MINISTÉRIO DA EDUCAÇÃO
UNIVERSIDADE FEDERAL DO RIO GRANDE DO SUL
ESCOLA DE ENGENHARIA
Programa de Pós-Graduação em Engenharia de Minas, Metalúrgica e de Materiais
PPGE3M

AVALIAÇÃO DO IMPACTO AMBIENTAL DE RESÍDUOS DE ELASTÔMEROS TERMOPLÁSTICOS SEBS/PP COM PROPRIEDADES ANTIMICROBIANAS

DAIANE TOMACHESKI

Tese para obtenção do título de Doutor em Engenharia

Porto Alegre
2017

DAIANE TOMACHESKI

AVALIAÇÃO DO IMPACTO AMBIENTAL DE RESÍDUOS DE ELASTÔMEROS TERMOPLÁSTICOS SEBS/PP COM PROPRIEDADES ANTIMICROBIANAS

Tese submetida ao Programa de Pós-Graduação em Engenharia de Minas, Metalúrgica e de Materiais (PPGE3M) da Universidade Federal do Rio Grande do Sul, como requisito parcial à obtenção do título de Doutora em Engenharia.

Área de Concentração: Ciência e Tecnologia dos Materiais

Orientadora: Prof. Dra. Ruth Marlene Campomanes Santana
Coorientadora: Dra. Michele Pittol

Porto Alegre

2017

DAIANE TOMACHESKI

AVALIAÇÃO DO IMPACTO AMBIENTAL DE RESÍDUOS DE ELASTÔMEROS TERMOPLÁSTICOS SEBS/PP COM PROPRIEDADES ANTIMICROBIANAS

TESE DE DOUTORADO

Esta tese foi analisada e julgada adequada para a obtenção do título de Doutora em Engenharia, área de concentração de Ciência e Tecnologia dos Materiais, e aprovada em sua forma final, pelo orientador e pela Banca Examinadora do Programa de Pós-Graduação.

_____
Professora orientadora: Dra. Ruth Marlene Campomanes Santana

_____
Coorientadora: Dra. Michele Pittol

Aprovado em: __/__/__

BANCA EXAMINADORA:

_____
Professora: Dra. Duclerc Fernandes Parra
Instituto de Pesquisas Energéticas e Nucleares

_____
Professor: Dr. André Luis Catto
Centro Universitário UNIVATES

_____
Professora: Dra. Maria Madalena de Camargo Forte
Universidade Federal do Rio Grande do Sul

Aos meus pais, Ineu e Helena.

AGRADECIMENTOS

À Deus, por cuidar para que as portas estejam sempre abertas.
Aos meus pais, pelo apoio incondicional na minha vida acadêmica.
À Michele Pittol, amiga, parceira de projeto e co-orientadora.
À minha orientadora Ruth Santana e aos professores, pela transmissão de conhecimentos.
À Softer Brasil Compostos Termoplásticos, pela infraestrutura. Ao FINEP, pelo apoio financeiro. E especialmente à Vanda Ribeiro que fez esta participação possível.
Aos colegas de laboratório da Softer Brasil Compostos Termoplásticos.

Science:

If you don't make mistakes, you're doing it wrong.

If you don't correct those mistakes, you're doing it really wrong.

If you can't accept that you're mistaken, you're not doing it all.

Anon.

PARTICIPAÇÕES EM CONGRESSOS

Parte dos resultados obtidos durante o doutorado foram publicados nos seguintes eventos de âmbito internacional:

- TOMACHESKI, D.; PITTOL, M.; RIBEIRO, V.F.; SANTANA, R.M. C. Organic additives as antimicrobial agents in thermoplastics compounds. **XXIV International Materials Research Congress**. Cancun, México, 16 a 20 de Agosto de 2015.
- TOMACHESKI, D.; PITTOL, M.; RIBEIRO, V.F.; SANTANA, R.M. C. Silver phosphate glass and silver nanoparticles as antimicrobials in thermoplastic elastomer compounds. **XI Simposio Argentino de Polímeros**. Santa Fé, Argentina, 20 a 23 de outubro de 2015.
- TOMACHESKI, D.; PITTOL, M.; RIBEIRO, V.F.; SANTANA, R.M. C. Influence of the processing conditions on the antimicrobial and mechanical properties. **XI Simposio Argentino de Polímeros**. Santa Fé, Argentina, 20 a 23 de outubro de 2015.
- TOMACHESKI, D.; PITTOL, M.; RIBEIRO, V.F.; SANTANA, R.M. C. Investigation of factors affecting microbial growth in elastomeric materials**.** **XXXVII Congreso Chileno de Microbiologia**. La Serena, Chile, 01 a 04 de dezembro de 2015.

PUBLICAÇÃO DE ARTIGOS

Os capítulos desta tese foram publicados ou submetidos para publicação nas seguintes revistas científicas:

- TOMACHESKI, D.; PITTOL, M.; FERREIRA, V. F.; SANTANA, R. M. C. Efficiency of silver based antibacterial additives and its influence in thermoplastic elastomers. **Journal of Applied Polymer Science**, v. 133, p. 43956, 2016. doi: 10.1002/app.43956
    - Classificação Qualis Engenharias II: A1
    - Fator de impacto: 1,866

- TOMACHESKI, D.; PITTOL, M.; LOPES, A. P. M.; SIMÕES, D. N.; FERREIRA, V. F.; SANTANA, R. M. C. Effects of weathering on mechanical, antimicrobial properties and biodegradation process of silver loaded TPE compounds. **Journal of Polymers and the Environment**, 2017. Doi: 10.1007/s10924-016-0927-8
    - Classificação Qualis Engenharias II: A1
    - Fator de impacto: 1,969

- TOMACHESKI, D.; PITTOL. M.; SIMÕES, D. N.; FERREIRA, V. F.; SANTANA, R. M. C. Effect of natural ageing on surface of silver loaded TPE and its influence in antimicrobial efficacy. **Applied Surface Science**, v. 405, p. 137-145, 2017. Doi: 10.1016/j.apsusc.2017.02.036
    - Classificação Qualis Engenharias II: A1
    - Fator de impacto: 3,150

- TOMACHESKI, D.; PITTOL, M.; SIMÕES, D. N.; FERREIRA, V. F.; SANTANA, R. M. C. Effects of silver adsorbed on fumed silica, silver phosphate glass, bentonite organomodified with silver and titanium dioxide in aquatic indicator organisms. **Journal of Environmental Sciences**, 2017. doi: 10.1016/j.jes.2016.07.018
    - Fator de impacto: 2,208

- TOMACHESKI, D.; PITTOL, M.; SIMÕES, D. N.; FERREIRA, V. F.; SANTANA, R. M. C. Impact of silver ions and silver nanoparticles on the plant grown and soil microorganisms. **Global Journal of Environmental Science and Management**, 3(4): …-… 2017 (*In press*). Doi: 10.22034/gjesm.2017.03.04.00*

RESUMO

A preocupação com a saúde tem levado ao uso de produtos com propriedades antimicrobianas, visando reduzir a proliferação de micro-organismos patogênicos. Ao mesmo tempo em que aditivos antimicrobianos são benéficos, pois reduzem a transmissão de doenças, os efeitos negativos, ainda, não estão bem elucidados. Estes aditivos podem afetar organismos essenciais ao meio ambiente e no desenvolvimento de plantas de interesse agrícola. Este trabalho tem o objetivo de avaliar o impacto ambiental causado por resíduos de elastômeros termoplásticos aditivados com três antimicrobianos comerciais à base de prata e pelos aditivos puros: (1) nanopartículas de prata adsorvida em sílica pirogênica (AgNp_sílica); (2) bentonita organomodificada com prata (Ag^+_bentonita) e (3) prata em vidro fosfato (Ag^+_fosfato). Os aditivos foram incorporados em uma formulação de composto termoplástico, a base de copolímero em bloco estireno-etileno/butileno-estireno (SESB), polipropileno (PP) e óleo mineral por mistura no estado fundido em extrusora dupla rosca e moldados por injeção. Os aditivos foram caracterizados por tamanho, forma e composição com o objetivo de avaliar a influência destas características nas seguintes propriedades do composto: mecânicas, térmicas, químicas, físicas, morfológicas e antimicrobianas. Além disso, foram avaliadas a variação na degradação abiótica e biótica dos compostos termoplásticos. A influência na degradação abiótica e a consequente redução de vida útil dos compostos foram avaliadas pelo ensaio de intemperismo. Já para a avaliação do impacto no solo foi realizado ensaio de biodegradação em câmara respirométrica (degradação biótica) e germinação de plantas no solo contendo os aditivos. O microcrustáceo aquático *Daphnia magna (D. magna)* foi utilizado como bioindicador de toxicidade dos aditivos na água. Os resultados indicam que compostos com AgNp_sílica possuem melhor propriedade antibacteriana que os demais aditivos testados, eliminando mais de 95% da população de *Escherichia coli* e 80% da população de *Staphylococcus aureus* após 24 horas de contato. A incorporação dos aditivos teve pouco efeito sobre as propriedades mecânicas, térmicas, químicas, físicas e morfológicas dos compostos. Os compostos aditivados e sem aditivo não apresentaram diferença no ensaio de intemperismo. No ensaio respirométrico, as amostras aditivadas tiveram pouca variação na produção de gás carbônico em comparação ao composto padrão. No teste de toxicidade em água com *D. magna*, houve mortalidade de todos os organismos, mesmo na concentração de 0,0001 mg L^{-1} de aditivo. No ensaio de germinação, os resultados foram adversos, não possibilitando estabelecer um padrão de toxicidade. Por fim, conclui-se que com o manejo adequado dos resíduos, compostos termoplásticos antimicrobianos são ambientalmente seguros, além de auxiliar no controle da propagação de doenças.

Palavras chave: Compostos termoplásticos, aditivo antimicrobiano, prata, impacto ambiental.

ABSTRACT

The concern with health has led to the use of products with antimicrobial properties aiming to reduce the proliferation of pathogenic microorganisms. At the same time that antimicrobial additives are useful to reduce the transmission of disease, adverse effects under human and environmental health still not well understood. These additives can affect organisms essential to the environment and plant development. The objective of this work was to evaluate the environmental impact caused by residues from thermoplastic elastomers (TPE) containing three commercial, silver-based antimicrobial additives and the pure additives. The additives tested were: (1) silver nanoparticles adsorbed on fumed silica (AgNp_silica); (2) bentonite organomodified with silver (Ag^+_bentonite) and (3) silver phosphate glass (Ag^+_phosphate). The additives were incorporated into a thermoplastic compound formulation, based on styrene-ethylene/butylene-styrene block copolymer (SESB), polypropylene (PP) and mineral oil by melt-blend in a twin-screw extruder and injection molded. A non loaded sample (standard) was used as control. The additives were characterized according to their size, shape and composition to evaluate the influence of these characteristics on the properties of the compound (mechanical, thermal, chemical, physical, morphological and antimicrobial). The influence on the abiotic degradation and consequent reduction in the life cycle of the compounds was evaluated by weathering test. To evaluate the impact of loaded TPE in soil, a soil biodegradation test was carried out in a respiratory chamber (biotic degradation) and germination of plants. The aquatic microcrustacean *Daphnia magna* (*D. magna*) was used as a bioindicator of toxicity of the additives in water. The results indicate that AgNp_silica compounds have better antibacterial properties than the other additives tested, eliminating more than 95% of the *Escherichia coli* population and 80% of the *Staphylococcus aureus* population after 24 h of contact. The incorporation of the additives had little effect on the mechanical, thermal, chemical, physical and morphological properties of the compounds. The results indicated that the additives presented a moderate effect on the properties of the above-mentioned metal loaded TPE compounds. The loaded and standard samples showed no difference in the weathering tests. In the respirometric assay, loaded samples had little variation in the production of carbon dioxide compared to the standard one. In the *D. magna* assay, there was mortality of all organisms, even at the concentration of 0.0001 mg L^{-1} of additive. In the germination test, the results were inconsistent and it was not possible to determine the toxicity potential of the additives tested. Lastly, it is possible to conclude that, taking into account the correct final disposition of TPE residues; thermoplastic compounds are environmentally safe and can assist in the control of diseases.

Keywords: Thermoplastic compounds, antimicrobial, silver, environmental impact

LISTA DE FIGURAS

Figure 4.1 Diffractograms of samples: (a) AgNp_silica, (b) Ag^+_phosphate and (c) Ag^+_bentonite.....31

Figure 4.2 Micrographs of SEM (left) and TEM (right) of additives: (a, b) AgNp_silica, (c, d) Ag^+_phosphate and (e, f) Ag^+_bentonite.....33

Figure 4.3 FTIR-ATR spectra of (a) AgNp_silica, (b) Ag^+_phosphate and (c) Ag^+_bentonite.....35

Figure 4.4 FTIR-ATR spectra of the (a) standard sample and compounds with (b) 2.0% of Ag^+_bentonite, (c) 0.3% of Ag^+_phosphate and (d) 0.05% of AgNp_silica.....36

Figure 4.5 Variation in tensile properties of the compounds: (-●-) AgNp_silica, (-▲-) Ag^+_phosphate (-■-) and Ag^+_bentonite. 36

Figure 4.6 DSC curves of the (a) standard sample and compounds (b) 0.05% of AgNp_silica (c) 0.3% of Ag^+_phosphate and (d) 2.0% of Ag^+_bentonite.....37

Figure 4.7 Micrographs of SEM (a, d and g) and TEM of the compounds with 0.05% of AgNp_silica (a, b, c); 0.3% of Ag^+_phosphate (d, e, f) and 2.0% of Ag^+_bentonite (g, h, i).....39

Figure 4.8 Variation in (a) *E. coli* and (b) *S. aureus* colony forming unit per square centimeter (CFU cm^{-2}) in (-●-) AgNp_silica 0.025%, (-○-) AgNp_silica 0.05%, (-▲-) Ag^+_phosphate 0.1%, (-◊-) Ag^+_phosphate 0.3%, (-♦-) Ag^+_bentonite 0.5%, (-◊-) Ag^+_bentonite 2.0% compounds 40

Figure 5.1 (a) Weathering experiment; values of (b) rainfall, temperature and (c) solar radiation during the period evaluated 52

Figure 5.2 Variation in mechanical properties over the weathering exposure: (-♦-) Standard, (-■-) Ag^+_bentonite, (-▲-) Ag^+_phosphate, (-x-) AgNp_silica 56

Figure 5.3 FTIR-ATR of (a) Standard sample and compounds with (b) 2.0 % of Ag^+_bentonite, (c) 0.3 % of Ag^+_phosphate and (d) 0.05 % of AgNp_silica.....58

Figure 5.4 FTIR-ATR of Standard sample (a) no weathering, (b) after three, (c) six and (d) nine months of weathering exposure 58

Figure 5.5 Scanning electron microscopy from the surface of TPE samples of (a) Standard, (b) Ag^+_bentonite, (c) Ag^+_phosphate and (d) AgNp_silica after 3 months of weathering exposure 59

Figure 5.6 Variation in (a) *E. coli* and (b) *S. aureus* population in silver loaded compounds during weathering exposure.....60

Figure 5.7 Standard sample characteristics after weathering exposure and burial in soil 62

Figure 5.8 (a) Cumulative CO_2 emissions from unexposed samples, (b) exposed to weathering for 3 and (c) exposed to weathering for 6 months. (-♦-) Standard, (-■-) Ag^+_bentonite, (-▲-) Ag^+_phosphate, (-x-) AgNp_silica, (-●-) cellulose.....63

Figure 5.9 FTIR-ATR of Standard sample (a) no weathering, (b) buried in soil, no weathering, (c) buried in soil after 3 months of weathering and (d) buried in soil after 6 months of weathering 64

Figure 6.1 Micrographs and average diameter determined by transmission electron microscopy (TEM), diameter determined by laser diffraction, surface specific area (SSA), and zeta potential at different pH determined for (a) AgNp_silica, (b) Ag^+_phosphate, and (c) Ag^+_bentonite 72

Figure 6.2 Growth of (a) *S. aureus* and (b) *E. coli* on SEBS-based TPE compounds 76

Figure 6.3 Antibacterial activity of loaded TPE samples against (a) *E. coli* and (b) *S. aureus* population after zero, three, six and nine months of natural ageing exposure. (-●-) Standard, (-♦-) Ag^+_bentonite, (-■-) Ag^+_phosphate, (-▲-) AgNp_silica 76

Figure 6.4 Aged-TPE samples exposed to fungal growth 77

Figure 6.5 Carbonyl index (a, -●-) Standard, (b, -♦-) Ag^+_bentonite, (c, -■-) Ag^+_phosphate and (d, -▲-) AgNp_silica 78

Figure 6.6 Modifications in sample wettability before (right) and after (left) nine months of exposure: (a) Standard, (b) Ag^+_bentonite, (c) Ag^+_phosphate and (d) AgNp_silica 79

Figure 6.7 Water contact angle (-●-) Standard, (-♦-) Ag^+_bentonite, (-■-) Ag^+_phosphate and (-▲-) AgNp_silica 79

Figure 6.8 Representative 20 µm x 20 µm AFM 3-D images of (a) Standard initial; (b) Standard after nine months; (c) Ag^+_bentonite initial; (d) Ag^+_bentonite after nine months; (e) Ag^+_phosphate initial; (f) Ag^+_phosphate after nine months; (g) AgNp_silica initial and (h) AgNp_silica after nine months 83

Figure 7.1 Micrographs obtained by TEM, diameter, specific surface area (SSA) and zeta potential of the additives: (a) AgNp_silica, (b) Ag^+_phosphate, (c) Ag^+_bentonite and (d) TiO_2 94

Figure 7.2 Zeta potential of (-▲-) AgNp_silica; (-■-) Ag^+_phosphate; (-♦-) Ag^+_bentonite and (-x-) TiO_2 96

Figure 7.3 Total of dead *Daphnia magna* after 48 h in contact with TiO_2 suspensions 97

Figure 7.4 *Ceriodaphnia dubia* neonates produced during the 7-days in contact with TiO_2 suspensions 98

Figure 8.1 Transmission electron microscopy of the additives evaluated: (a) AgNp_silica, (b) Ag^+_phosphate and (c) Ag^+_bentonite 114

Figure 8.2 Germination assay: (a) greenhouse used in the test and (b) vessels arrangement within the greenhouse. 115

Figure 8.3 Oat cultivated in soils containing (a) Control, (b) Ag^+_bentonite, (c) Ag^+_phosphate and (d) AgNp_silica 118

Figure 8.4 Lettuce cultivated in soils containing (a) Control, (b) Ag^+_bentonite, (c) Ag^+_phosphate and (d) AgNp_silica 118

Figure 8.5 Radish cultivated in soils containing (a) Control, (b) Ag^{+}_bentonite, (c) Ag^{+}_phosphate and (d) AgNp_silica.....119

LISTA DE TABELAS

Table 4.1 Specific surface area determined by BET 32

Table 4.2 Values of average diameter, D_{10}, D_{50} and D_{90} determined by laser diffraction.....34

Table 4.3 DSC results of the second heating of TPE samples.....38

Table 4.4 Variation of antimicrobial efficacy. 40

Table 5.1 Thermal characteristics (melting temperature T_m, and crystallinity index X_{cPP}) of TPE samples from the first heating scan before and after 3, 6 and 9 months of weathering exposure. 57

Table 5.2 Total amount of silver in samples before and after nine months of weathering.....61

Table 6.1 Surface free energy of samples before and after six and nine months of exposure 81

Table 7.1. Mean values of the aqueous suspensions parameters.....96

Table 7.2. Evaluation of metal aqueous suspensions (AgNp_silica, Ag^+_phosphate and Ag^+_bentonite) to *Daphnia magna*.....97

Table 8.1 Physical-chemical characteristics of the additives evaluated 114

Table 8.2 Physicochemical characteristics of metal loaded soil.....117

Table 8.3 Oat, lettuce and radish germination (%), relative germination (%, comparing loaded soil with the control), root growth (mm) and dry mass (g) 118

Table 8.4 Soil microbiota after harvest.....121

LISTA DE ABREVITURAS, SIGLAS E SÍMBOLOS

ΔHc	Crystallization enthalpy (Entalpia de cristalização)
ΔHm	Melting enthalpy (Entalpia de fusão)
$\Delta H°_{(PP)}$	Polypropylene melting enthalpy (Entalpia de fusão do polipropileno)
ΔH^*	Thermoplastic elastomer melting enthalpy (Entalpia de fusão do elastômero termoplástico)
A	Absorbância
ABNT	Associação Brasileira de Normas Técnicas
AFM	Atomic Force Microscopy (Microscopia de Força Atômica)
Ag^+_bentonite	Bentonite organomodified with silver (Bentonita organomodificada com prata)
Ag^+_phosphate	Silver phosphate glass (Prata vidro fosfato)
AgNp	Silver nanoparticle (Nanopartículas de prata)
AgNp_silica	Silver nanoparticle adsorbed on fumed silica (Nanopartículas de prata adsorvidas em sílica pirogênica)
ANOVA	Analysis of variance (Análise de Variança)
ASTM	American Society for Testing and Materials (Sociedade Americana para Testes e Materiais)
A_t	Average logarithm numbers of viable bacteria after inoculation on antibacterial samples after 24 h (Média do número logaritmo de bactérias viáveis após inoculação nos corpos de prova antibacterianos após 24 h)
ATP	Adenosine triphosphate (Adenosina trifosfato)
BET	Brunauer–Emmett–Teller Method (Método Brunauer–Emmett–Teller)
C. dubia	*Ceriodaphnia dubia*
CFU	Colony forming units (Unidades formadoras de colônia)
D. magna	*Daphnia magna*
DNA	Deoxyribonucleic Acid (Ácido desoxirribonucleico)
DSC	Differential scanning calorimetry (Calorimetria Diferencial de Varredura)
EC_0	Effective concentration that cause effect on 0% of test organisms (Concentração efetiva que causa efeito em 0% dos organismos teste)
EC_{50}	Effective concentration that cause effect on 50% of test organisms (Concentração efetiva que causa efeito em 50% dos organismos teste)
EDS	Energy dispersive X-ray (Raios-X por energia dispersiva)
Ef	Reduction of bacterial population (%) (Redução da população bacteriana)
FEG	Field emission gun (Canhão de emissão de campo)
FTIR-ATR	Fourier Transform Infrared Spectroscopy - Attenuated total reflection (Espectroscopia no Infravermelho por Transformada de Fourier - Refletância Total Atenuada)
JIS	Japanese Industrial Standards (Norma Industrial Japonesa)
LC_{50}	Lethal concentration (Concentração letal)
M	Molar
M_n	Massa molar ponderal média
w	Polypropylene mass fraction (Fração mássica do Polipropileno)

M_w	Massa molar-z média
NOEC	No-observed-effect concentration (Concentração que não causa efeitos)
Np	Nanoparticle (Nanopartícula)
OM	Organic matter (Matéria orgânica)
P_f	Final bacterial population (População bacteriana final)
P_i	Initial bacterial population (População bacteriana inicial)
PP	Polypropylene (Polipropieleno)
R	Antibacterial activity (Atividade antibacteriana)
r	Rotações
Ra	Rugosidade
ROS	Reactive Oxygen Species (Espécies Reativas de Oxigênio)
rpm	Rotações por minuto
S	Sul
SD	Standard deviation (Desvio padrão)
SEBS	Styrene-ethylene/butylene-styrene (Estireno-etileno/butileno-estireno)
SEM	Scanning electron microscopy (Microscopia eletrônica de varredura)
SFE	Surface free energy (Energia livre de superfície)
SSA	Specific surface area (Área Superficial Específica)
T	Transmitância
T_c	Crystallization temperature
TEM	Transmission electron microscopy (Microscopia eletrônica de transmissão)
T_m	Melting temperature (Temperatura de fusão)
TPE	Thermoplastic elastomer (Elastômero Termoplástico)
U_t	Average of logarithm numbers of viable bacteria after inoculation on standard (additive free) samples (Média do número logaritmo de bactérias viáveis após inoculação nos corpos de prova não tratados após 24 h)
UV	Ultravioleta
v	Volume
W	Oeste
X_c	Crystallinity degree (Grau de cristalinidade)
ZP	Zeta Potencial (Potencial zeta)
γ	Surface free energy (Energia Livre de Superfície)
γ^-	Lewis base polar force (Força polar básica)
γ^+	Lewis acid polar force (Força polar ácida)
γ^D	Dispersive force (Força dispersiva)
γ_L	Liquid surface tension (Tensão superficial do líquido)
γ_L^-	Liquid Lewis base polar force (Força polar básica do líquido)
γ_L^+	Liquid Lewis acid polar force (Força polar ácida do líquido)
γ_L^D	Liquid dispersive force (Força dispersiva do líquido)
γ_{LS}	Interfacial free energy (Energia interfacial livre)
γ^P	Polar (Lewis) force (Força polar)

γ_S	Solid surface tension (Tensão superficial do sólido)
γ_S^-	Solid Lewis base polar force (Força polar básica do sólido)
γ_S^+	Solid Lewis acid polar force (Força polar ácida do sólido)
γ_S^D	Solid dispersive force (Força dispersiva do sólido)
Θ	Liquid-solid contact angle (Ângulo de contato entre líquido e sólido)

SUMÁRIO

1 INTRODUÇÃO GERAL 19
1.1 INTRODUÇÃO 19
1.2 REFERENCIAS 20

2 OBJETIVO GERAL 23

3 INTEGRAÇÃO DE ARTIGOS 24

4 EFFICIENCY OF SILVER BASED ANTIBACTERIAL ADDITIVES AND ITS INFLUENCE IN THERMOPLASTIC ELASTOMERS 25
4.1 INTRODUCTION 25
4.2 EXPERIMENTAL 27
4.2.1 Materials 27
4.2.2 Compounds preparation 27
4.2.3 Compounds and additives characterization 28
4.3 RESULTS AND DISCUSSION 31
4.3.1 Additives characterization 31
4.3.2 Compounds characterization 35
4.4 CONCLUSIONS 42
4.5 REFERENCES 43

5 EFFECTS OF WEATHERING ON MECHANICAL, ANTIMICROBIAL PROPERTIES AND BIODEGRADATION PROCESS OF SILVER LOADED TPE COMPOUNDS 49
5.1 INTRODUCTION 49
5.2 EXPERIMENTAL 51
5.2.1 Materials 51
5.2.2 TPE compounds preparation 51
5.2.3 Natural ageing experiments 52
5.2.4 Biodegradation in soil 52
5.2.5 Analytical methods 53
5.3 RESULTS 55
5.3.1 Influence of natural ageing 55
5.3.2 Aerobic biodegradation in soil 62
5.4 CONCLUSIONS 65
5.5 REFERENCES 65

6 EFFECT OF NATURAL AGEING ON SURFACE OF SILVER LOADED TPE AND ITS INFLUENCE IN ANTIMICROBIAL EFFICACY 70
6.1 INTRODUCTION 70
6.2 MATERIALS AND METHODS 71
6.2.1 Materials 71
6.2.2 TPE compounds preparation 72
6.2.3 Natural ageing experiments 72
6.2.4 Analytical methods 73
6.2.5 Statistical analysis 75
6.3 RESULTS AND DISCUSSION 75

6.3.1 Bacterial development 75
6.3.2 Antimicrobial properties 76
6.3.3 Modifications on the surface and their influence in antimicrobial properties 78
6.4 CONCLUSIONS 84
6.5 REFERENCES 84

7 EFFECTS OF SILVER ADSORBED ON FUMED SILICA, SILVER PHOSPHATE GLASS, BENTONITE ORGANOMODIFIED WITH SILVER AND TITANIUM DIOXIDE IN AQUATIC INDICATOR ORGANISMS 89
7.1 INTRODUCTION 89
7.2 MATERIAL AND METHODS 91
7.2.1 Characterization of the particles 91
7.2.2 *Daphnia magna* preparation to the acute toxicity assays 92
***7.2.3* Preparation of solutions 92**
7.2.4 Exposure 92
7.2.5 *Ceriodaphnia dubia* preparation to the chronic assay 93
7.2.6 Exposure 93
7.2.7 Data analysis 93
7.3 RESULTS 94
7.3.1 Particles characterization 94
7.3.2 Abiotic variables 96
7.3.3 Acute toxicity 96
7.3.4 Chronic toxicity 98
7.4 DISCUSSION 98
7.4.1 Size dependent toxicity 99
7.4.2 Metal ion release and associated damage 99
7.4.3 Metal binding process and toxicity 100
7.4.4 TiO_2 properties and its toxic behavior 101
7.5 CONCLUSIONS 104
7.6 REFERENCES 104

8 IMPACT OF SILVER IONS AND SILVER NANOPARTICLES ON THE PLANT GROWTH AND SOIL MICROORGANISMS 112
8.1 INTRODUCTION 112
8.2 MATERIAL AND METHODS 113
8.2.1 Germination assay 115
8.2.2 Soil characterization 116
8.2.3 Isolation of soil microorganisms 116
8.3 RESULTS AND DISCUSSION 117
8.4 CONCLUSIONS 122
8.5 REFERENCES 123

9 CONCLUSÃO GERAL 129

1 INTRODUÇÃO GERAL

1.1 INTRODUÇÃO

A utilização de antimicrobianos em polímeros tem como objetivo inibir o crescimento e proliferação de bactérias e fungos, principalmente, na fabricação de utensílios suscetíveis aos mesmos ou em aplicações biomédicas.

Os elastômeros termoplásticos à base do copolímero em bloco estireno-etileno/butileno-estireno (SEBS) são frequentemente utilizados em blendas com polipropileno (PP) e óleo mineral para fabricação de materiais emborrachados para uso em produtos como calçados hospitalares e vedações de geladeira. Devido à característica de toque suave são aplicados também em produtos com contato direto com as mãos, como cabos de escovas de dente e brinquedos. Em todas estas aplicações os objetos produzidos são propícios à contaminação por fungos e bactérias patogênicas [1-4], e a incorporação de aditivos com propriedades antimicrobianas na formulação do produto pode contribuir para a redução da formação de biofilme.

Em âmbito comercial, os aditivos antimicrobianos que se destacam são os de base prata, na forma de nanopartículas ou íons. Nos últimos anos, muitos estudos têm sido realizados para aprimorar a eficácia deste tipo de aditivo [5-7]. Estudos mostram que as características do polímero também influenciam na eficácia do aditivo antimicrobiano, devido às características como polaridade, cristalinidade, superfície, etc. [8, 9]. Ou seja, a eficácia dos polímeros com propriedades antimicrobianas ainda não está consolidada e necessita de mais estudos.

Apesar da ampla possibilidade de aplicação dessas substâncias, o uso e o descarte incorreto podem ocasionar problemas ambientais; uma vez que, além de inibir o crescimento de micro-organismos nocivos, também pode interferir na biota local ocasionando danos ao ambiente [10, 11]. Além disso, essas substâncias podem alterar o processo natural de biodegradação [12-14], bem como a absorção de nutrientes pelas plantas [15-17] e até mesmo ser letal para pequenos organismos aquáticos [18-20].

No processo de gestão do resíduo sólido urbano brasileiro, somente 5,2% dos resíduos potencialmente recicláveis são reciclados [21]. Nesse contexto, mesmo que a indústria tenha o cuidado necessário para evitar que o aditivo puro entre em

contato com o solo e corpos hídricos, o aditivo incorporado no produto final pode ser lixiviado para o solo nos aterros sanitários.

Para o desenvolvimento deste trabalho foram selecionados três aditivos antimicrobianos comerciais, que possuem íons ou nanopartículas de prata como princípio ativo, sendo eles: (1) prata em vidro fosfato (Ag^+_fosfato); (2) bentonita organomodificada com prata (Ag^+_bentonita) e (3) nanopartículas de prata adsorvidas em sílica pirogênica (AgNp_silica).

A importância científica desta pesquisa está no fato de ser o primeiro projeto a estudar o efeito da incorporação de aditivos antimicrobianos a base de prata nas propriedades de compostos termoplásticos de SEBS/PP/óleo e também avaliar o impacto ambiental deste produto. Quanto maior a compreensão de como as características do aditivo, do polímero e do meio externo interagem, mais eficaz e seguro será o desenvolvimento de um polímero com propriedades antimicrobianas.

1.2 REFERENCIAS

1. MERRIMAN, E.; CORWIN, P.; IKRAM, R. Toys are a potential source of cross-infection in general practitioners' waiting rooms. **British Journal of General Practice**, v. 52, p. 138-140, 2002.
2. GARCIA-CRUZ, C. P.; AGUILAR, M. J. N.; ARROYO-HELGUERA, O. E. Fungal and bacterial contamination on indoor surfaces of a hospital in Mexico. **Jundishapur Journal of Microbiology**, v. 5, n. 3, p. 460-464, 2012. Doi: 10.5812/jjm.2625
3. FRAZELLE, M. R.; MUNRO, C. L. Toothbrush Contamination: A Review of the Literature. **Nursing Research and Practice**, Article ID 420630, 6 pages, 2012. Doi: 10.1155/2012/420630
4. OTU-BASSEY, I. B.; EWAOCHE, I. S.; OKON, B. F.; IBOR, U. A. Microbial contamination of house hold refrigerators in Calabar Metropolis-Nigeria. **American Journal of Epidemiology and Infectious Disease**, v. 5, n. 1, p. 1-7, 2017. Doi: 10.12691/ajeid-5-1-1
5. FIORI M. A.; PAULA, M. M. S.; BERNARDIN, A. M.; RIELLA, H. G.; ANGIOLETTO, E. Bactericide glasses developed by Na^+/Ag^+ ionic exchange. **Materials Science and Engineering C**, v. 29, p. 1569–1573, 2009.
6. LALUEZA, P.; MONZÓN, M.; ARRUEBO, M.; SANTAMARÍA. Bactericidal effects of different silver-containing materials. **Materials Research Bulletin**, v. 46, p. 2070-2076, 2011. Doi: 10.1016/j.materresbull.2011.06.041
7. FERREIRA, L.; FONSECA, A.M.; BOTELHO, G.; ALMEIDA-AGUIAR, C.; NEVES, I.C. Antimicrobial activity of faujasite zeolites doped with silver**. Microporous and Mesoporous Materials**, v. 160, p. 126–132, 2012. Doi:

10.1016/j.micromeso.2012.05.006

8. KUMAR, R.; MÜNSTEDT, H. Silver ion release from antimicrobial polyamide/silver composites. **Biomaterials**, v. 26, p. 2081–2088, 2005. Doi: 10.1016/j.biomaterials.2004.05.030

9. CARVALHO, D.; SOUSA, T.; MORAIS, P. .; PIEDADE, A. P. Polymer/metal nanocomposite coating with antimicrobial activity against hospital isolated pathogen. **Applied Surface Science**, v. 379, p. 489–496, 2016. Doi: 10.1016/j.apsusc.2016.04.109

10. CALDER, A. J.; DIMKPA, C. O.; MCLEAN, J. E.; BRITT, D. W.; JOHNSON, W.; ANDERSON, A. J. Soil components mitigate the antimicrobial effects of silver nanoparticles towards a beneficial soil bacterium, *Pseudomonas chlororaphis* O6. **Science of the Total Environment**, v. 429, p. 215-22, 2012. Doi: 10.1016/j.scitotenv.2012.04.049

11. SHIN, Y-J.; KWAK, J. I.; AN, Y-J. Evidence for the inhibitory effects of silver nanoparticles on the activities of soil exoenzymes. **Chemosphere**, v. 88, p. 524-529, 2012. Doi: 10.1016/j.chemosphere.2012.03.010

12. LUNA-DELRISCO, M.; ORUPOLD, K.; DUBOURGUIER, H-C. Particle-size effect of CuO and ZnO on biogas and methane production during anaerobic digestion. **Journal of Hazardous Materials**, v. 189, p. 603–608, 2011. Doi: 10.1016/j.jhazmat.2011.02

13. YANG, Y.; XU, M.; WALL, J. D.; HU, Z. Nanosilver impact on methanogenesis and biogas production from municipal solid waste. **Waste Management**, v. 32, p. 816–825, 2012. Doi: 10.1016/j.wasman.2012.01.009

14. LAZIC, V.; RADOICIC, M.; SAPONJIC, Z.; RADETIC, T.; VODNIK, V.; NIKOLIC, S.; DIMITRIJEVIC, S.; RADETIC, M. Negative influence of Ag and TiO_2 nanoparticles on biodegradation of cotton fabrics. **Cellulose**, v. 22, p. 1365–1378, 2015. Doi: 10.1007/s10570-015-0549-7

15. KAVEH, R.; LI, Y-S.; RANJBAR, S.; TEHRANI, R.; BRUECK, C. L.; AKEN, B. V. Changes in Arabidopsis thaliana Gene Expression in Response to Silver Nanoparticles and Silver Ions. **Environmental Science & Technology**, v. 47, p. 10637−10644, 2013. Doi: 10.1021/es402209w

16. WANG, J.; KOO, Y.; ALEXANDER, A.; YANG, Y.; WESTERHOF, S.; ZHANG, Q.; SCHNOOR, J. L.; COLVIN, V. L.; BRAAM, J.; ALVAREZ, P. J. J. Phytostimulation of poplars and *Arabidopsis* exposed to silver nanoparticles and Ag^+ at sublethal concentrations. **Environmental Science and Technology**, v. 47, p. 5442−5449, 2013. Doi: 10.1021/es4004334

17. MUSTAFA, G.; SAKATA, K.; HOSSAIN, Z.; KOMATSU, S. Proteomic study on the effects of silver nanoparticles on soybean under flooding stress. **Journal of Proteomics**, v. 122, p. 100-118, 2015. Doi: 10.1016/j.jprot.2015.03.030

18. POYNTON, H. C.; LAZORCHAK, J. M.; IMPELLITTERI, C. A.; BLALOCK, B. J.; ROGERS, K.; ALLEN, H. J.; LOGUINOV, A.; HECKMAN, J. L.; GOVINDASMAWY, S. Toxicogenomic responses of nanotoxicity in *Daphnia magna* exposed to silver nitrate and coated silver nanoparticles. **Environmental Science and Technology**, v. 46, p. 6288−6296, 2012. Doi:

10.1021/es3001618

19. RIBEIRO, F.; GALLEGO-URREA, J. A.; JURKSCHAT, K.; CROSSLEY, A.; HASSELLÖV, M.; TAYLOR, C.; SOARES, A.M.V.M.; LOUREIRO, S. Silver nanoparticles and silver nitrate induce high toxicity to *Pseudokirchneriella subcapitata*, *Daphnia magna* and *Danio rerio.* **Science of the Total Environment**, v. 466–467, p. 232–241, 2014. Doi: 10.1016/j.scitotenv.2013.06.101

20. SAKAMOTO, M.; HA, J-Y.; YONESHIMA, S.; KATAOKA, C.; TATSUTA, H.; KASHIWADA, S. Free silver ion as the main cause of acute and chronic toxicity of silver nanoparticles to cladocerans. **Archives of Environmental Contamination and Toxicology**, v. 68, p. 500–509, 2015. Doi: 10.1007/s00244-014-0091-x

21. SISTEMA NACIONAL DE INFORMAÇÕES SOBRE SANEAMENTO (SNIS). **Diagnóstico do manejo de resíduos sólidos urbanos – 2014**. Brasil. Ministério das Cidades. Secretaria Nacional de Saneamento Ambiental. Brasília: SNSA/MCIDADES, 2016.

2 OBJETIVO GERAL

O principal objetivo do trabalho é avaliar o impacto ambiental causado por resíduos de elastômeros termoplásticos SEBS/PP contendo aditivos antimicrobianos comerciais à base de prata. Objetiva-se também avaliar o impacto causado pelos aditivos puros quando em contato com o solo e corpos hídricos. Com isso, busca-se à obtenção de dados para a produção de um produto polimérico que contribua para a redução da transmissão de doenças e com baixo dano ao meio ambiente.

Objetivos Específicos:

- Avaliar a influência de aditivos antimicrobianos nas propriedades mecânicas, físicas, térmicas, químicas, morfológicas e antimicrobianas do composto de base SEBS/PP;
- Avaliar a influência de aditivos antimicrobianos sobre a expectativa de vida útil do produto através do ensaio de intemperismo (degradação abiótica);
- Avaliar o impacto de compostos antimicrobianos no solo, através do ensaio de compostagem em solo simulado com uso de câmara respirométrica (degradação biótica);
- Avaliar o impacto de aditivos antimicrobianos no ciclo de vida de organismos aquáticos, através do ensaio com microcrustáceos;
- Avaliar o impacto das características físicas e químicas de aditivos antimicrobianos (tamanho, forma e composição) e sua influência no meio ambiente, através de testes no solo e em organismos aquáticos;
- Avaliar o impacto de aditivos antimicrobianos no solo, através do ensaio de germinação.

3 INTEGRAÇÃO DE ARTIGOS

Os artigos foram elaborados de forma a dividir os resultados em três partes.

A primeira parte (Capítulo 4) apresenta as características dos aditivos comerciais à base de prata avaliados, bem como o procedimento para incorporação dos mesmos nas blendas do copolímero em bloco estireno-etileno/butileno-estireno (SEBS) com polipropileno (PP) e óleo mineral. As blendas obtidas foram caracterizadas quanto às propriedades mecânicas, térmicas, químicas, morfológicas e antimicrobianas. As blendas aditivadas obtidas neste Capítulo foram utilizadas nos estudos realizados e cujos resultados foram publicados nos Capítulos 5 e 6.

A segunda parte (Capítulos 5 e 6) refere-se à análise sobre o impacto ambiental, com a avaliação da redução da vida útil do material (ensaio de intemperismo natural) após a incorporação dos aditivos e o impacto no processo de biodegradação, através do ensaio de respirometria em solo simulado (câmara respirométrica). O Capítulo 5 mostra os resultados das alterações mecânicas, térmicas, químicas e antimicrobianas que ocorreram nos compostos após a degradação abiótica e biótica. A perda de propriedades mecânicas e antimicrobianas, bem como mudanças na estrutura molecular do composto, foi avaliada em corpos de prova expostos ao intemperismo por períodos de 3, 6 e 9 meses (de agosto/2015 a maio/2016). Após degradação abiótica por 0, 3 e 6 meses as amostras foram enterradas em solo para avaliar a influência do aditivo na degradação biótica. As amostras sem aditivo de prata e que não passaram por degradação abiótica foram utilizadas como referência para comparação. O Capítulo 6 contém os resultados do estudo sobre as variações na superfície dos compostos expostos ao intemperismo para compreender as mudanças que causaram o decréscimo da propriedade antimicrobiana dos mesmos.

A terceira parte (Capítulos 7 e 8) contém os resultados sobre o impacto ambiental dos aditivos, caso estes sejam descartados diretamente ou lixiviados do composto em corpos hídricos ou no solo. Os aditivos foram avaliados segundo o efeito dos mesmos na sobrevivência do microcrustáceo *Daphnia magna* (*D. magna*), no crescimento de plantas comestíveis (alface, rabanete e aveia) e na microbiota do solo. Nos ensaios com *D. magna* o dióxido de titânio (TiO_2) foi incluído para enriquecer a discussão dos resultados.

4 EFFICIENCY OF SILVER BASED ANTIBACTERIAL ADDITIVES AND ITS INFLUENCE IN THERMOPLASTIC ELASTOMERS[1]

Abstract

Styrene-ethylene/butylene-styrene (SEBS) based thermoplastic elastomers (TPE) are polymers with soft touch properties that are widely used for manufacturing devices that involve hand contact. However, when contaminated with microorganisms these products can contribute to spreading diseases. The incorporation of antibacterial additives can help maintain low bacteria counts. This work evaluated the antibacterial action of TPE loaded with silver ions and silver nanoparticles. The additives nanosilver on fumed silica (AgNp_silica), silver phosphate glass (Ag^+_phosphate), and bentonite organomodified with silver (Ag^+_bentonite) were added to the TPE formulation. The compounds were evaluated for tensile and thermal properties and antimicrobial activity against Escherichia coli (E. coli) and Staphylococcus aureus (S. aureus). All the additives eliminated over 90% of E. coli, but only AgNp_silica killed more than 80% of S. aureus population. The better effect of AgNp_silica was attributed to the additive's high specific surface area, which promoted greater contact with bacteria cells.

Key words: Elastomers; Nanoparticles; Nanowires and nanocrystals; Properties and characterization; Thermoplastics.

4.1 INTRODUCTION

Styrene-ethylene/butylene-styrene (SEBS) based thermoplastic elastomers (TPE) are polymers with soft touch properties that are widely used for manufacturing medical and personal devices that involve hand contact such as toothbrush cables, cell phones, keyboards, wheelchair handlebars, and pens [1]. These objects are susceptible to biofilm formation, contributing to spreading diseases, mainly in hospital environments, where infections can be transmitted through health care worker's hand [2]. Moreover, the microbial attack causes damage to the mechanical properties, surface degradation and staining, resulting in a deteriorated appearance [3-4]. Microbial adherence to a polymeric surface is a requirement for biofilm formation [5] On this basis, the development and use of polymers with an antibacterial feature, together with disinfection protocols, can prevent the dissemination of pathogens in several environments [6-7].

Despite numerous studies about silver in polymeric matrices such as polypropylene [8, 9], polyethylene [10, 11], polyamide [12], polyethylene

[1] Publicado como: TOMACHESKI, D.; PITTOL, M.; FERREIRA, V. F.; SANTANA, R. M C. Efficiency of silver based antibacterial additives and its influence in thermoplastic elastomers**. Journal of Applied Polymer Science**, v. 133, p. 43956., 2016. Doi: 10.1002/app.43956

terephthalate and polyvinyl chloride [13], polystyrene [14] and even thermoplastic polyurethane [15], to our knowledge, no studies have been conducted regarding antibacterial properties of silver in SEBS-based TPE.

Antibacterial materials containing a set of organic and inorganic substances have been developed [16, 17]. Inorganic biocides have attracted much interest for bacterial control due their heat resistance, durability and selectivity towards microorganisms [18, 19]. In the case of silver (Ag)-based materials, the low volatility, broad microbial spectrum killing, and rare cases of bacterial resistance are relevant characteristics for its choice as an antibacterial agent [20]. Moreover, efforts have been made aiming to improve its biocide efficiency.

It is well known that bioavailability of silver species will impact on metal antibacterial characteristics [21]. Elements such as particle size [15], surface specific area [12], and precursor materials [21] of particles may contribute to metal availability and bactericidal performance of polymer incorporated with silver. It is assumed that in order to obtain an antibacterial effect, silver ions must be released from the bulk to the aqueous medium, in this way, further on silver elemental form, a range of silver modifications have been tried, such as carbon nanotubes with silver [22], silver/silica nanocomposites [23], colloidal silver [24], zeolites doped with silver [25], silver nanoparticles [26] and silver nanocomposites with bacterial and cellulosic fibers [27]. Also, the processes in which silver particles are incorporated into the polymeric matrix (blending, embedding or coating) can influence the biocide action by affecting the molecular contact between the silver and the polymer surface [28-30]. Ag-based TPE systems must be capable of being manufactured by model processing, and the product should be extruded and injection molded, while keeping proper antibacterial agent concentration. In addition, depending on the type of application, the materials have to possess certain mechanical, rheological, thermal and chemical resistance, and stability under harsh processing situations [8]. Particles with Ag can be incorporated into thermoplastic elastomers during the extrusion process by melt blending, which is the most usual method to provide biocide properties to polymers [31].

Understanding the mechanisms of action between the type of silver used and their mechanical performance and antibacterial efficiency will lead to proper selection of an agent for manufacturing antibacterial thermoplastic elastomer products. In the present study, the TPE/silver compounds were prepared via extrusion process, with

the aim of to evaluate the effects of nanosilver adsorbed on fumed silica (AgNp_silica), silver ions supported in phosphate glass (Ag^+_phosphate) and bentonite organomodified with silver (Ag^+_bentonite) on the mechanical and antibacterial properties of thermoplastic materials.

4.2 EXPERIMENTAL

4.2.1 Materials

The additives tested were nanosilver adsorbed on fumed silica (AgNp_925-SiO, supplied by TNS Nanotecnologia Ltda. and named here as “AgNp_silica”) silver ions supported in phosphate glass (named here as “Ag^+_phosphate”) and bentonite organomodified with silver (Bactiblock 101 R1.43, supplied by Nanobiomatters BactiBlock, S.L. and named here “Ag^+_bentonite”) as biocide. The proportions used were those recommended by the additive suppliers; 0.025-0.05%, 0.1-0.3% and 0.5-2.0%, respectively. The additives were added to a TPE formulation compounded by styrene-ethylene/butylene-styrene copolymer (SEBS, 32% styrene, ethylene/butylene 32/68, linear, M_w 214.8 g mol^{-1}, M_w/M_n = 1.3), polypropylene homopolymer (PP, melt flow index 1.5 g 10 min^{-1} at 230°C) and white mineral oil (64% paraffinic and 36% naphtenic), in the ratio of 30/20/50, respectively. Antioxidant Irganox 1010 (0.1%) was added to avoid thermal degradation during processing. A standard sample (additive free) was also used.

4.2.2 Compounds preparation

The samples were prepared using a co-rotating double screw extruder (L/D 40 and 16 mm screw diameter, AX Plásticos) with temperature profile from 170°C to 190°C, speed screw of 300 rpm, feed rate of 1.5 kg h^{-1} and melt discharge temperature of 200°C. The extrusion parameters were kept constant throughout the tests. Specimen in plate form of 2 mm thick were prepared using injection molding machine (Haitian, PL860) at 190°C and an injection pressure of 17 bars. After molding, the specimens were conditioned at 23 ± 2°C and 50 ± 5% relative humidity for 24 h before testing.

4.2.3 Compounds and additives characterization

4.2.3.1 Additive's mineral compositions

The additive's mineral compositions were determined by qualitative analysis by X-ray diffraction in Pan Analytical X'pert PRO and X'Pert HighScore software.

4.2.3.2 Particle size measurement

Particle size distribution was determined by laser diffraction in a CILAS 1180 particle size analyzer with scanning range from 0.04 µm to 2500 µm. AgNp_silica and Ag^{+}_phosphate were predispersed in deionized water using ultrasound (60 s) and Ag^{+}_bentonite was predispersed in isopropyl alcohol.

4.2.3.3 Particles specific surface area

The specific surface area (SSA) of particles was measured by nitrogen adsorption using the Brunauer–Emmett–Teller (BET) method. Measurements were performed by a Quantachrome Nova 1000e surface area analyzer. Samples were dried in an oven at 110°C for 24 h and then in vacuum at 200°C for 3 h.

4.2.3.4 Analysis of fourier transform infrared spectroscopy spectra

Fourier transformed infrared spectroscopy attenuated total reflection (FTIR–ATR) was recorded on a PerkinElmer spectroscope (Frontier). Each spectrum was recorded with a total of 10 scans; at a resolution of 4 cm^{-1} at room temperature. The Spectrum software was used for spectra analysis.

4.2.3.5 Scanning electron microscopy analysis

Morphological analysis of the samples was performed with scanning electron microscopy (SEM), where the samples were deposited in carbon type stuck to stub, metalized with gold, compounds were cryogenically broken in liquid nitrogen. For image acquisition, a SEM of field emission (SEM-FEG) (Inspect F50, FEI) was used with 20 kV, spot 3 and working distanceh of 10 mm.

4.2.3.6 Transmission electron microscopy analysis

For transmission electron microscopy (TEM) (Tecnai, G2 T20) additives were dispersed in ethanol by ultrasound for 30 minutes. The samples were prepared by placing a drop of the ethanol suspension onto a small carbon film coated copper grid (300 mesh). For compounds images, ultrathin sections (70 nm) were prepared with a Leica EM FC7 ultramicrotome with a diamond knife. For image acquisition an acceleration voltage of 200 kV was used. The average particle diameter was calculated using ImageJ version 1.40g software.

4.2.3.7 Mechanical properties

The mechanical properties of the compounds were obtained by tensile test and analyzed according to ASTM D 412C, in the EMIC DL 2000 machine. The cross-head speed and gauge length of the apparatus were 500 mm min^{-1} and 25 mm, respectively.

4.2.3.8 Differential scanning calorimetry

Thermal analysis of the samples by differential scanning calorimetry (DSC) was performed in a DSC Q100 (TA Instruments, USA). The samples were subjected to heating from -30°C to 200°C at a heating rate of 10°C min^{-1}. The desired temperature was maintained for 5 minutes and cooled to -30°C at the same rate, and reheated under a nitrogen atmosphere. Crystallinity values were obtained in the heating second cycle. Nitrogen was used at a flow rate of 50 mL min^{-1}. The degree of crystallinity X_c, normalized to crystalline phase of compositions, PP, as suggested by Karakaya [32] by applying the equation (1):

$$X_c = \frac{\Delta H^*}{w\ x\ \Delta H^0_{PP}}\ x\ 100 \quad (1)$$

where ΔH^* is the melting enthalpy per gram, *w* is the PP fraction found in the compound and $\Delta H^0_{(PP)}$ is the melting enthalpy per gram of 100% crystalline PP (209 J g^{-1}) [33].

4.2.3.9 Antimicrobial studies

Japan industrial standard (JIS) Z 2801 [34] was applied to evaluate antibacterial efficiency of samples against *Staphylococcus aureus* ATCC 6538 (*S. aureus*) and *Escherichia coli* ATCC 8739 (*E. coli*) strains. TPE specimens (50 mm x 50 mm) were placed in a sterile Petri dish and 400 µL of 6 x 10^6 CFU cm^{-2} of *E. coli* and 3 x 10^6 CFU cm^{-2} of *S. aureus* suspension were inoculated on the specimen surface. All of them were incubated for 24 h at 35 ± 1°C. The result was expressed as a microbial value calculated from the difference between the number of colony forming units (CFU) per square centimeter at zero hour (initial) and after 24 h of incubation, equation (2):

$$Ef\ (\%) = \frac{Pi - Pf}{Pi} \quad (2)$$

Where *Ef* is the reduction of bacterial population (percentage, %), Pi and Pf are, respectively, initial and final bacterial population (colony forming units per square centimeter, CFU cm^{-2}).

Antibacterial activity - *R*, was validated in accordance with JIS Z 2801, with the equation (3):

$$R = U_t - A_t \quad (3)$$

Where *Ut* is average of logarithm numbers of viable bacteria after inoculation on standard (additive free) samples after 24 h and *At* is average logarithm numbers of viable bacteria after inoculation on antibacterial samples after 24 h. To be considered effective, *R* must be ≥ 2.0.

4.2.3.10 Statistical analysis

Statistical analysis of variance (ANOVA) was applied in tensile strength, modulus, elongation at break and antibacterial results using MYSTAT, student version 12 (Systat Software, Inc., CA, USA). The level of significance was set at 0.05.

4.3 RESULTS AND DISCUSSION

4.3.1 Additives characterization

4.3.1.1 Additive's mineral compositions.

X-ray diffraction detected the presence of SiO_2 (JCPDS 01-082-1557) and Ag (JCPDS 01-087-0720) in the AgNp_silica sample (Figure 4.1a). The Ag^+_phosphate sample has an amorphous structure, so it was not possible to characterize its composition through this method (Figure 4.1b). The Ag^+_bentonite sample contain montmorillonite-22A (JCPDS 00-029-1499) and cristobalite (JCPDS 01-077-1317) (Figure 4.1c).

Figure 4.1 Diffractograms of samples: (a) AgNp_silica, (b) Ag^+_phosphate and (c) Ag^+_bentonite

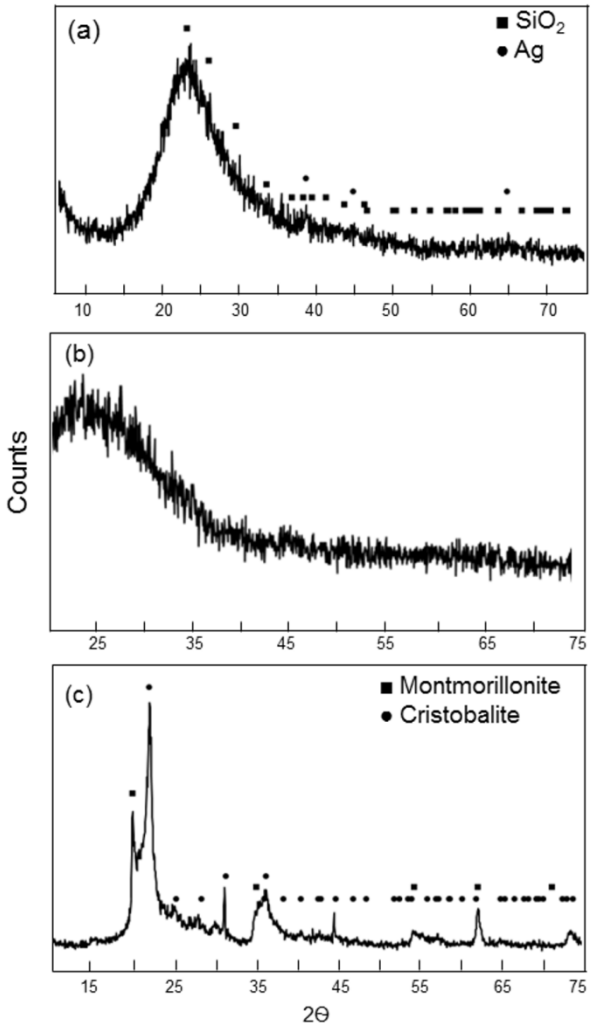

4.3.1.2 Particles specific surface area.

The specific surface area (SSA) of the additives is shown in Table 4.1. AgNp_silica showed the highest SSA, 293.9 m^2 g^{-1}, as expected for nanoparticles [23]. Ag^+_phosphate have the lowest SSA, 6.16 m^2 g^{-1}. The SSA found in Ag^+_bentonite, 36.73 m^2 g^{-1}, is in accordance with the literature inspection [35-36].

Table 4.1 Specific surface area determined by BET

	AgNp_silica	Ag^+_phosphate	Ag^+_bentonite
SSA, m^2 g^{-1}	293.90	6.16	36.73

BET: Brunauer–Emmett–Teller method

4.3.1.3 Morphological analysis.

Figure 4.2 shows images obtained by SEM (left) and TEM (right). Figure 4.2a and Figure 4.2b show micrographs of AgNp_silica sample obtained in SEM and TEM, respectively. In SEM images it was possible to observe blocks with irregular geometry and the same size determined before in laser diffraction (between 5 and 30 µm). The TEM images confirmed nanoscale of this additive, with nanoparticles of silica (20 nm) and silver (10 nm), both in spherical forms. In this study, as reported previously by Egger et al. [23] in SEM image of AgNp_silica were observed the silver nanoparticles located on the surface of the silica matrix and also embedded in a matrix of amorphous silicon dioxide (SiO_2). This shape provides a quick availability of silver to the compound.

As seen on Figure 4.2c and Figure 4.2d, Ag^+_phosphate presented a non-crystalline planar form. In a study performed by Suenaga et al. [37] the authors found that the silver ions present a tetrahedral molecular configuration and create a two-dimensional sheet composition including dimeric units. In SEM image, the particles presented 2 µm, the same size determined by granulometric assay. The results obtained in granulometric and SEM assay reflect the agglomerate patterns of the Ag^+_phosphate particles. In TEM images the particles presented 200 nm in size.

Ag^+_bentonite (Figure 4.2f) showed a typical platelet form found in montmorillonite clay [38]. In this sample, difference in size was observed between the SEM and granulometric results. In SEM and granulometric assay particles presented an average size of 10 µm, while in TEM their size was 1 µm. The difference in size

can be attributed to the agglomerated sheets configuration which prevents measurements.

Figure 4.2 Micrographs of SEM (left) and TEM (right) of additives: (a, b) AgNp_silica, (c, d) Ag^+_phosphate and (e, f) Ag^+_bentonite

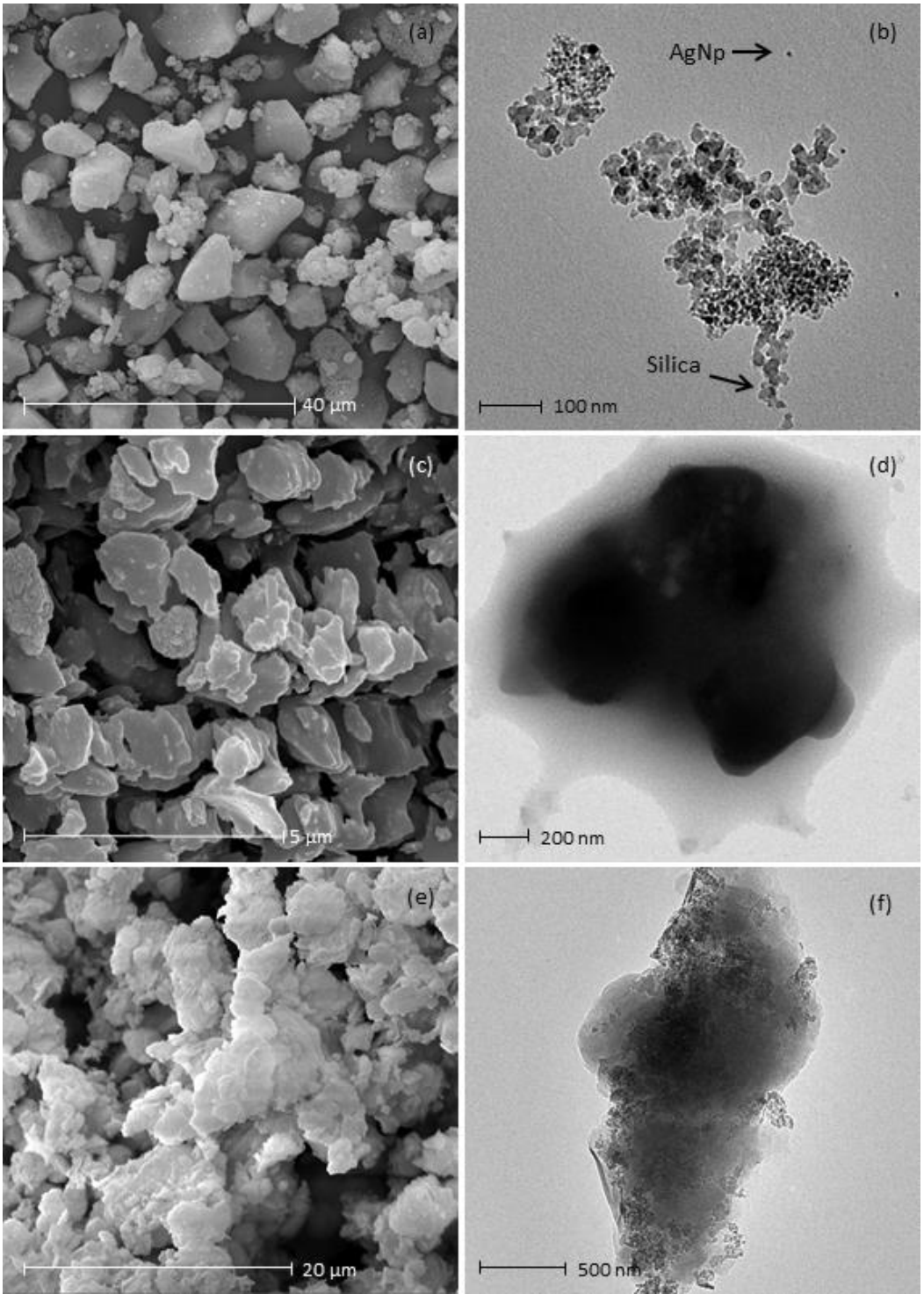

It was not possible to identify traces of silver in the spectrograms of additives Ag^+_phosphate and Ag^+_bentonite.

4.3.1.4 Particle size measurement

Values of average diameter, D_{10}, D_{50} and D_{90} determined by laser diffraction are shown in Table 4.2. It was noted that the average size of the AgNp_silica (12.97 µm) showed a value above the nanoscale. This result reflects the size of the AgNp_silica clusters, as observed in TEM and SEM images shown above. Ag^+_phosphate have an average size of 1.6 µm. Ag^+_bentonite has an average size of 7.30 µm, ranging from 2.08 to 13.92 µm.

Table 4.2 Values of average diameter, D_{10}, D_{50} and D_{90} determined by laser diffraction.

	Average diameter, µm	D_{10}, µm	D_{50}, µm	D_{90} µm
AgNp_silica	12.97	4.7	9.2	28.99
Ag^+_phosphate	1.61	0.86	1.50	2.49
Ag^+_bentonite	7.30	2.08	6.32	13.92

4.3.1.5 Analysis of fourier transform infrared spectroscopy spectra

Figure 4.3 shows the infrared spectra of AgNp_silica, Ag^+_phosphate and Ag^+_bentonite, in the region ranging from 1600 to 650 cm^{-1}.

In the AgNp_silica spectra (Figure 4.3a), a peak on 1070 cm^{-1} was observed and attributed to Si–O–Si asymmetric stretching [41]. An ideal stoichiometric silicon dioxide is 1080 cm^{-1}. The Si-O stretching peaks are at 792 cm^{-1}. In silicon dioxide infrared, there was a dependence of the peak position and the oxygen dose, ranging from 1015 to 1080 cm^{-1}, the higher the oxygen amount the greater will be the peak position (SiOx, with x≈2) [39-40]. Also, the absorption of around 800 and 960 cm^{-1} is related to the rocking, bending and stretching vibrational modes of the Si–O–Si units, respectively [40-41].

In Figure 4.3b, symmetric stretching of P-O-P in P_2O_7 can be seen at 737 cm^{-1}, symmetric stretching of P-O in PO_3 and PO_4, and asymmetric stretching of P-O-P in P_2O_7 can be seen at 929 cm^{-1}. Asymmetric stretching of P-O in PO_3 and PO_4 can be seen at 1102 cm^{-1} and 1233 cm^{-1}. As observed in the Ag^+_phosphate FTIR analysis, phosphate peak can be superimposed by other peaks [42-43].

Figure 4.3c shows the infrared of Ag^+_bentonite, the peaks in 1009 cm^{-1} and 1070 cm^{-1} can be attributed to Si-O-Si bonds [39-42]; peaks 842 and 914 cm^{-1} are attributed to deformations in MgAlOH and AlAlOH [35, 44]. Silicon and oxygen are common to all clay minerals. Their combination with other elements, such as

aluminum, magnesium, iron, sodium, calcium, and potassium, and the ways in which these elements can be linked provide a large number of configurations [38].

Figure 4.3 FTIR-ATR spectra of (a) AgNp_silica, (b) Ag^+_phosphate and (c) Ag^+_bentonite

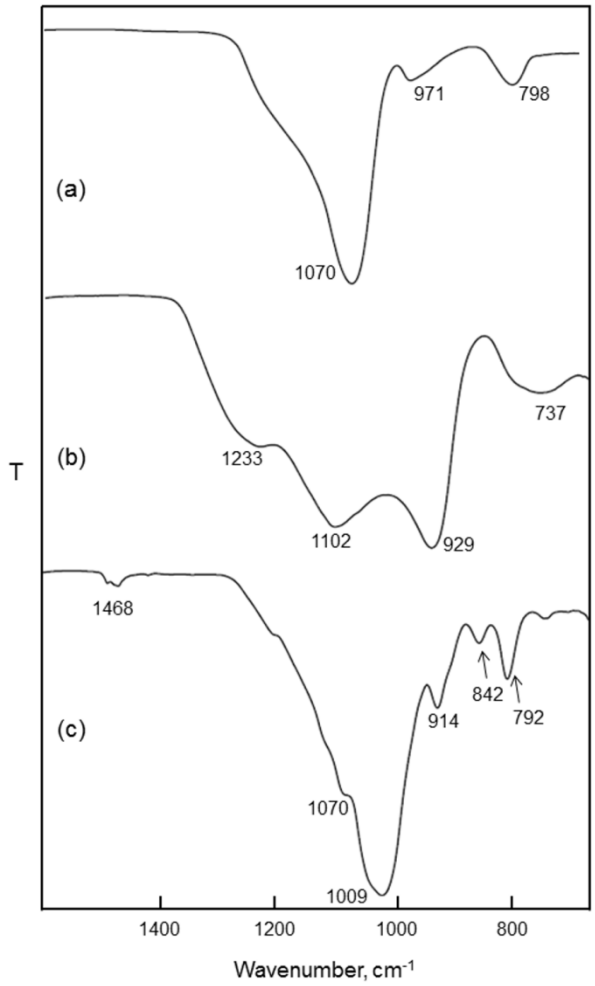

4.3.2 Compounds characterization

4.3.2.1 Analysis of fourier transform infrared spectroscopy spectra.

Infrared spectra from standard and additived compounds with 0.05% of AgNp_silica, 0.3% of Ag^+_phosphate and 2.0% of Ag^+_bentonite were analyzed to evaluate possible modifications in molecular organization due to the incorporation of additives. There were not changes in the region 1200-600 cm^{-1} as show on Figure 4.4. It was possible to notice the characteristics bands of SEBS in 699 cm^{-1} and 759 cm^{-1} due to out-of-plan bending of C-H in aromatic monosubstituted ring of styrene units [45]. Skeletal vibrations representing C=C stretching of aromatic styrene ring appeared at 1493 cm^{-1} [45] and rocking vibration of CH_2 from ethylene appear at 720

cm^{-1} [46]. Bands in 1452 cm^{-1} and 1376 cm^{-1} were in plane bending of the C-H from CH_2 and CH_3, common to all components of the blend [45-46].

Figure 4.4 FTIR-ATR spectra of the (a) standard sample and compounds with (b) 2.0% of Ag^+_bentonite, (c) 0.3% of Ag^+_phosphate and (d) 0.05% of AgNp_silica

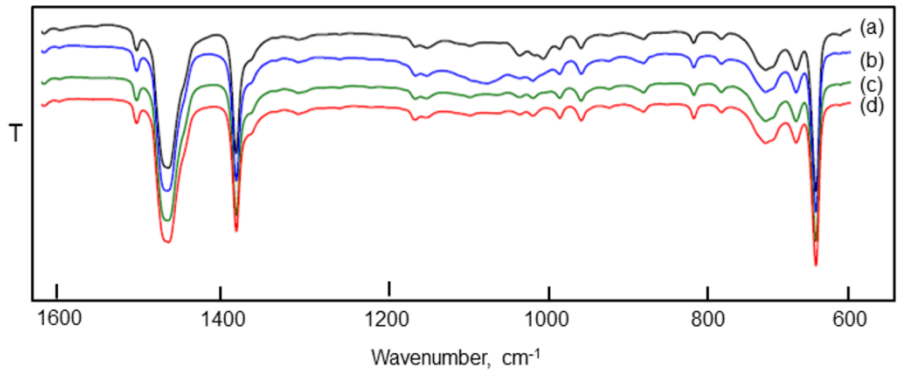

4.3.2.2 Tensile properties

Figure 4.5 shows the results of tensile properties of the compounds.

Figure 4.5 Variation in tensile properties of the compounds: (-●-) AgNp_silica, (-▲-) Ag^+_phosphate (-■-) and Ag^+_bentonite.

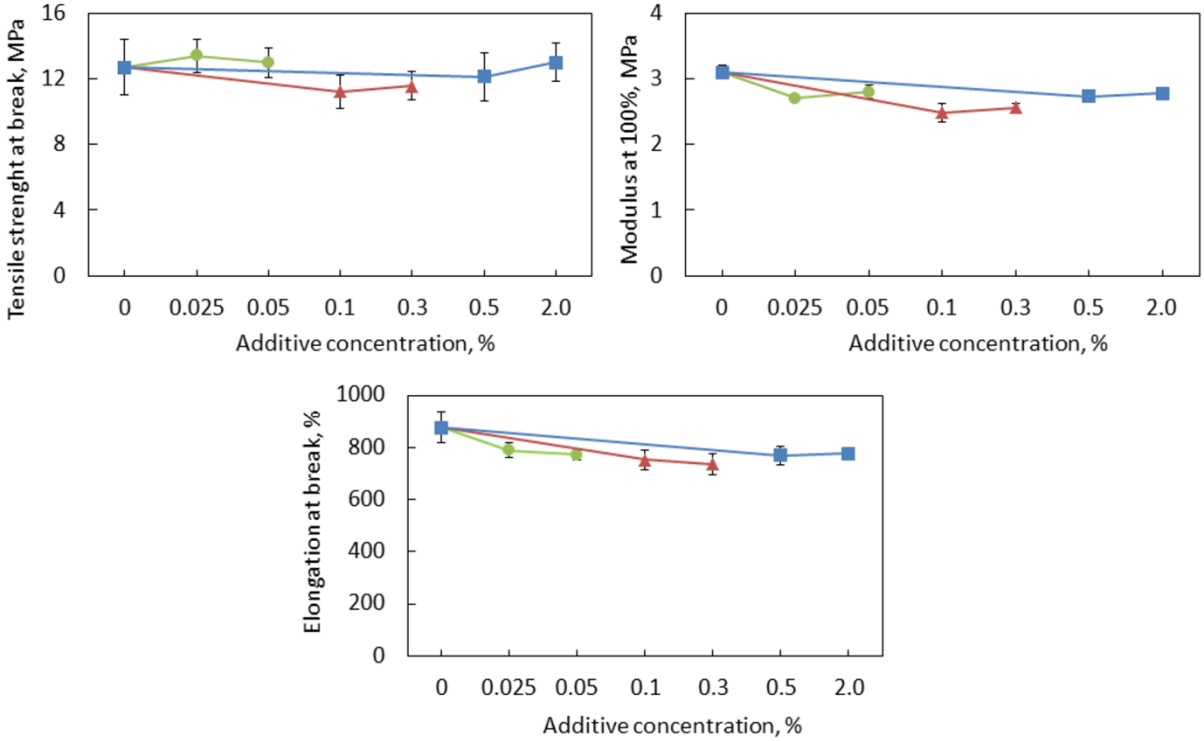

Note: ANOVA test: Tensile strength ($F_{6,28}$=2.223; p=0.07), modulus ($F_{6,28}$=25.461; p<0.05) and elongation at break ($F_{6,28}$=2.124; p=0.08).

There were not significant changes in tensile strength and elongation at break values of specimens with biocide when compared to the standard specimen.

However, the modulus values presented a significant difference when compared with loaded compounds ($p<0.05$), but it cannot be related to a particular additive. Modulus can be affected by moduli of the two phases, as well as volume fraction, particle geometry, degree of agglomeration, and size distribution of particles [48].

Wu and coworkers [47] found that surface characteristics of particles are very important to improve dispersion and interface between particle and matrix. Also, high interfacial stiffness improves polymer modulus. If particle and matrix are not properly matched, the contact point between both surfaces will be a weak point that will reduce the modulus [48, 49]. Based on this information, it could be concluded that there was no interfacial adhesion between the additives and polymer.

4.3.2.3 Differential scanning calorimetry

In Figure 4.6 are shown overlapping curves of exothermic and endothermic events corresponding to the crystallization and melting of polypropylene. It was observed a slight shift to the right of the crystallization temperature in loaded samples compared to sample standard (additive free, curve a). Regarding to the endothermic curves, there was no significant difference in the melting temperatures between standard sample and loaded samples.

Figure 4.6 DSC curves of the (a) standard sample and compounds (b) 0.05% of AgNp_silica (c) 0.3% of Ag^+_phosphate and (d) 2.0% of Ag^+_bentonite

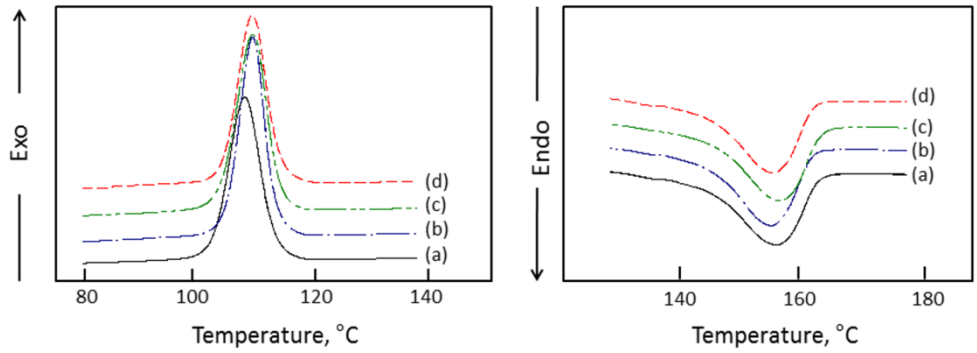

Table 4.3 shows the values of melting temperature (T_m), melting enthalpy (ΔH_m), crystallization temperature (T_c), crystallization enthalpy (ΔH_c) and crystallinity degree (X_c) of the compounds.

The crystallization temperature of pure PP used in this work was 103°C, in the form of the compound it was increased to 107°C, and with the incorporation of additives increase to 108°C.

Table 4.3 DSC results of the second heating of TPE samples

Sample	T_m, °C	ΔH_m, J g^{-1}	T_c, °C	ΔH_c, J g^{-1}	X_c, %
PP	166	89	103	90,6	43
Standard	153	21	107	21,4	48
Ag^+_phosphate (0.1%)	152	21	108	21,2	48
Ag^+_phosphate (0.3%)	152	20	108	20,1	45
AgNp_silica (0.025%)	152	20	108	20,9	46
AgNp_silica (0.050%)	153	21	108	21,8	48
Ag^+_bentonite (0.5%)	153	20	108	20,8	46
Ag^+_bentonite (2.0%)	152	21	108	21,3	48

As shown in Table 4.3, all the samples had a T_m around 153°C, lower than melt temperature of pure PP that was 166°C. This result confirms that the addition of SEBS and oil into PP restricts the mobility e packing of PP chains. In a study realized by Karakaya et al. [32], the addition of filler increases the crystallinity degree and was attributed to action of the particles as nucleating agents. In general, there was a slight increase in X_c values with the additives incorporation, but this values were similar to standard sample, and therefore may be considered not significant.

PP is strongly susceptible to additives that change its crystallization feature by accelerating crystallization [49]. In an experiment performed by Chan [50], the addition of calcium carbonate ($CaCO_3$) did not change crystallinity of PP, but the crystallization temperature increased by about 10°C. The size of the spherulites decreased with the increase of $CaCO_3$, since it works as a nucleating agent. In sum, the particles of the additive acted as nucleation sites, reducing the spherulites size, which increase the crystallinity and, consequently, the modulus [51-52].

In this study, the incorporation of the additives resulted in a slight difference in the crystallinity values. Whereas that to some authors the polymer crystallinity influences the additive efficiency, by promoting the silver migration to the surface of the compound [12-15] and in the case of silver nanoparticles, water must be diffused by the amorphous portion of the compound, it could be assumed that the better antibacterial activity of AgNp_silica was related to the portion of amorphous area presented in the compound.

4.3.2.4 Morphology

Figure 4.7 shows scanning (a, d and g) and transmission microscopies of the compounds with 0.05% of AgNp_silica (a, b, c); 0.3% of Ag^+_phosphate (d, e, f) and 2% of Ag^+_bentonite (g, h, i). As immiscible components, blends of SEBS, PP and oil always will form two separated phases: a SEBS/oil and PP/oil domains. In TEM images, these domains were presented as dark (SEBS/oil) and bright (PP/oil) areas [53]. The SEM images did not provide any information, because of the little size of the additives. In Figure 4.7g it was possible to see a sheet of bentonite.

Figure 4.7 Micrographs of SEM (a, d and g) and TEM of the compounds with 0.05% of AgNp_silica (a, b, c); 0.3% of Ag^+_phosphate (d, e, f) and 2.0% of Ag^+_bentonite (g, h, i)

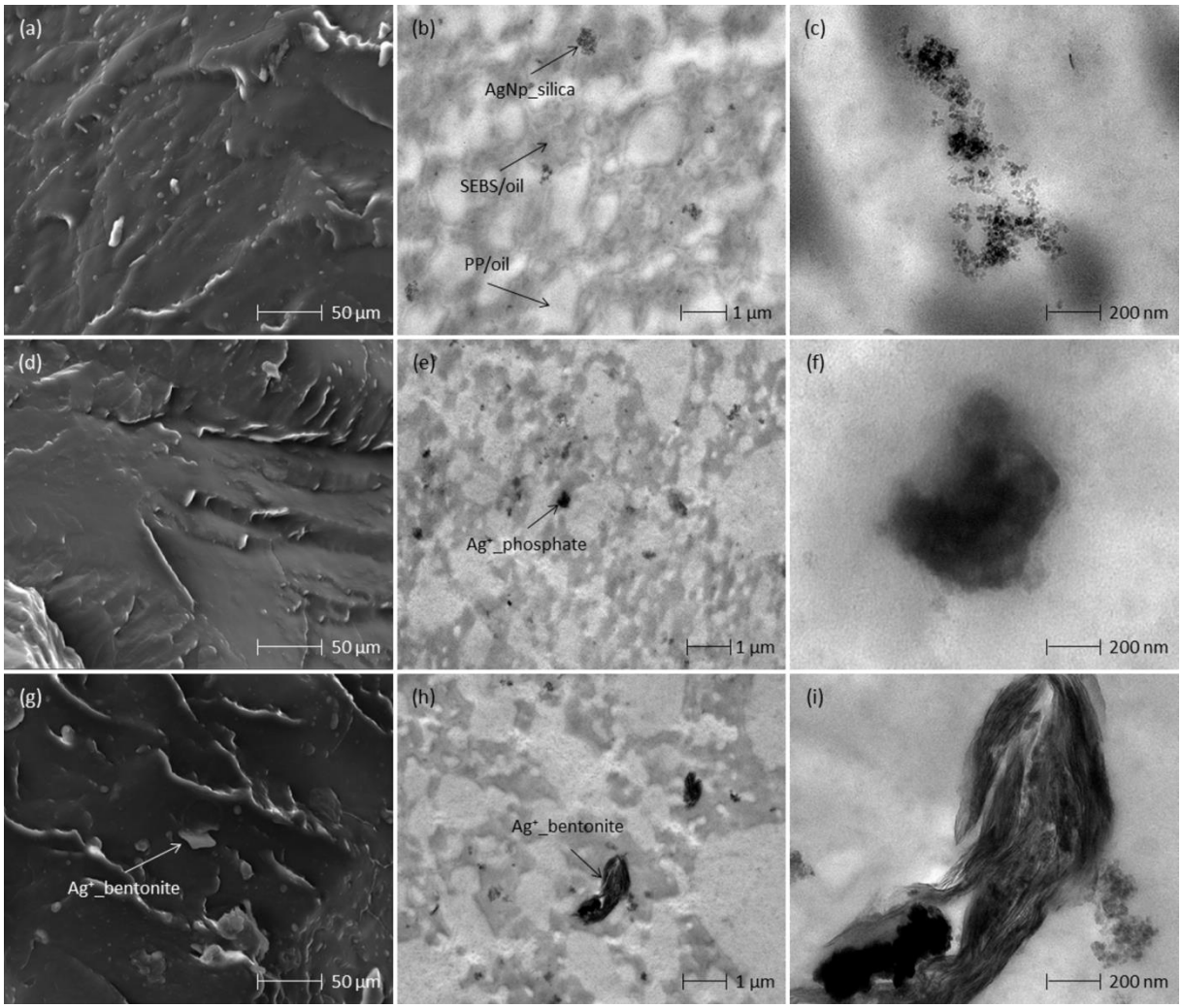

In TEM analysis, in the first images for all additives was remarkable the preference of the particles to SEBS/oil phase. For AgNp_silica, it was noted that the silica particles formed agglomerates (Figure 4.7b and c). The bentonite sheets did not exfoliate; instead of this they formed clusters (Figure 4.7h and 4.7i).

4.3.2.5 Antimicrobial studies

Table 4.4 shows bacterial reduction (%) and antibacterial efficacy (R) values in metal loaded TPE toward *E. coli* and *S. aureus* populations. Figure 4.8a and Figure 4.8b show bacterial reduction of *E. coli* and *S. aureus* populations, respectively, in additived TPE monitored in a 24-h period.

E. coli ($F_{5,12}$=11.5521; p<0.05) and *S. aureus* ($F_{5,12}$=7.509; p<0.05) final population differs significantly between the antibacterial additives. All the samples eliminated more than 90% of *E. coli* CFU after 24 h. Only AgNp_silica eliminated more than 80% of *S. aureus*. This suggested differences in antimicrobial activity. None of the additives reached the value of R required by standard JIS Z 2801, even in the maximum dose recommended by the additive suppliers.

Table 4.4 Variation of antimicrobial efficacy.

	E. coli		***S. aureus***	
	Reduction, %	**R**	**Reduction, %**	**R**
Ag^+_bentonite (0.5%)	95.3	0.5	26.8	0.6
Ag^+_bentonite (2.0%)	95.3	0.5	76.4	1.1
Ag^+_phosphate (0.1%)	95.6	0.5	57.3	0.8
Ag^+_phosphate (0.3%)	92.0	0.2	43.4	0.7
AgNp_silica (0.025%)	96.4	0.6	81.9	1.2
AgNp_silica (0.050%)	95.6	0.5	80.6	1.1

It was noted that the sample with 0.1% Ag^+_phosphate was more effective than the sample 0.3%, the same occured with sample AgNp_silica, which could be due to inefficient dispersion of the additive during processing.

Figure 4.8 Variation in (a) *E. coli* and (b) *S. aureus* colony forming unit per square centimeter (CFU cm^{-2}) in (-●-) AgNp_silica 0.025%, (-○-) AgNp_silica 0.05%, (-▲-) Ag^+_phosphate 0.1%, (-◊-) Ag^+_phosphate 0.3%, (-♦-) Ag^+_bentonite 0.5%, (-◊-) Ag^+_bentonite 2.0% compounds

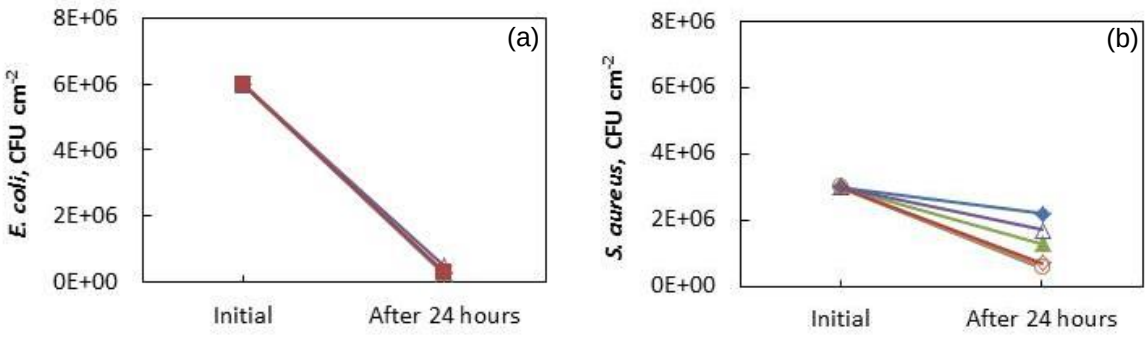

It was reported that the contact of silver ions (positively charged) with the bacterial wall (negatively charged) causes an electrostatic imbalance that induces a sequence of events leading to a disturbance of bacterial cell structure, and may hinder microbial proliferation [54-55]. In addition, ionic silver can block DNA transcription and suspend bacterial respiration and adenosine triphosphate (ATP) synthesis [56]. According to Kim et al. [57] bacterial membranes possess sulfur-containing proteins and silver nanoparticles penetrate the cell by connecting to these proteins. After entering the bacterial cell, silver nanoparticles react with the respiratory chain of bacteria and inhibit their respiration.

The biocidal activity of nanoparticles is amplified by its topography, that improves contact with the microorganisms [58]. Silver nanoparticles are a small form of elemental silver and still there is no consensus on its way of action. Martinez-Abad [59] describes silver nanoform with unstable behavior resembling an ion in action. Tolaymat et al. [60] mention that when silver nanoparticles come in contact with the dissolved oxygen ($O_{2(aq.)}$) in water, they release silver ions according to the following equation (4):

$$O_{2(aq.)} + 4H_3O+ + 4Ag_{(s)} \rightarrow + 4Ag^{+}_{(aq.)} + 6H_2O \quad (4)$$

E. coli was more responsive to the toxic effects of silver. This configuration may be due to the thin peptidoglycan layer found in Gram-negative cell walls that allows the permeation of silver particles into the cytoplasm. Sondi and Salopek-Sondi [61] studied the interaction between *E. coli* and silver at the nanometer scale. They found indications of deterioration similar to pits in the surface membrane of bacteria. This characteristic kills the bacteria by raising membrane permeability, which prevents an appropriate control of molecule being transported across the membrane. In addition, Morones et al. [62] described the bactericidal action of silver nanoparticles by association and harm to DNA, indicating a nano-size dependent relationship in biocide effect.

It is noteworthy that, as in our study, previous research using silver-based additives reported a level of tolerance to silver in Gram-positive bacteria [18, 23]. These results could be due the thick peptidoglycan cell wall of Gram-positive bacteria that protects its cell from silver penetration [63]. Thus, the form of incorporation of silver into different bacterial cell walls influence its efficiency, especially toward the bacterium *S. aureus*, which is known to have a higher resistance.

One aspect that remains to be established concerns the identification of exactly which of the physical and chemical properties of nano-Ag are responsible for the effective antibacterial activities of silver compounds materials [64]. Since that high surface area means more contact area available [65], the enhanced effect of AgNp_silica can be explained by the high specific surface area observed in these additives (45x bigger than Ag^+_phosphate and 8x bigger than Ag^+_bentonite). As describe by Magaña et al. [44] the antibacterial properties of silver exchanged montmorillonites have been attributed to the attraction of the negatively charged membrane of the bacteria to the surface of the clay, where silver ions kills the bacteria or renders them unable to replicate. In this study, the low SSA and overlapping sheets of the additive Ag^+_bentonite may have limited the contact of bacteria with the bentonite surfaces coated with silver.

The high crystalinnity of the compound (almost 50%) may have hindered the release of ions to the specimen surface. The additives evaluated herein have been developed and are recommended for use in thermoplastics such as polypropylene, polystyrene and polyethylene. However, as previously mentioned, the use of antibacterial additives in thermoplastic elastomers in a SEBS base is a market innovation. Thus, the morphological differences between these polymeric groups can affect the release of silver in its ionic or nano form, which require a higher concentration of the additive into the compound.

4.4 CONCLUSIONS

Despite being of different composition, structure and size, the additives tested here had no significant effect in tensile strength and elongation at break properties when compared to the standard sample. From an industrial point of view, changes on modulus were not considered an excluding factor for final product utilization. The AgNp_silica additive provided better efficacy, with a decrease over 90% of *E. coli* and over 80% of *S. aureus* population, probably due to its high specific surface area that provides a high contact with the bacteria cell, even in small amounts. Thus, the incorporation of AgNp_silica by extrusion / injection is the process that presented promising features to be applied as a biocide in SEBS-based thermoplastic elastomers with no relevant changes to usual industrial procedures.

The process of additives dispersion should be reviewed to prevent agglomeration of the particles and achieve the maximum antimicrobial protection guaranteed by the additives suppliers.

4.5 REFERENCES

1. DROBNY, J. G. **Handbook of thermoplastic elastomers**. New York: William Andrew Publishing, 2007. ISBN 978-0-8155-1549-4
2. ULGER, F.; ESEN, S.; DILEK, A.; YANIK, K.; GUNAYDIN, M.; LEBLEBICIOGLU, H. Are we aware how contaminated our mobile phones with nosocomial pathogens? **Annals of Clinical Microbiology and Antimicrobials**, v. 8, n. 7, p. 1-14, 2009. Doi: 10.1186/1476-0711-8-7.
3. SINGH, S. K.; ANAMIKA, J.; DIPAK, S.; ARTI, D. Synthesis and antimicrobial activity of polysiloxanes polyurethane biocidal polymers as surface modifiers. **Der Chemica Sinica**, v. 2, p. 111-117, 2011.
4. NANDEKAR, K.A.; DONTULWAR, J.R.; GURNULE, W. B. J. Antimicrobial screening and thermoanalytical studies of newly synthesized copolymer derived from p-hydroxybenzoic acid, and thiosemicarbazide. **Journal of Chemical and Pharmaceutical Research**, v. 4, p. 3628-3636, 2012.
5. GRAY, J. E.; NORTONA, P. R.; ALNOUNO, R.; MAROLDA, C. L.; VALVANO, M. A.; GRIFFITHS; K. Biological efficacy of electroless-deposited silver on plasma activated polyurethane. **Biomaterials**, v. 24, p. 2759–2765, 2003. Doi: 10.1016/S0142-9612(03)00057-7
6. TEMIZ, A.; TOĞAY, S. O.; SENER, A.; GÜVEM, G.; RZAEV, Z. M. O.; PISKIN, E. J. Antimicrobial poly(n-vinyl-2-pyrrolidone-alt-maleic anhydride)/poly(ethylene imine) macrocomplexes. **Journal of Applied Polymer Science**, v. 102, p. 5841–5847, 2006. Doi: 10.1002/app.24903
7. AHMED, N. A. A. M. Bacterial resistance and challenges of biocides plastics. In: LAGARÓN, J.M.; OCIO, M. J.; LÓPEZ-RUBIO, A. **Antimicrobial Polymers**. Hoboken: Wiley, 2012. p. 23-49. ISBN 978-0-470-59822-1
8. RADHESHKUMAR, C.; MÜNSTEDT, H. Morphology and mechanical properties of antimicrobial polyamide/silver composites. **Materials Letters**, v. 59, p. 1949-1953, 2005. Doi: 10.1016/j.matlet.2005.02.033
9. OLIANI, W. L.; PARRA, D. F.; LIMA, L. F. C. P.; LINCOPAN, N.; LUGAO, A. B. J. Development of a nanocomposite of polypropylene with biocide action from silver nanoparticles. **Journal of Applied Polymer Science**, v. 132, p. 42218, 2015. Doi: 10.1002/app.42218.
10. SÁNCHEZ-VALDES, S.; ORTEGA-ORTIZ, H.; RAMOS-DE VALLE, L. F.; MEDELLÍN-RODRÍGUEZ, F. J.; GUEDEA-MIRANDA, R. Mechanical and antimicrobial properties of multilayer films with a polyethylene/silver nanocomposite layer. **Journal of Applied Polymer Science**, v. 111, p. 953–962, 2009. Doi: 10.1002/app.29051
11. JOKAR, M.; RAHMAN, R. A.; IBRAHIM, N. A.; ABDULLAH, L. C.; TAN, C. P. Melt production and antimicrobial efficiency of low-density polyethylene (LDPE)-

silver nanocomposite film. **Food Bioprocess Technology**, v. 5, p. 719–728, 2012. Doi: 10.1007/s11947-010-0329-1

12. KUMAR, R.; MÜNSTEDT, H. Silver ion release from antimicrobial polyamide/silver composites. **Biomaterials**, v. 26, p. 2081–2088, 2005. Doi: 10.1016/j.biomaterials.2004.05.030

13. PONGNOP, W.; SOMBATSOMPOP, K.; KOSITCHAIYONG, A.; SOMBATSOMPOP, N. J. Effects of incorporating technique and silver colloid content on antibacterial performance for thermoplastic films. **Journal of Applied Polymer Science**, v. 122, p. 3456-3465, 2011. Doi: 10.1002/app.34448

14. PALOMBA, M.; CAROTENUTO, G.; CRISTINO, L.; DI GRAZIA, M. A.; NICOLAIS, F.; NICOLA, S. D. J. Activity of antimicrobial silver polystyrene nanocomposites. **Journal of Nanomaterials**, Article ID 185029, 7 pages, 2012. Doi: 10.1155/2012/185029.

15. TRIEBEL, C.; VASYLYEV, S.; DAMM, C.; STARA, H.; OZPINAR, C.; HAUSMANN, S.; PEUKERT, W.; MUNSTEDT, H. J. Polyurethane/silver-nanocomposites with enhanced silver ion release using multifunctional invertible polyesters. **Journal of Materials Chemistry**, v. 21, p. 4377-4383, 2011. Doi: 10.1039/c0jm03487h

16. NICHOLS, D. Available active ingredients. In: NICHOLS, D. **Biocides in Plastics**. v. 15. United Kingdom: Rapra Review Reports, 2004. p. 19-28, 2004. ISBN 978-1-859757-512-3

17. MUÑOZ-BONILLA, A.; FERNANDEZ-GARCIA, M. Polymeric materials with antimicrobial activity. **Progress in Polymer Science**, v. 37, p. 281–339, 2012. Doi: 10.1016/j.progpolymsci.2011.08.005

18. JUNG, W.K.; KOO, H.C.; KIM, K.W.; SHIN, S.; KIM, S.H.; PARK, Y.H. Antibacterial activity and mechanism of action of the silver ion in *Staphylococcus aureus* and *Escherichia coli*. **Applied and Environmental Microbiology**, v. 74, p. 2171–2178, 2008.

19. NAWAZ, H. R.; SOLANGI, B. A.; ZEHRA, B.; NADEEM, U. Preparation of nano zinc oxide and its application in leather as a retanning and antibacterial agent. **Canadian Journal on Scientific and Industrial Research**, v. 2, n. 4, p. 164-170, 2011.

20. SILVER, S. Bacterial silver resistance: molecular biology and uses and misuses of silver compounds. **FEMS Microbiology Reviews**, v. 27, p. 341-353, 2003. Doi: 10.1016/S0168-6445(03)00047-0.

21. LALUEZA, P.; MONZÓN, M.; ARRUEBO, M.; SANTAMARÍA. Bactericidal effects of different silver-containing materials. **Materials Research Bulletin**, v. 46, p. 2070-2076, 2011. doi:10.1016/j.materresbull.2011.06.041

22. RANGARI, V. K.; MOHAMMAD, G. M.; JEELANI, S.; HUNDLEY, A.; VIG, K.; SINGH, S. R.; PILLAI, S. Synthesis of Ag/CNT hybrid nanoparticles and fabrication of their Nylon-6 polymer nanocomposite fibers for antimicrobial applications. **Nanotechnology**, v. 21, p. 1-11, 2010,

23. EGGER, S.; LEHMANN, R. P.; HEIGHT, M. J.; LOESSNER, M. J.; SCHUPPLER, M. Antimicrobial properties of a novel silver-silica

nanocomposite material. **Applied and Environmental Microbiology**, v. 75, p. 2973–2976, 2009. Doi: 10.1128/AEM.01658-08

24. TAKAMIYA, A.S. **Adição de Nanopartículas de Prata ao Poli (metil metacrilato) – Análise Microbiológica**. 2010. 115 f. Dissertação (Mestrado em Odontologia) - Faculdade de Odontologia do Campus de Araçatuba, Universidade Estadual Paulista Júlio de Mesquita Filho, Araçatuba, 2010.
25. FERREIRA, L.; FONSECA, A.M.; BOTELHO, G.; ALMEIDA- AGUIAR, C.; NEVES, I.C. Antimicrobial activity of faujasite zeolites doped with silver**. Microporous and Mesoporous Materials**, v. 160, p. 126–132, 2012. Doi: /10.1016/j.micromeso.2012.05.006
26. KONG, H.; JANG, J. Antibacterial properties of novel poly(methyl methacrylate) nanofiber containing silver nanoparticles. **Langmuir**, v. 24, p. 2051-2056, 2008.
27. PINTO, R.J.B.; MARQUES, P. A.A.P.; NETO, C.P.; TRINDADE, T.; DAINA, S.; SADOCCO, P. Antibacterial activity of nanocomposites of silver and bacterial or vegetable cellulosic fibers. **Acta Biomaterialia**, v. 5, p. 2279-2289, 2009.
28. JEONG, S. H.; YEO, S. Y.; YI, S. Y. The effect of filler particle size on the antibacterial properties of compounded polymer/silver fibers. **Journal of Materials Science**, v. 40, p. 5407-5411, 2005.
29. CHOI, O.; DENG, K. K.; KIM, N-J.; ROSS, L.J.; SURAMPALLI, R.Y.; HU, Z. The inhibitory effects of silver nanoparticles, silver ions, and silver chloride colloids on microbial growth. **Water Research**, v. 42, p. 3066-3074, 2008. Doi: 10.1016/j.watres.2008.02.021
30. KUMAR, A.; VEMULA, P. K.; AJAYAN, P. M.; JOHN, G. Silver-nanoparticle-embedded antimicrobial paints based on vegetable oil. **Nature Matererials**, v. 7, p. 236-241, 2008. Doi: 10.1038/nmat2099
31. SAUVET, G.; DUPOND, S.; KAZMIERSKI, K.; CHOJNOWSKI, J. Biocidal polymers active by contact. v. synthesis of polysiloxanes with biocidal activity. **Journal of Applied Polymer Science**, v. 75, p. 1005–1012, 2000.
32. KARAKAYA, N.; ERSOY, O.G.; ORAL, M. A.; GONUL, T.; DENIZ, V. Effect of different fillers on physical, mechanical, and optical properties of styrenic-based thermoplastic elastomers. **Polymer Engineering and Science**, p. 6777-688, 2010. Doi: 10.1002/pen.21569.
33. MACHADO, LU. D. B.; MATOS, J. do R. Análise térmica diferencial e calorimetria exploratória diferencial. In: CANEVAROLO JR., SEBASTIÃO V. (ed). **Técnicas de Caracterização de Polímeros**. São Paulo: Artliber Editora, 2007. ISBN 85-88098-19-9
34. JAPANESE INDUSTRIAL STANDARD. **JIS Z 2801**: Antibacterial products - Test for antibacterial activity and efficacy. 27 p., 2010.
35. CAGLAR, B.; AFSIN, B.; TABAK, A.; EREN, E. Characterization of the cation-exchanged bentonites by XRPD, ATR, DTA/TG analyses and BET measurement. **Chemical Engineering Journal**, v. 149, p. 242–248, 2009. Doi: 10.1016/j.cej.2008.10.028
36. TIAN, L.; OULIAN, L.; ZHIYUAN, L.; LIUIMEI, H.; XIAOSHENG, W. Preparation and characterization of silver loaded montmorillonite modified with sulfur amino

acid. **Applied Surface Science**, v. 305, p. 386–395, 2014. Doi: 10.1016/j.apsusc.2014.03.098

37. SUENAGA, Y.; KONAKA, H.; SUGIMOTO T.; KURODA-SOWA, T.; MAEKAWA, M.; MUNAKATA, M. Crystal structure and photo-induced property of two-dimensional silver(I) complex with 1,3,5-tris(benzylsulfanyl)benzene. **Inorganic Chemistry Communications**, v. 6, p. 389-393, 2003. Doi: 10.1016/S1387-7003(02)00780-3
38. KAMENA, K. Nanoclays and their emerging markets. In: XANTHOS, M. **Functional Fillers for Plastics**, 2ª ed. Wiley-VCH Verlag GmbH & Co. KGaA: Weinheim, 2010. p. 177-187. ISBN 978-3-527-60442-5
39. ONO, H.; IKARASHI, T.; OGURA, A. Infrared studies of silicon oxide formation in silicon wafers implanted with oxygen. **Applied Physics Letters**, v. 72, n. 22, p. 2853-2855, 1998. Doi: 10.1063/1.121479
40. DONCHEV, V.; NESHEVA, D.; TODOROVA, D.; GERMANOVA, K.; VALCHEVA, E. Characterization of Si–SiOx nanocomposite layers by comparative analysis of computer simulated and experimental infra-red transmission spectra. **Thin Solid Films**, v. 520, p. 2085–2091, 2012. Doi: 10.1016/j.tsf.2011.08.009
41. LACONA, F.; FRANZÒ, G.; SPINELLA, C. Correlation between luminescence and structural properties of Si nanocrystals. **Journal of Applied Physics**, v. 87, n. 3, p. 1295-1303, 2000. Doi: 10.1063/1.372013
42. TOLOMAN, D.; MAGDAS, D. A.; BRATU, I.; GIURGIU, L. M.; ARDELEAN, I. Infrared spectra of calcium phosphate glasses. **International Journal of Modern Physics B**, v. 24, p. 351-358, 2010,
43. ESSEHLI, R.; BALI, B. E.; BENMOKHTAR, S.; FUESS, H.; SVOBODA, I. OBBADE, S. Synthesis, crystal structure and infrared spectroscopy of a new non-centrosymmetric mixed-anion phosphate $Na_4Mg_3(PO_4)_2(P_2O_7)$. **Journal of Alloys and Compounds**, v. 493, p. 654–660, 2010. doi: 10.1016/j.jallcom.2009.12.181
44. MAGAÑA, S. M.; QUINTANA, P.; AGUILAR, D. H.; TOLEDO, J. A.; ANGELES-CHÁVEZ, C.; CORTÉS, M. A.; LÉON, L.; FREILE-PELEGRÍN, Y.; LÓPEZ, T.; TORRES SÁNCHEZ, R. M. Antibacterial activity of montmorillonites modified with silver. **Journal of Molecular Catalysis A: Chemical**, v. 281, p. 192–199, 2008. Doi:10.1016/j.molcata.2007.10.024
45. ORLOV, A. S.; KISELEV, S. A.; KISELEVA, E. A.; BUDEEVA, A. V.; MASHUKOV, V. I. Determination of styrene-butadiene rubber composition by attenuated total internal reflection infrared spectroscopy. **Journal of Applied Spectroscopy**, v. 80, n. 1, p. 47-53, 2013.
46. LIN, J-H.; PAN, Y-J.; LIU, C-F.; HUANG, C-L.; HSIEH, C-T.; CHEN, C-K.; LIN, Z-I.; LOU, C-W. Preparation and compatibility evaluation of polypropylene/high density polyethylene polyblends. **Materials**. v. 8, p. 8850–8859. 2015. Doi: 10.3390/ma8125496
47. WU, C. L.; ZHANG, M. Q.; RONG, M. Z.; FRIEDRICH, K. Silica nanoparticles filled polypropylene: effects of particle surface treatment, matrix ductility and particle species on mechanical performance of the composites. **Composites**

Science and Technology, v. 65, p. 635–645, 2005. Doi: 10.1016/j.compscitech.2004.09.004

48. XANTHOS, M. Polymer and Polymer Composites. In: XANTHOS, MARINO. **Functional Fillers for Plastics**, 2ª ed. Wiley-VCH Verlag GmbH & Co. KGaA, Weinheim, 2010. p. 3-17. ISBN 978-3-527-60442-5
49. STRIBECK, N.; ZEINOLEBADI, A.; SARI, M. G.; BOTTA, S.; JANKOVA, K.; HVILSTED, S.; DROZDOV, A.; KLITKOU, R.; POTARNICHE, C-G.; CHRISTIANSEN, J. DEC.; ERMINI, V. Properties and semicrystalline structure evolution of polypropylene/montmorillonite nanocomposites under mechanical load. **Macromolecules**, v. 45, p. 962−973, 2012. Doi: 10.1021/ma202004f
50. CHAN, C-M.; WU, J.; LI, J-X.; CHEUNG, Y-K. Polypropylene/calcium carbonate nanocomposites. **Polymer**, v. 43, p. 2981-2992, 2002.
51. WAY, J. L.; ATKINSON, J. R.; NUTTING, J. The effect of spherulite size on the fracture morphology of polypropylene. **Journal of Materials Science**, v. 9, p. 293-299, 1974.
52. PARENTEAU, T.; AUSIAS, G.; GROHENS, Y.; PILVIN, P. Structure, mechanical properties and modelling of polypropylene for different degrees of crystallinity. **Polymer**, v. 53, p. 5873-5884, 2012. Doi: 10.1016/j.polymer.2012.09.053
53. SENGUPTA, P. **Morphology of olefinic thermoplastic elastomer blends: A comparative study into the structure-property relationship of EPDM/PP/oil based TPVs and SEBS/PP/oil blends***.* 2004. 207 f. PhD. Thesis, University of Twente, The Netherlands, 2004.
54. HAMOUDA, T.; BAKER, J.R. Jr. Antimicrobial mechanism of action of surfactant lipid preparations in enteric Gram-negative bacilli. **Journal of Applied Microbiology**, v. 89, p. 397-403, 2000.
55. STOIMENOV, P. K.; KLINGER R. L.; MARCHIN G. L.; KLABUNDE, K. J. Metal oxide nanoparticles as bactericidal agents. **Langmuir**, v. 18, p. 6679-6686, 2002.
56. TREVORS, J. T. Silver resistance and accumulation in bacteria. **Enzyme and Microbial Technology**, v. 9, p. 331-333, 1987.
57. KIM, S. S.; PARK, J. E.; LEE, J. Properties and antimicrobial efficacy of cellulose fiber coated with silver nanoparticles and 3-mercaptopropyltrimethoxysilane (3-MPTMS). **Journal of Applied Polymer Science**, v.119, p. 2261–2267, 2011.
58. RAGHUPATHI, K. R.; KOODALI, R. T.; MANNA, A. C. Size-dependent bacterial growth inhibition and mechanism of antibacterial activity of zinc oxide nanoparticles. **Langmuir**, v. 27, p. 4020–4028, 2011. Doi: 10.1021/la104825u
59. MARTÍNEZ-ABAD, A. Silver- and nanosilver-based plastic Technologies. In: LAGARÓN, J.M.; OCIO, M. J.; LÓPEZ-RUBIO, A. **Antimicrobial Polymers**. Hoboken: Wiley, 2012. p. 287-316. ISBN 978-0-470-59822-1
60. TOLAYMAT, T. M.; EL BADAWY, A. M.; GENAIDY, A.; SCHECKEL, K. G.; LUXTON, T.P.; SUIDAN, M. An evidence-based environmental perspective of manufactured silver nanoparticle in syntheses and applications: A systematic

review and critical appraisal of peer-reviewed scientific papers. **Science of the Total Environment**, v. 408, p. 999–1006, 2010. Doi: 10.1016/j.scitotenv.2009.11.003

61. SONDI, I.; SALOPEK-SONDI, B. Silver nanoparticles as antimicrobial agent: a case study on *E. coli* as a model for Gram-negative bactéria. **Journal of Colloid and Interface Science**, v. 275, p. 177–182, 2004. Doi: 10.1016/j.jcis.2004.02.012
62. MORONES, J. R.; ELECHIGUERRA, J. L.; CAMACHO, A.; HOLT, K.; KOURI, J. B; RAMÍREZ, J. T.; YACAMAN, M. J. The bactericidal effect of silver nanoparticles. **Nanotechnology**, v. 16, 2346–2353, 2005. Doi: 10.1088/0957-4484/16/10/059
63. FORTUNATI, E.; ARMENTANO, I.; ZHOUC, Q.; IANNONI, A.; SAINO, E.; VISAI, L.; BERGLUND, L. A.; KENNY, J. M. Multifunctional bionanocomposite films of poly(lactic acid), cellulose nanocrystals and silver nanoparticles. **Carbohydrate Polymers**, v. 87, p. 1596-1605, 2012. Doi: 10.1016/j.carbpol.2011.09.066
64. LOK, C-N; HO, C-M.; CHEN, R.; HE, Q-Y.; YU, W-Y.; SUN, H.; TAM, P. K-H.; CHIU, J-F.; CHE, C-M. Silver nanoparticles: partial oxidation and antibacterial activities. **Journal of Biological Inorganic Chemistry**, v. 12, p. 527–534, 2007. doi: 10.1007/s00775-007-0208-z
65. CIULLO, P.A. **Industrial Minerals and Their Uses: A Handbook and Formulary**; Westwood: Noyes Publication, 1996. ISBN: 0-8155-1408-5

5 EFFECTS OF WEATHERING ON MECHANICAL, ANTIMICROBIAL PROPERTIES AND BIODEGRADATION PROCESS OF SILVER LOADED TPE COMPOUNDS[2]

Abstract

The incorporation of antimicrobial metals such as silver is an alternative to protect the material against microbial attack. However, loaded polymer can lose its antimicrobial properties after some time of use, and the additive may even leak out into the environment becoming harmful to non-target organisms. This study aims to evaluate the mechanical properties and antimicrobial activity of silver containing thermoplastic elastomer (TPE) samples exposed to weathering and the influence of additive incorporation in material biodegradation in the soil. For this purpose, silver ions (Ag^+_bentonite, Ag^+_phosphate) and silver nanoparticles (AgNp_silica) based additives were blended in a formulation of SEBS, polypropylene and mineral oil. The test samples were exposed to natural ageing over nine months, and were then evaluated according to their mechanical properties, antimicrobial activity, and degree of crystallinity and surface characteristics. The biodegradation process before and after natural ageing was evaluated through the generation of carbon dioxide. The results show that the action of natural ageing reduced the mechanical properties of loaded and unloaded TPE, and modified the degree of crystallinity and the chemical characteristic of the TPE surface. The presence or type of additive did not influence material resistance after being exposed to weathering. A decrease in antimicrobial activity in samples after natural ageing was observed. At a variable level and according to the chemical content, generation of carbon dioxide from TPE samples was greater in aged samples than in unexposed ones.

Key words: Thermoplastic elastomers; Weathering; Degradation; Silver; Carbon dioxide.

5.1 INTRODUCTION

In general, polymers deteriorate by physical or chemical factors such as light, heat and moisture [1], which results in embrittlement, cracking, chalking, discoloration and, lastly, loss of mechanical properties [2]. Polymer characteristics that are affected by degradation include chemical structure, molecular weight, crystallinity, glass-transition, melting temperatures and melting enthalpy [3]. These modifications can be analyzed by visual observations (roughening of the surface, formation of holes or cracks, de-fragmentation and color changes).

[2] Publicado como: TOMACHESKI, D.; PITTOL, M.; LOPES, A. P. M.; SIMÕES, D. N.; FERREIRA, V. F.; SANTANA, R. M. C. Effects of weathering on mechanical, antimicrobial properties and biodegradation process of silver loaded TPE compounds. **Journal of Polymers and the Environment**, 2017. Doi: 10.1007/s10924-016-0927-8

The biodeterioration process is defined as a change in the chemical or physical properties of a material resulting from the action of microorganisms [4]. This process takes place following the growth of microorganisms on the surface or/and within a given material [5], usually after previous abiotic degradation, and will vary in function of the physicochemical constitution of the surface [6]. Few fungal species, and recently described bacteria species, have the ability to degrade undamaged plastics [7]. The resistance to biodegradation in undamaged plastics is due to their long carbon chain and ultra-hydrophobic surfaces, which are poorly bonded by microorganisms [1, 8].

Styrene-ethylene/butylene-styrene (SEBS) is applied together with polypropylene and mineral oil to create thermoplastic elastomers (TPE's) that possess soft touch qualities. The devices produced with this polymer comprise hand contact surfaces such as toothbrush handles, sporting goods, home appliances, which are exposed to the action of a range of pathogenic and non-pathogenic microorganisms. The incorporation of silver-based antimicrobial additive in polymer blends is a good alternative to prevent microbial proliferation without modifying the characteristics of the end product. The use of antimicrobial additives such as silver in polymeric matrices like polypropylene [9]; polyethylene [10], and polystyrene [11] has been reported as being successful.

However, a study realized by Sun et al. [12] depicted that in the European Union (EU), the major part of AgNp released from consumer goods accumulates in waste incineration plants (340 µg Kg^{-1}), followed by solid waste in landfill (79 µg Kg^{-1}) and sewage treatment plants (61 µg Kg^{-1}). In Brazil, waste incineration is not a usual practice, with 97% of urban solid waste going to landfill sites [13] and only 41% of the sewage generated in Brazil is directed to treatment plants [14]. Based on this information, we may suppose that the levels of AgNp in Brazilians landfill sites and treatment plants are even higher than those in the EU. Moreover, harmful effects in microorganisms that are important to the ecosystem have been reported in nitrogen, sulfur, carbon and phosphorous cycles [15]. Calder et al. [16] found that 1 mg L^{-1} of silver ions was enough to eliminate a population of *Pseudomonas chlororaphis* from the soil. Instead, Gitipur et al. [17] added 2 mg kg^{-1} of silver ions or silver nanoparticles to soil and determined that this amount was not enough to have an influence in composting of municipal solid waste. Controversial results can be

ascribed to the fact that silver can interact with inorganic and organic anions in the medium, forming soluble metal complexes, precipitating and reducing its toxicity [15].

In this scenario, the environmental concern with the use of antimicrobial polymers rests on the fact that if leaching occurs, the additives may cause an environmental issue and, when it becomes waste, the polymer degradation time may be even greater than that of non-antimicrobial materials. As far as the authors are aware, this is the first evaluation of the effects of weathering in mechanical, antimicrobial properties of silver loaded TPE compounds. In that sense, further research is necessary to ensure product performance to the final consumers and assess the environmental impact of these silver containing materials. The purpose of the present study was to evaluate the mechanical properties and antimicrobial activity of silver containing TPE samples exposed to natural ageing. A further objective was to evaluate whether the additive incorporation affects material biodegradation in soil before and after exposure to weathering.

5.2 EXPERIMENTAL

5.2.1 Materials

The additives tested were bentonite organomodified with silver (referred to here as "Ag^+_bentonite"), silver ions supported in phosphate glass (referred to here as "Ag^+_phosphate") and nanosilver adsorbed on fumed silica (referred to here as "AgNp_silica"). The proportions used were recommended by the additive suppliers, 2.0%, 0.3% and 0.05% respectively. The additives were added to a TPE formulation compounded by styrene-ethylene/butylene-styrene copolymer (SEBS, 32% styrene, ethylene/butylene 32/68, linear, Mw 214.8 Da) polypropylene homopolymer (PP, melt flow index 1.5 g 10 min^{-1} at 230°C), white mineral oil (64 % paraffinic and 36% naphtenic), at a ratio of 30/20/50 respectively. An antioxidant was added at a proportion of 0.1% to prevent thermal degradation during processing. A compound with no antimicrobial additive (Standard) was also tested.

5.2.2 TPE compounds preparation

The samples were prepared using a co-rotating double screw extruder (L/D 40 and 16 mm screw diameter, AX Plásticos) with a temperature profile from 170°C

to 190°C, speed of 300 rpm, feed rate of 1.5 kg h^{-1} and melt discharge temperature of 200°C. Test specimens in plate form of 2 mm thickness were prepared using injection molding machine (Haitian, PL860) at 190°C and an injection pressure of 17 bars.

5.2.3 Natural ageing experiments

The specimens were exposed to weathering for 9 months (from August 2015 to May 2016), under real climatic conditions in accordance with ASTM 1435. The specimens were exposed in an outdoor station at an inclination of 30° to the ground (Figure 5.1a), located in Campo Bom city, southern Brazil (29º40'54"S and 51º03'25"W), 20 meters elevation above sea level. Samples were collected every 3 months to study the effects of weathering. During the experiment, solar radiation, temperature and rainfall data were obtained from Inmet (National Institute of Meteorology, Brazil) [18] and reported in Figure 5.1b and c.

Figure 5.1 (a) Weathering experiment; values of (b) rainfall, temperature and (c) solar radiation during the period evaluated

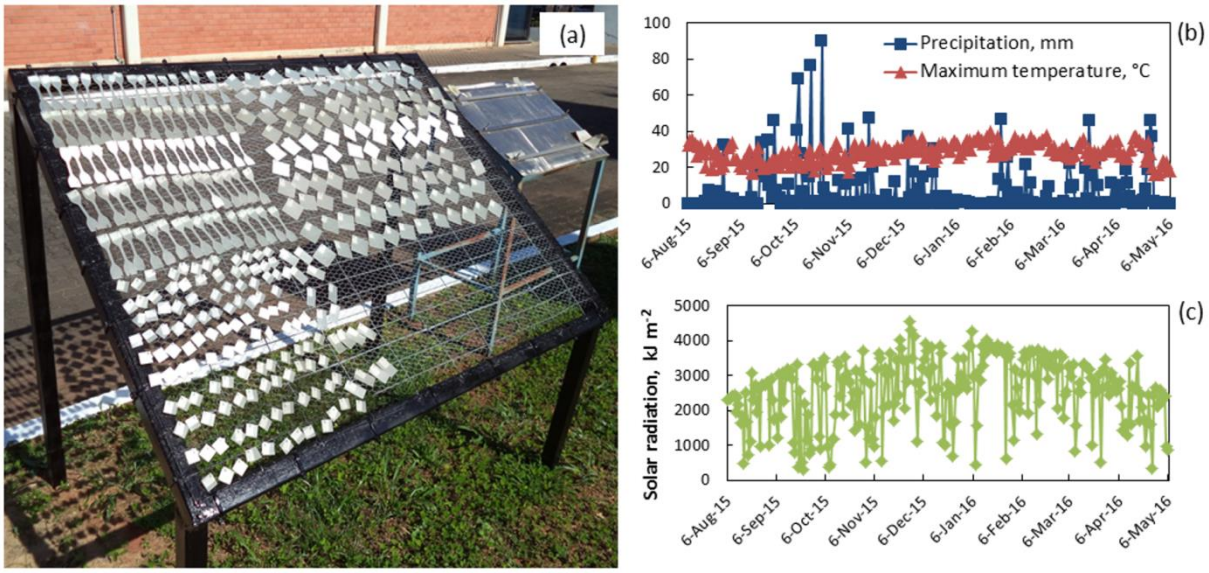

5.2.4 Biodegradation in soil

The method used for biodegradation testing was based on parameters reported by Montagna et al. [19] and Catto et al. [20] using a biometer flask adapted according to ASTM D 5338 and ASTM D 5988. These test methods determine the degree and rate of aerobic biodegradation for plastic materials exposed to a controlled-composting environment under laboratory conditions at thermophilic

temperatures (50-60°C). The level of biodegradation was estimated through the mineralization of the polymer carbon atoms evolving to CO_2, which were trapped by the NaOH solutions. The biodegradation tests were performed in an Erlenmeyer flask (250 mL capacity) with a multilayer substrate comprising a mixture of 60 g of soil and approximately 0.8-1.0 g of samples to be biodegraded. The mixture was sandwiched between two layers of 3 g perlite, and wetted with 30 mL of distilled water. The respirometric apparatus was kept at 58 ± 2°C and open every 7 days for titration of the NaOH solution. Prior to the titration, 3 mL of 35 m/v (%) $BaCl_2$ solution was added to the NaOH (30 mL) used for the titration, with a drop of phenolphthalein. The amount of carbon dioxide (CO_2) produced during the incubation period was determined as mg of the theoretical quantity of CO_2 produced by the blank samples (soil without carbon source) during the incubation time. Cellulose (cardboard packaging) was used as a positive control.

5.2.5 Analytical methods

The changes in physical properties of the polymer which occurred as a result from biotic and abiotic degradation were monitored through the determination of mechanical properties, degree of crystallinity (X_c), and surface chemical changes by attenuated total reflectance fourier transform infrared spectroscopy (ATR-FTIR). Also, scanning electron microscopy (SEM) images were applied to search for microbial growth on the of the sample surfaces.

5.2.5.1 Mechanical properties

The changes in mechanical characteristics were monitored by tensile properties (tensile at break, modulus at 100% and elongation at break), according to ASTM D 412C. Test specimens type C was tested using a universal machine EMIC DL 2000, operating at a speed of 500 mm min^{-1} with a grip distance of 25 mm.

5.2.5.2 Microbiological Studies

Japan Industrial Standard (JIS) Z 2801 was applied to evaluate antimicrobial abilities of TPE samples against *Staphylococcus aureus* ATCC 6538 (*S. aureus*) and *Escherichia coli* ATCC 8739 (*E. coli*). These bacterial species are representative of Gram-positive and Gram-negative bacteria and are the most common bacteria used

in antibacterial studies. After weathering exposure, the TPE specimens (50 mm x 50 mm) were placed in a sterile Petri dish and 400 µL of bacterial suspension of *E. coli* and *S. aureus* were inoculated on the specimen surface. All of them were incubated for 24 h at 35 ± 1°C. The results were expressed as a microbial value calculated from the difference between the number of Colony Forming Units (CFU) per square centimeter, at zero hour (initial) and after 24 h of incubation.

5.2.5.3 Thermal properties

Thermal analysis by differential scanning calorimetry (DSC) was performed in a DSC Q100 (TA Instruments, USA) according to ASTM D 3418. The samples were subjected to heating from -30°C to 200°C at a rate of 10°C min^{-1} under a nitrogen atmosphere. Nitrogen was used at a flow rate of 50 mL min^{-1}. The percentage of crystallinity of PP phase, X_c, was calculated from the melting enthalpy (ΔH^*), $\Delta H°_{(PP)}$ of pure PP (209 J g^{-1}) and its mass fraction, *w*, as expressed in equation (1)

$$X_c = \frac{\Delta H^*}{w\ x\ \Delta H^0_{PP}}\ x\ 100 \quad (1)$$

5.2.5.4 Chemical characterization

Attenuated Total Reflection Fourier Transformed Infrared Spectroscopy (ATR-FTIR) was recorded in a PerkinElmer spectroscope (Frontier MIR, PerkinElmer). Each spectrum was recorded with a total of 10 scans at a resolution of 4 cm^{-1} at room temperature on the surface of the sample exposed to the sun. The Spectrum software was used for spectra analysis.

5.2.5.5 Scanning electron microscopy of microbial growth

Scanning Electron Microscopy (SEM) was performed to verify microbial growth in the surface of TPE samples exposed to weathering for 3 months. TPE samples were immersed in a glutaraldehyde buffer (1.2 mL glutaraldehyde 25%, 5.0 mL 0.2M PO_4^{3-} buffer and 3.8 mL H_2O). The fixed samples were rinsed three times with phosphate buffer (0.2 M in distillated water 1:1) to remove the traces of glutaraldehyde. The samples were dehydrated through a series of dehydrating solutions (30, 50, 70, and 90 % acetone for 10 min each; 90 and 100 % acetone for 20 min) and then subjected to critical point drying. The TPE samples were deposited

in a carbon type stuck to stub, metalized with gold. For image acquisition, a SEM of field emission (SEM-FEG) (Inspect F50, FEI) was used with 20 kV, spot 3 and working distance of 10 mm.

5.2.5.6 Inductively Coupled Plasma Atomic Emission Spectroscopy (ICP-OES)

The unexposed and nine months exposed polymer samples were digested according to the norm EN 1122. Total silver was analyzed by Inductively Coupled Plasma Optical Emission Spectrometry (ICP-OES), Thermo Scientific iCAP 6300 Model. The silver curve was in the range of 10 µg L^{-1} to 2 mg L^{-1}.

5.2.5.7 Statistical analysis

Statistical Analysis of Variance (ANOVA) was applied in tensile strength, modulus at 100%, elongation at break and antibacterial results using MYSTAT, student version 12 (Systat Software, Inc., CA, USA). The level of significance was set at 0.05.

5.3 RESULTS

5.3.1 Influence of natural ageing

5.3.1.1 Mechanical properties

Figure 5.2 shows variations in mechanical properties of TPE samples exposed to weathering. After 3 months there were great decreases in tensile at break ($p<0.05$), modulus values had little but significant reduction ($p<0.05$) and elongation at break was reduced by half ($p < 0.05$). After 9 months TPE samples were almost completely degraded. Since both loaded and unloaded TPE had the same loss of mechanical properties, it can be concluded that the presence of additive did not influence on the mechanical resistance of the material exposed to weathering.

In polymer degradation, the reduction in tensile properties can be assigned to an extensive chain scission [21, 22]. The TPE samples used in this study are based in SEBS, polypropylene (PP) and oil. According to Allen et al. [23] the degradation of SEBS occurs as a result of scission of styrene chains connected with the ethylene-butylene group. PP degradation occurs due to chain scission, initiated by autoxidation of the PP, and gives sequence to a series of reactions that will lead to

formation of carbonyl groups [24]. This kind of degradation is consistent with the reduction in mechanical properties observed here and previously reported by Zhang et al. [25].

As observed in Figure 5.1b and Figure 5.1c, it was rainy and warm in the first three months, with an accumulated rainfall of 635 mm and temperature between 4°C and 36°C. In the second quarter, the accumulated precipitation was 380 mm and the temperatures ranged from 13°C to 40°C. Whereas that temperature is the factor that most influence polymer degradation [26], the warmest temperature in the second quarter may have accelerated the degradation process and the decay in modulus value.

Figure 5.2 Variation in mechanical properties over the weathering exposure: (-♦-) Standard, (-■-) Ag^+_bentonite, (-▲-) Ag^+_phosphate, (-x-) AgNp_silica

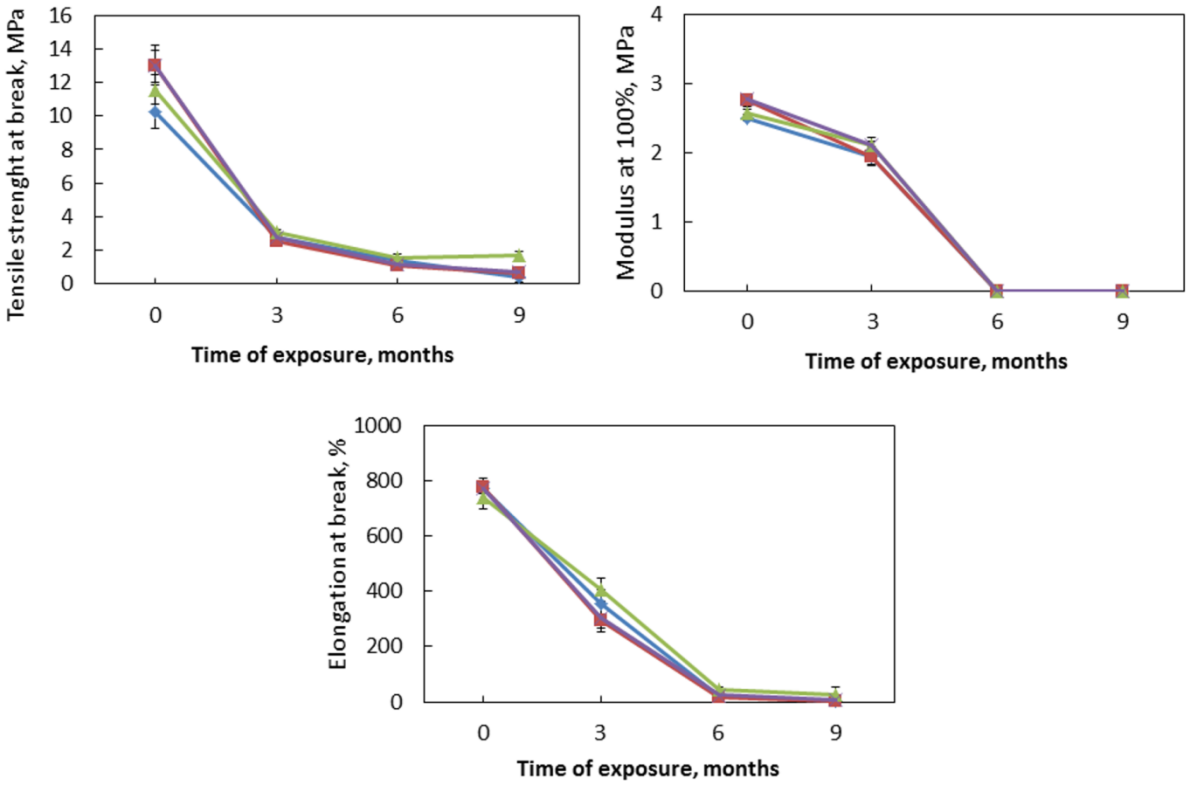

5.3.1.2 Degree of crystallinity

Table 5.1 shows the melting temperature and crystallinity degree in TPE samples with or without Ag, calculated from the first heating.

Table 5.1 Thermal characteristics (melting temperature T_m, and crystallinity index X_{cPP}) of TPE samples from the first heating scan before and after 3, 6 and 9 months of weathering exposure.

Sample	Initial		3 months		6 months		9 months	
	T_m, °C	X_{cPP}, %	T_m, °C	X_{cPP}, %	T_m, °C	X_{cPP}, %	T_m, °C	X_{cPP}, %
Standard	154.2	39.7	153.0	42.3	152.7	45.0	152.0	46.0
Ag^+_bentonite	152.1	45.6	153.0	42.2	152.3	39.2	151.8	35.9
Ag^+_phosphate	153.4	44.8	153.3	41.4	152.4	41.6	153.0	42.7
AgNp_silica	152.5	42.5	153.0	41.8	152.1	40.7	152.0	39.7

In the Standard sample there was an increase in crystallinity degree throughout the exposure time. The crystallinity values of Ag^+_bentonite loaded compound had higher decline during the 9 months of experiment than other loaded compounds (Ag^+_phosphate and AgNp_silica). In TPE formulation, Ag^+_bentonite were loaded in a greater amount than the other additives, which may have caused an elevated level of defects, further hindering crystallization. According to Rabello and White [24] the increase in crystallinity with chain scission is explained by the chemi-crystallization effect, where chain scissions lead to the rejection of chromophore impurities and are related to strained or entangled molecules. Also, further crystallization takes place through the rearrangement of free molecule segments. Moreover, the reduction in molecular size favors crystallization [27]. The increase in PP crystallinity after UV exposure was also reported by Rajakumar et al. [21]. With the exposure time, chain oxidation occurs in extraneous groups and the rise in chain scissions renders crystallization [24, 28].

5.3.1.3 FTIR analysis

The incorporation of silver additives did not change the FTIR surface profile (Figure 5.3). It was possible to notice the characteristics bands of SEBS in 699 cm^{-1} and 759 cm^{-1} due to out-of-plan bending of C-H in aromatic monosubstituted ring of styrene units [29]. Skeletal vibrations representing C=C stretching of aromatic styrene ring appeared at 1493 cm^{-1} [29] and rocking vibration of CH_2 from ethylene appear at 720 cm^{-1} [30]. Bands in 1452 cm^{-1} and 1376 cm^{-1} were in plane bending of the C-H from CH_2 and CH_3, common to all components of the blend [29, 30]. The chemical reactions that occur in plastic materials during environmental exposures involve free radical chain reaction that leads to the cleavage of the chain and the rise of functional groups such as carboxyl and carbonyl groups [31].

Figure 5.3 FTIR-ATR of (a) Standard sample and compounds with (b) 2.0 % of Ag^+_bentonite, (c) 0.3 % of Ag^+_phosphate and (d) 0.05 % of AgNp_silica

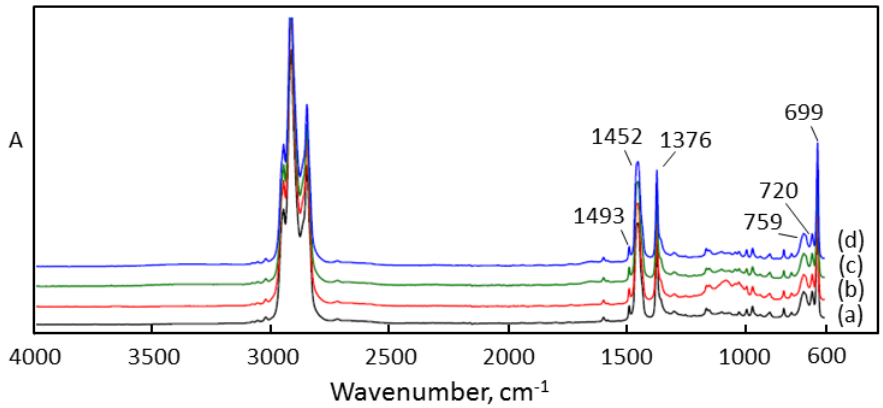

After exposure, all the samples featured the same band profile with different intensity. To make it clean and clear, Figure 5.4 shows the modifications only on the surface of the Standard sample. Default of the bands between 3400 cm^{-1} and 3000 cm^{-1} assigned to –OH showed that there was little formation of hidroperoxides [32, 33]. The FTIR profile was the same at 3, 6 and 9 months, with increase in intensity of new bands in comparison with unexposed samples (initial). The region between 1780 cm^{-1} and 1620 cm^{-1} is usually attributed to the presence of carbonyl groups like ketones, ester and ethers [23, 26, 32-34].

Figure 5.4 FTIR-ATR of Standard sample (a) no weathering, (b) after three, (c) six and (d) nine months of weathering exposure

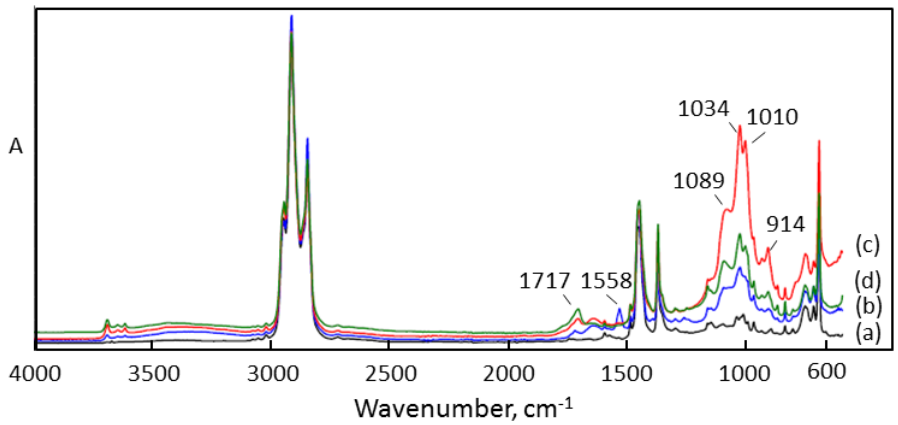

The region between 1280 cm^{-1} and 1000 cm^{-1} was assigned to a mixture of aliphatic esters, ethers, ozonides and adsorbed water. There was a large shoulder that can be related to C-O-C vibration (1151 cm^{-1}); C-O-H stretching vibration (1077 cm^{-1}); C-C rocking vibrations (1016 cm^{-1}) and ozonides (1050-1000 cm^{-1}) [23, 33].

In the present study the low intensity of bands in the region of 1780-1620 cm^{-1} showed that there was no oxidation or that all groups formed in oxidation reactions were subsequently photo-oxide and thermo-oxide [35]. One possibility is that the

relation of water molecules to the oxidation products resulted in a rinsing of the oxidation products [35].

5.3.1.4 Microbial growth on the TPE surface analyzed by SEM microscopy

To verify the development of microorganisms on loaded TPE surfaces, samples exposed to weathering for 3 months were analyzed by SEM microscopy. Figure 5.5 shows biofilm formed by microbial-like structures on a TPE surface after 3 months of weathering exposure. In Figure 5.5a, b and c bacterial-like cells can be observed and hyphal network in Figure 5.5d.

Figure 5.5 Scanning electron microscopy from the surface of TPE samples of (a) Standard, (b) Ag^+_bentonite, (c) Ag^+_phosphate and (d) AgNp_silica after 3 months of weathering exposure

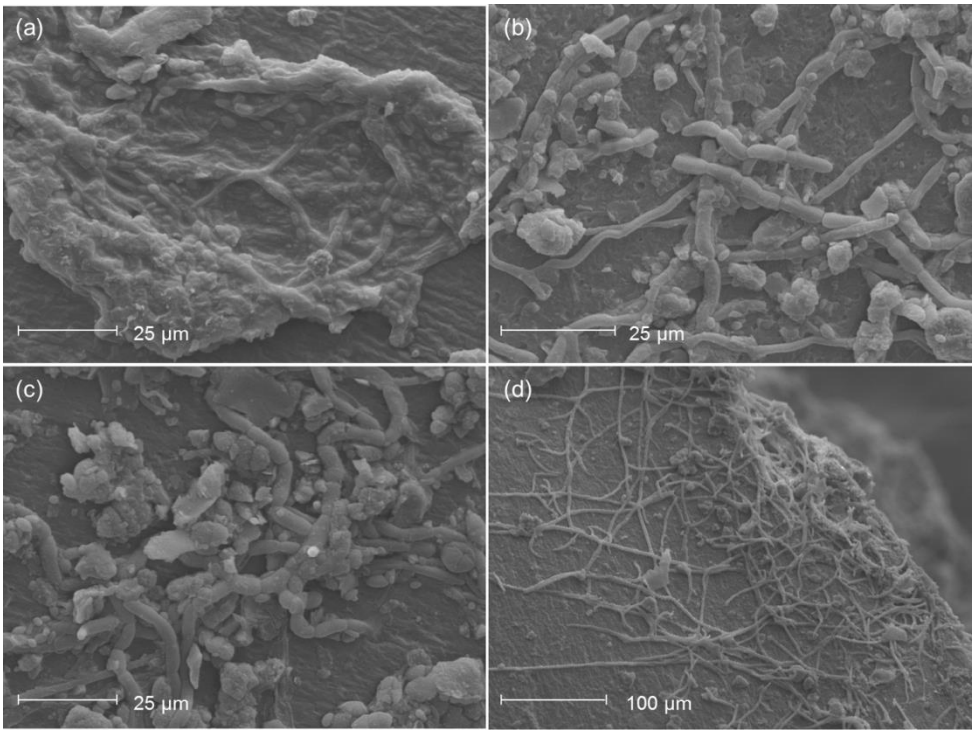

Throughout the exposure time, the TPE samples were subjected to a wide source of organisms and dirt. The results shows that the same samples that present antimicrobial action also exhibited microbial cells bonded to their surfaces. In this study, the methodology used in microscopy analysis does not allow to know whether the organisms in the sample were biologically active at the time of the test.

5.3.1.5 Variation in bacterial population

Figure 5.6 shows the variation in bacterial population over the time of study. After 3 months a significant decrease was observed in antimicrobial properties against *E. coli* in all TPE loaded samples compared to counts from the initial time. This pattern was intensified over time with an increment in *E. coli* population after 9 months of exposure (Figure 5.6a).

Figure 5.6 Variation in (a) *E. coli* and (b) *S. aureus* population in silver loaded compounds during weathering exposure

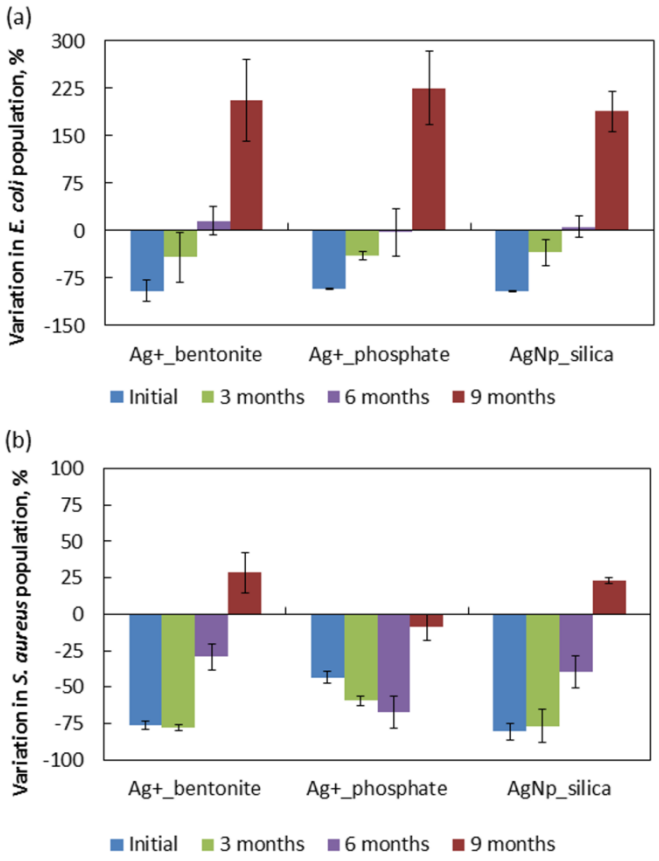

In Figure 5.6b it can be observed that after 3 months of weathering exposure the TPE loaded samples presented no significant difference in antimicrobial properties against *S. aureus* when compared to the initial time. In this way, it can be supposed that the microbial cells observed in the microcopy (Figure 5.5) were not biologically active or were present in low numbers to significantly impact the antimicrobial result. However, after 6 months of weathering Ag^+_bentonite and AgNp_silica presented a great reduction in antimicrobial efficiency that get even worse after 9 months of exposure. After 9 months Ag^+_bentonite and AgNp_silica samples presented proliferation of *S. aureus*, while Ag^+_phosphate maintained its

antibacterial activity, eliminating around 10 % of the *S. aureus* population (Figure 5.6b).

In the present study it was observed that the more degraded the polymer the most susceptible to microbial attack. Studies have shown that when polymer cracks occur, the presence of oxygen and availability of molecular chains makes the polymer suitable for microbial consumption [36, 37].

Oxidized groups (like carbonyl and carboxyl) are promptly degraded by microorganisms [38]. Polymer oxidation increases surface hydrophilicity, which provides a friendly environment to microorganisms due to water retention [39]. Also, differences in antimicrobial efficacy over time may be ascribed to the formation of a layer on the polymer surface from degradation products, which were verified in infrared spectrogram after 3, 6 and 9 months of exposure. This layer provides a shield between the bacteria and the silver ions and silver nanoparticles. Moreover, the variation of polymer crystallinity, which can imprison or release ions and silver nanoparticles, may have had a consequence on bacterial deactivation.

To verify the possibility of loss of additive by leaching, samples were analyzed by ICP-AES before and after nine months of exposure; results are show in Table 5.2.

Table 5.2 Total amount of silver in samples before and after nine months of weathering

Sample	Calculated initial value* (mg kg^{-1})	Observed values in unexposed samples (mg kg^{-1})	Observed values after nine months of exposure (mg kg^{-1})
Ag^+_bentonite 2.0 %	1000	4.39	47.2
Ag^+_phosphate 0.3 %	3000	6.98	13.8
AgNp_silica 0.05 %	0.5 to 10	<2.00	<2.00

*Note: *Values calculated based on the silver concentration in the formulation of the additives.*

It was notable that the concentration of additives found in samples after 9 months of exposure was higher than in unexposed samples, but lower than expected. The extraction of metal during the process of polymer digestion may have been facilitated by the advanced state of compound degradation. Anyway, it is not possible to correlate changes in silver content with loss of antibacterial activity neither with CO_2 production rates.

5.3.2 Aerobic biodegradation in soil

Figure 5.7 shows the aspect of the Standard samples after weathering exposure and burial in soil. It is notable that the modification in the aspect of the samples was more prominent in those samples exposed to a temperature of 60°C (buried in soil). Pre-ageing by weathering contributed to complete change in color and loss of transparency.

Figure 5.7 Standard sample characteristics after weathering exposure and burial in soil

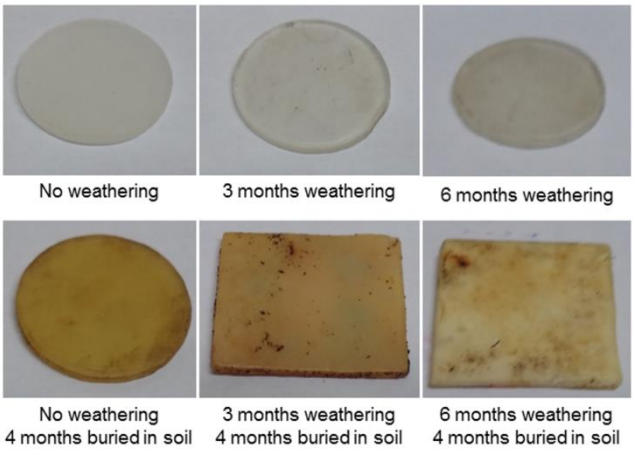

Microbial cells produce enzymes which support the degradation and assimilation of the polymer through their cellular membranes [38, 40]. For a truly biodegradable plastic, the ultimate result is a reduction in the molar mass (length) of polymers, followed by biodigestion and/or biological conversion of the polymer breakdown products, and ultimately, biological conversion to carbon dioxide and/or methane, and water [3].

Figure 5.8a shows the results of carbon dioxide generation from the biodegradation test of unexposed samples conducted for 120 days in a controlled setting (buried in soil; 60°C). It was noted that there was no difference in CO_2 generation between the positive control samples (cellulose), Standard samples, and samples loaded with 0.3% of Ag^+_phosphate and 2.0% of Ag^+_bentonite. But in the experiment with 0.05% of AgNp_silica, CO_2 generation dropped after 58 days. This result supports the idea that the AgNp additive was released into the soil and killed the bacteria responsible for biodegradation. Recent studies reports that the presence of silver nanoparticles in soil reduces soil microbial activity [15, 16, 41, 42].

Figure 5.8b shows the results of carbon dioxide generation from the biodegradation test conducted for 120 days in a controlled setting (buried in soil;

60°C) in samples exposed to weathering for 3 months. It was notable that the samples exposed for 3 months (Figure 5.8b) produced much more CO_2 during the assay than the unexposed samples (Figure 5.8a). As verified by Albertsson et al. [38] and Bonhomme et al. [43], the action of light or heat acts as a pioneer to biodegradation by producing articles with low molar mass that can be assimilated by thermophilic microorganisms. High respiratory activity after biotic degradation was also observed by Luz et al. [44]. In samples exposed for 3 months, Ag^+_bentonite, Ag^+_phosphate and AgNp_silica loaded samples produced more CO_2 than the Standard sample and cellulose.

Figure 5.8 (a) Cumulative CO_2 emissions from unexposed samples, (b) exposed to weathering for 3 and (c) exposed to weathering for 6 months. (-♦-) Standard, (-■-) Ag^+_bentonite, (-▲-) Ag^+_phosphate, (-x-) AgNp_silica, (-●-) cellulose

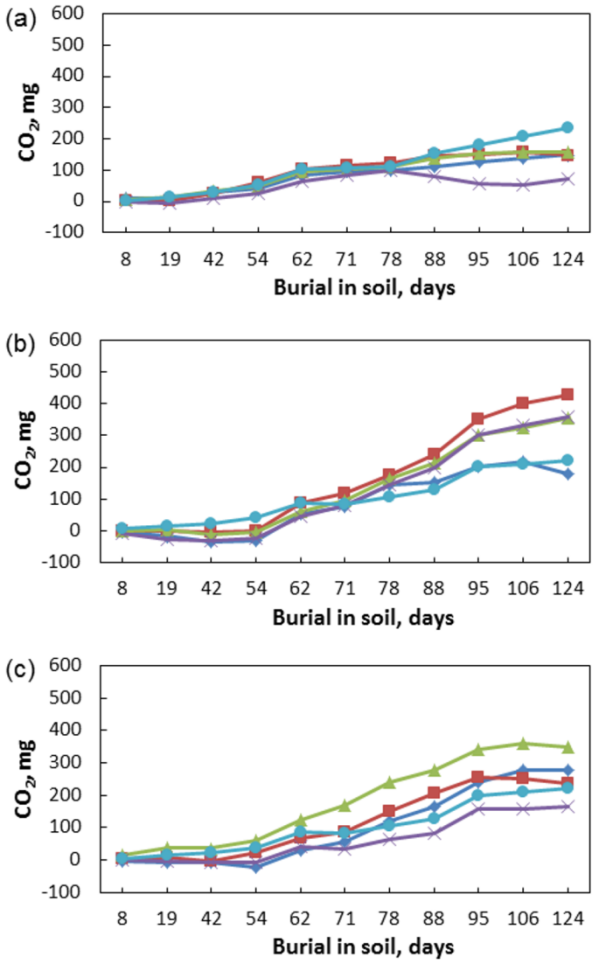

In Figure 5.8c it is possible to the see that CO_2 production in samples buried in soil after 6 months of exposure was lower than that in samples aged for 3 months. There are two possibilities for this result: (1) after 6 months of exposure, the samples became too degraded to offer any nutrients to microorganisms; (2) as can be verified

in the ICP-OES assay, silver becomes more widely available in degraded polymer; thus after a long contact time with soil the silver may have produced a harmful effect to soil microorganisms. In Figure 5.9 shows the change in FTIR profile from Standard samples after burial in soil. As verified in the infrared assay, there was no reduction in characteristic bands of polymer, only the appearance of new bands due to the formation of oxidized groups, as previously discussed. This way, the second alternative would be the most acceptable.

Figure 5.9 FTIR-ATR of Standard sample (a) no weathering, (b) buried in soil, no weathering, (c) buried in soil after 3 months of weathering and (d) buried in soil after 6 months of weathering

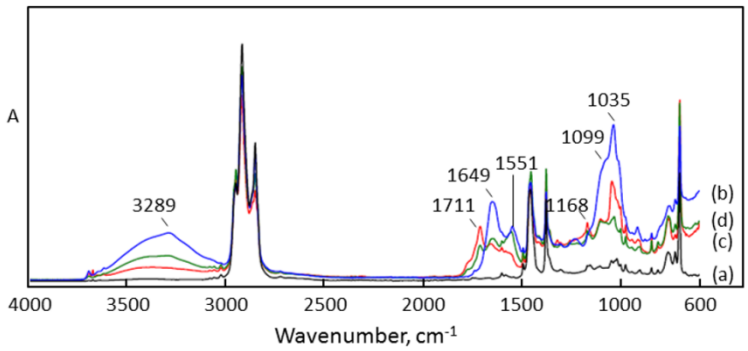

According to studies realized by Bonhomme et al. [43], when polymer is exposed to microbial action, the modifications observed in the FTIR profile are similar to those in samples exposed to weathering. Those authors reported bands in the region around 1088 cm^{-1} and assigned them to polysaccharides, which are the metabolites produced by microorganisms and the major constituents of biofilms. Formation of proteomic material was assigned to bands at 1655 cm^{-1}, 1636 cm^{-1}, 1539 cm^{-1} and 1523 cm^{-1} (that can be overlapped in Figure 5.9). The FTIR profiles from all loaded samples exposed to weathering and buried in soil were similar. The spectra from sub-products of polymer decomposition and biofilm formation were very similar, not being possible to assign the new bands to polymer degradation or biofilm formation.

It can be noted that there was an increase in band intensity in the region between 1800 cm^{-1} and 1500 cm^{-1} on the samples during weathering (Figure 5.9). And after burial in soil, those values increased even further. The samples presented a decrease in the region between 1280 cm^{-1} and 1000 cm^{-1} after burial in soil which was originated from oxidized groups.

It is accepted that in the presence of microorganisms the concentrations of these functional surface groups will increase or decrease due to microbial production or consumption [4]. Moreover, the production or consumption of functional groups will depend on the balance rates of oxidation and degradation, abiotic factors and the nature of the microorganisms present [4].

5.4 CONCLUSIONS

Regardless of additive content, a loss of mechanical characteristics was observed after weathering exposure in loaded and non-loaded compounds. At a variable level, the antibacterial properties of loaded TPE were verified during the first six months. After nine months of weathering exposure the samples lost their antibacterial properties and provided conditions for bacterial development. Samples exposed to weathering presented better biodegradation rate than unexposed samples.

It can be concluded that the incorporation of silver based additives in TPE formulation does not guarantee better mechanical resistance of the compounds after intense exposure weatherproof. Even after being subjected to intense abiotic action, the loaded TPE compounds showed antimicrobial properties. However, despite those properties, silver loaded compounds presented susceptibility to biodegradation by soil microbiota.

5.5 REFERENCES

1. SHAH, A. A.; HASAN, F.; HAMEED, A.; AHMED, S. **Role of microorganisms in biodegradation of plastics: Basics and methods in biodegradation of synthetic and natural plastics**. Saarbrücken: VDM Verlag, 2009. ISBN-13 978-3639118087
2. WRIGHT, D. **Failure of plastics and rubber products: causes, effects and case studies involving degradation**. Shawbury, Shrewsbury, Shropshire: Rapra Technology Limited, 2001. ISBN 1-85957-517-X
3. LUCAS, N.; BIENAIME, C.; BELLOY, C.; QUENEUDEC, M.; SILVESTRE, F.; NAVA-SAUCEDO, J-E. Polymer biodegradation: Mechanisms and estimation techniques. **Chemosphere**, v. 73, p. 429-442, 2008. Doi: 10.1016/j.chemosphere.2008.06.064
4. RESTREPO-FLÓREZ, J-M.; BASSI, A.; THOMPSON, M. R. Microbial degradation and deterioration of polyethylene - A review. **International Biodeterioration & Biodegradation**, v. 88, p. 83-90, 2014. Doi:

10.1016/j.ibiod.2013.12.014

5. HUECK, H. J. The Biodegradation of Materials – An appraisal. **International Biodeterioration and Biodegradation**, v. 48, p. 5-11, 2001.

6. WANG, R.; NEOH K. G.; SHI, Z.; KANG, E-T.; TAMBYAH, P. A.; CHIONG, E. Inhibition of *Escherichia coli* and *Proteus mirabilis* adhesion and biofilm formation on medical grade silicone surface. **Biotechnology and Bioengineering**, v.109, n. 2, p. 336-345, 2012. Doi: 10.1016/j.polymer.2012.02.046

7. YOSHIDA, S.; HIRAGA, K.; TAKEHANA, T.; TANIGUCHII, Y. H.; MAEDA, Y.; TOYOHARA, K.; MIYAMOTO, K.; KIMURA, Y.; ODA, K. A bacterium that degrades and assimilates poly(ethylene terephthalate). **Science**, v. 351, n. 6278, p. 1196-1199, 2016. Doi: 10.1126/science.aad6359

8. DESAI, N. P.; SYED, F. A.; HUBBELL, H.; HUBBELL, J. A. Surface-immobilized polyethylene oxide for bacterial repellence. **Biomaterials**, v. 13, n. 7, p. 417-420, 1992.

9. OLIANI, W. L.; PARRA, D. F.; LIMA, L. F. C. P.; LINCOPAN, N.; LUGAO, A. B.; Development of a nanocomposite of polypropylene with biocide action from silver nanoparticles. **Journal of Applied Polymer Science**, v. 132, p. 42218, 2015. Doi: 10.1002/APP.42218

10. JOKAR, M.; RAHMAN, R.A.; IBRAHIM, N. A.; ABDULLAH, L.C.; TAN, C. P. Melt Production and antimicrobial efficiency of low-density polyethylene (LDPE)-silver nanocomposite film. **Food Bioprocess Technology**, v. 5, p. 719–728, 2012. Doi: 10.1007/s11947-010-0329-1

11. PALOMBA, M.; CAROTENUTO, G.; CRISTINO, L.; DI GRAZIA, M. A.; NICOLAIS, F.; NICOLA, S. D. J. Activity of antimicrobial silver polystyrene nanocomposites. **Journal of Nanomaterials**, Article ID 185029, 7 pages, 2012. Doi: 10.1155/2012/185029.

12. SUN, T. Y.; BORNHÖFT, N. A.; HUNGERBÜHLER, K.; NOWACK, B. Dynamic probabilistic modeling of environmental emissions of engineered nanomaterials. **Environmental Science and Technology**, v. 50, p. 4701-4711, 2016. Doi: 10.1021/acs.est.5b05828

13. SISTEMA NACIONAL DE INFORMAÇÕES SOBRE SANEAMENTO (SNIS). **Diagnóstico do manejo de resíduos sólidos urbanos – 2014**. Brasil. Ministério das Cidades. Secretaria Nacional de Saneamento Ambiental. Brasília: SNSA/MCIDADES, 2016.

14. SISTEMA NACIONAL DE INFORMAÇÕES SOBRE SANEAMENTO (SNIS). **Diagnóstico dos serviços de água e esgotos – 2014**. Brasil. Ministério das Cidades. Secretaria Nacional de Saneamento Ambiental. Brasília: SNSA/MCIDADES, 2016.

15. SHIN, Y-J.; KWAK, J. I.; AN, Y-J. Evidence for the inhibitory effects of silver nanoparticles on the activities of soil exoenzymes. **Chemosphere**, v. 88, p. 524-529, 2012. Doi: 10.1016/j.chemosphere.2012.03.010

16. CALDER, A. J.; DIMKPA, C. O.; MCLEAN, J. E.; BRITT, D. W.; JOHNSON, W.; ANDERSON, A. J. Soil components mitigate the antimicrobial effects of silver nanoparticles towards a beneficial soil bacterium, *Pseudomonas chlororaphis*

O6. **Science of the Total Environment**, v. 429, p. 215-22, 2012. Doi: 10.1016/j.scitotenv.2012.04.049

17. GITIPOUR, A.; EL BADAWY, A.; ARAMBEWELA, M.; MILLER, B.; SCHECKEL, K.; ELK, M.; RYU, H.; GOMEZ-ALVAREZ, V.; DOMINGO, J. S.; THIEL, S.; TOLAYMAT, T. The impact of silver nanoparticles on the composting of municipal solid waste. **Environmental Science and Technology**, v. 47, p. 14385−14393, 2013. Doi: 10.1021/es402510a
18. INSTITUTO NACIONAL DE METEOROLOGIA (INMET). Estação Meteorológica de Observação de Superfície Automática de Campo Bom. Disponível em: http://www.inmet.gov.br/sonabra/pg_dspDadosCodigo.php?QTg4NA==
19. MONTAGNA, L. S.; FORTE, M. M. C.; SANTANA, R. M. C. Induced degradation of polypropylene with an organic pro-degradant additive. **Journal of Materials Science and Engineering A**, v. 3, n. 2, p. 123-131, 2013.
20. CATTO, A. L.; MONTAGNA, L. S.; SANTANA, R. M. C. Abiotic and biotic degradation of post-consumer polypropylene/ethylene vinyl acetate: wood flour composites exposed to natural weathering. **Polymer Composites**, 2015. Doi: 10.1002/pc.2361
21. RAJAKUMAR, K.; SARASVATHY, V.; CHELVAN, A. T.; CHITRA, R.; VIJAYAKUMAR, C. T. Natural weathering studies of polypropylene. **Journal of Polymer and the Environment**, v. 17, p. 191-202, 2009. Doi: 10.1007/s10924-009-0138-7
22. AL-SHABANAT, M. Study of the effect of weathering in natural environment on polypropylene and its composites: morphological and mechanical properties. **International Journal of Chemistry**, v. 3, n. 1, p. 129-141, 2011.
23. ALLEN, N. S.; EDGE, M.; MOURELATOU, D.; WILKINSON, A.; LIAUW, C.; PARELLADA, M. D.; BARRIO, J.; Influence of ozone on styrene–ethylene–butylene–styrene (SEBS) copolymer. **Polymer Degradation and Stability**, v. 79, p. 297–307, 2003.
24. RABELLO, M. S.; WHITE, J. R. Crystallization and melting behaviour of photodegraded polypropylene – 1: Chemi-crystallization. **Polymer**, v. 38, n. 26, p. 6379-6387, 1997.
25. ZHANG, Z.; WANG, S.; ZHANG, J. Large stabilizing effect of titanium dioxide on photodegradation of PVC/a-methylstyrene-acrylonitrile copolymer/impact modifier-matrix composites. **Polymer Composites**, v. 35, p. 2365, 2014. Doi: 10.1002/pc.22904
26. LV, Y.; HUANG, Y.; YANG, J.; KONG, M.; YANG, H.; ZHAO, J.; LI, G. Outdoor and accelerated laboratory weathering of polypropylene: A comparison and correlation study. **Polymer Degradation and Stability**, v. 112, p. 145-159, 2015. Doi: 10.1016/j.polymdegradstab.2014.12.023
27. RABELLO, M. S.; WHITE, J. R. Crystallization and melting behaviour of photodegraded polypropylene — II. Re-crystallization of degraded molecules. **Polymer**, v. 38, n. 26, p. 6389-6399, 1997. Doi: 10.1016/S0032-3861(97)00214-0

28. LONGO, C.; SAVARIS, M.; ZENI, M.; BRANDALISE, R. N.; GRISA, A. M. C. Degradation study of polypropylene (pp) and bioriented polypropylene (bopp) in the environment. **Materials Research**, v. 14, n. 4, p. 442-448, 2011. Doi: 10.1590/S1516-14392011005000080

29. ORLOV, A. S.; KISELEV, S. A.; KISELEVA, E. A.; BUDEEVA, A. V.; MASHUKOV, V. I. Determination of styrene-butadiene rubber composition by attenuated total internal reflection infrared spectroscopy. **Journal of Applied Spectroscopy**, v. 80, n. 1, p. 47-53, 2013.

30. LIN, J-H.; PAN, Y-J.; LIU, C-F.; HUANG, C-L.; HSIEH, C-T.; CHEN, C-K.; LIN, Z-I.; LOU, C-W. Preparation and compatibility evaluation of polypropylene/high density polyethylene polyblends. **Materials**, v. 8, p. 8850–8859, 2015. Doi: 10.3390/ma8125496

31. EGGINS, H. O. W.; MILLS, J.; HOLT, A.; SCOTT, G. Biodeterioration and biodegradation of synthetic polymers. IN: SYKES, G.; SKINNER, F. A. (Ed.). **Microbial aspects of pollution**. London: Academic Press, 1971. p. 267–277. ISBN: 0-12-648050-8

32. GULMINE, J. V.; AKCELRUD, L. FTIR characterization of aged XLPE. **Polymer Testing**, v. 25, p. 932–942, 2006.

33. ELANMUGILAN, M.; SREEKUMAR, P A.; SINGHA, N. K.; AL-HARTHI, M. A.; DE, S. K. Natural weather, soil burial and sea water ageing of low-density polyethylene: effect of starch/linear low-density polyethylene masterbatch. **Journal of Applied Polymer Science**, v. 129, p. 449-457, 2013. Doi: 10.1002/app.38769

34. RJEB, A.; TAJOUNTE, L.; IDRISSI, M. C. E.; LETARTE, S.; ADNOT, A.; ROY, D.; CLAIRE, Y.; PÉRICHAUD, A.; KALOUSTIAN, J. IR Spectroscopy study of polypropylene natural aging. **Journal of Applied Polymer Science**, v. 77, p.1742-1748, 2000.

35. WHITE, C. C.; TAN, K. T.; HUNSTON, D. L.; NGUYEN, T.; BENATTI, D. J.; STANLEY, D.; CHIN, J. W. Laboratory accelerated and natural weathering of styrene-ethylene-butylene-estyrene (SEBS) block copolymer. **Polymer Degradation and Stability**, v. 96, p. 1104-1110, 2011. Doi: 10.1016/j.polymdegradstab.2011.03.003

36. NICHOLS, D. Available active ingredients. In: NICHOLS, D. **Biocides in Plastics**. v. 15. United Kingdom: Rapra Review Reports, 2004. p. 19-28, 2004. ISBN 978-1-859757-512-3

37. SWIFT, G.; BACIU, R.; CHIELLINI, E. Environmentally degradable polyolefins. In: Celina, M. C.; Wiggins, J. S.; Billingham, N. C. **Polymer degradation and performance**. Washington: American Chemical Society Symposium Series, 2009. p. 2-16. ISBN: 978-0-8412-6978-1

38. ALBERTSSON, A-C.; BARENSTEDT, C.; KARLSSON, S.; LINDBERG, T. Degradation product pattern and morphology changes as means to differentiate abiotically and biotically aged degradable polyethylene. **Polymer**, v. 36, n. 16, p. 3075-3083, 1995.

39. TRIBEDI, P.; SIL, A. K. Cell surface hydrophobicity: a key component in the degradation of polyethylene succinate by *Pseudomonas sp*. AKS2. **Journal of**

Applied Microbiology, v. 116, p. 295-303, 2013. doi:10.1111/jam.12375

40. SCOTT, G. Initiation processes in polymer degradation. **Polymer Degradation and Stability,** v. 48, p. 315-324, 1995.
41. SILLEN, W. M. A.; THIJS, S.; ABBAMONDI, G. R.; JANSSEN, J.; WEYENS, N.; WHITE, J. C.; VANGRONSVELD, J. Effects of silver nanoparticles on soil microorganisms and maize biomass are linked in the rhizosphere. **Soil Biology and Biochemistry**, v. 91, p. 14-22, 2015. Doi: 10.1016/j.soilbio.2015.08.019
42. HE, S.; FENG, Y.; NI, J.; SUN, Y.; XUE, L.; FENG, Y.; YU, Y.; LIN, X.; YANG, L. Different responses of soil microbial metabolic activity to silver and iron oxide nanoparticles. **Chemosphere**, v. 147, p. 195-202, 2016. Doi: 10.1016/j.chemosphere.2015.12.055
43. BONHOMME, S.; CUER, A.; DELORT, A-M.; LEMAIRE, J.; SANCELME, M.; SCOTT, G. Environmental biodegradation of polyethylene. **Polymer Degradation and Stability**, v. 81, p. 441–452, 2003. Doi: 10.1016/S0141-3910(03)00129-0
44. LUZ, J. M. R.; PAES, S. A.; BAZZOLLI, D. M. S.; TÓTOLA, M. R.; DEMUNER, A. J.; KASUYA, M. C. M. abiotic and biotic degradation of oxo-biodegradable plastic bags by *Pleurotus ostreatus*. **Plos One**, v. 9, n. 11, p. 1-17, 2014. Doi: 10.1371/journal.pone.0107438.

6 EFFECT OF NATURAL AGEING ON SURFACE OF SILVER LOADED TPE AND ITS INFLUENCE IN ANTIMICROBIAL EFFICACY[3]

Abstract

The aim of this study is to characterize the modifications in silver loaded TPE surfaces exposed to weathering and their relation to susceptibility to microbial attack. Silver loaded TPE materials were exposed to natural ageing for nine months and modifications in antimicrobial properties and surface characteristics were evaluated. Chemical changes were investigated by using the infrared spectra. The average surface roughness and topography were determined by atomic force microscopy. Contact angle was measured to verify wettability conditions and surface free energy (SFE). After nine months of exposure, a decrease in the antimicrobial properties of loaded TPE compounds was observed. A reduction in surface roughness and improvement in wettability and high values of polar component of SFE were verified. The best antibacterial action was noticed in the sample with high Lewis acid force, lower roughness and lower carbonyl index.

Keywords: Thermoplastic elastomers; Surface properties; Antimicrobial; Silver, Natural ageing.

6.1 INTRODUCTION

Styrene-ethylene/butylene-styrene copolymer (SEBS)-based thermoplastic elastomers (TPE's) is widely used to produce devices with soft touch features. Bacterial contamination in SEBS-based TPE surfaces represents a health problem mainly in nosocomial settings. Despite SEBS-based TPE's is being used in a broad range of applications, there is a lack of information about the processes involved in microbial colonization of this type of surface. In addition, the different sorts of substances used in the processing of these polymers, such as the plasticizer (mineral oil) [1], can be a carbon source, with an influence on microbial proliferation by providing nutritional sources for the microorganisms' consumption [2, 3].

Biofilm formation begins with the attachment of microorganisms to a surface followed by the permeation of the cells inside extracellular substances originated from bacterial metabolism, ensuing biofilm maturation which is no longer possible to remove with usual cleaning methods [4]. To prevent biofilm formation, one strategy is to develop materials less susceptible to bacterial attachment. Seeking this aim, many

[3] Publicado como: TOMACHESKI, D.; PITTOL, M.; SIMÕES, D. N.; FERREIRA, V. F.; SANTANA, R. M. C. Effect of natural ageing on surface of silver loaded TPE and its influence in antimicrobial efficacy. **Applied Surface Science**, v. 405, p. 137-145, 2017. Doi: 10.1016/j.apsusc.2017.02.036

studies have been conducted to create antimicrobial materials either by incorporating biocidal additives [5, 6] or through surface modification [7-9].

A study performed by this research group proved the antimicrobial efficacy of silver loaded TPE [6]. An ensuing study showed that upon the exposition to natural ageing, even with the amount of silver unchanged, the loaded TPE compounds presented a reduction in their biocide action [10]. These results suggesting that, modifications in the polymer surface can be more significant to microbial colonization, than the leach of antimicrobial additive. This means that some characteristics of polymer surfaces can provide conditions to microbial attachment even in materials loaded with biocide substances. Pursuing this questioning, studies have been done relating the characteristic of surface of implantable materials and prostheses [11, 12] and the polymer biodegradation process [3, 13]. In all these studies the rating of wettability, carbonyl groups presence, modification in surface free energy and topography were addressed; however, further clarifications are needed.

Reckoning with the above discussions, the aim of this study is to characterize the modifications on silver loaded TPE surfaces exposed to weathering and to relate polymer surface characteristics to its susceptibility to microbial attack. The research hypotheses are that surface properties (wettability, surface free energy and topography) may have an effect on bacterial adherence and development in TPE surface and, thereafter, in the loss of antimicrobial efficacy of silver loaded compounds.

6.2 MATERIALS AND METHODS

6.2.1 Materials

The additives tested were bentonite organomodified with silver (referred to here as "Ag^+_bentonite"), silver ions supported in phosphate glass (referred to here as "Ag^+_phosphate") and nanosilver adsorbed on fumed silica (referred to here as "AgNp_silica"). The proportions used were 2.0%, 0.3% and 0.05% which were set in line with previous studies. The main characteristics of the additives are shown in Figure 6.1 based on a previous characterization reported in Tomacheski et al. [14]. The additives were incorporated into a TPE formulation compounded by styrene-ethylene/butylene-styrene copolymer (SEBS, 32% styrene, ethylene/butylene 32/68, linear, Mw 214.8 Da) polypropylene homopolymer (PP, melt flow index 1.5 g 10 min^{-1}

at 230°C), and white mineral oil (64% paraffinic and 36% naphtenic), at a ratio of 30/20/50, respectively. An antioxidant was added at a proportion of 0.1% to prevent thermal degradation during processing. An additive-free compound (Standard) was also used.

Figure 6.1 Micrographs and average diameter determined by transmission electron microscopy (TEM), diameter determined by laser diffraction, surface specific area (SSA), and zeta potential at different pH determined for (a) AgNp_silica, (b) Ag^+_phosphate, and (c) Ag^+_bentonite

	Micrographs obtained by TEM	Average diameter by TEM, µm	Diameter by laser diffraction, µm		SSA, $m^2 g^{-1}$	Zeta potential at pH, mV	
(a)	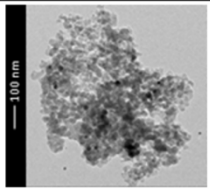	0.02	D_{10}	4.70	293.90	3	0.12
			D_{50}	9.20		5	-6.48
			D_{90}	28.99		7	-27.70
			Average	12.97		9	-27.53
						11	-35.77
(b)	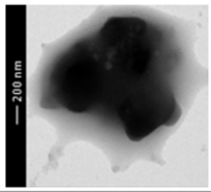	1.0	D_{10}	0.86	6.16	3	15.7
			D_{50}	1.50		5	6.82
			D_{90}	2.49		7	-21.80
			Average	1.61		9	-1.06
						11	-3.64
(c)	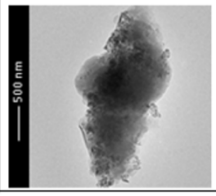	-	D_{10}	2.08	36.73	3	-8.31
			D_{50}	6.32		5	3.77
			D_{90}	13.92		7	-33.53
			Average	7.30		9	-32.17
						11	-42.30

6.2.2 TPE compounds preparation

The samples were prepared using a co-rotating double screw extruder (L/D 40 and 16 mm screw diameter, AX Plásticos) with temperature profile from 170°C to 190°C, speed of 300 rpm, feed rate of 1.5 kg h^{-1} and melt discharge temperature of 200°C. Test specimens in 2 mm thick plate form were prepared using injection molding machine (Haitian, PL860) at 190°C and an injection pressure of 17 bars.

6.2.3 Natural ageing experiments

The specimens were exposed to weathering for nine months (from August 2015 to May 2016), under real climatic conditions in accordance with ASTM 1435. The specimens were exposed in an outdoor station with 30° inclination from the ground located in Campo Bom city, southern Brazil (29º40'54"S and 51º03'25"W), 20 meters above sea level. The samples were collected every three months to study the effects of weathering.

6.2.4 Analytical methods

6.2.4.1 Microbiological studies

Japan Industrial Standard (JIS) Z 2801:2010 was applied to evaluate antimicrobial abilities of metal loaded TPE samples against *Staphylococcus aureus* ATCC 6538 (*S. aureus*) and *Escherichia coli* ATCC 8739 (*E. coli*). After weathering exposure, the TPE specimens (50 mm x 50 mm) were placed in a sterile Petri dish, and 400 µL of bacterial suspension of *E. coli* and *S. aureus* were inoculated on the specimen surfaces. All of them were incubated for 24 h at 35 ± 1°C. The results were expressed as a microbial value calculated from the difference between the number of colony forming units (CFU) per square centimeter at zero hour (initial) and after 24 h of incubation.

The Brazilian Association of Technical Standards (ABNT) NBR 15275 was used to evaluate the additive compounds' antimicrobial properties against the fungus *Aspergillus niger* (*A. niger*) ATCC 6275. TPE specimens (25 mm x 25 mm) were placed in a sterile Petri dish with agar, and 100 µL of fungus suspension were inoculated on the specimen surfaces. All of them were incubated for 7 days at 30 ± 2°C. The presence of inhibition zone (after 48 h of incubation) and hyphal growth (after 7 days of incubation) were evaluated with a stereoscopic microscope. The results were expressed as a percentage of the specimen area covered by the fungus.

6.2.4.2 Biofilm formation on SEBS-based TPE samples

Scanning electron microscopy (SEM) was performed to verify in vitro susceptibility of non-loaded TPE samples (Standard) exposed to the bacteria *Escherichia coli* ATCC 8739 (*E. coli*) and *Staphylococcus aureus* ATCC 6538 (*S. aureus*). To this end, the Standard sample was incubated for 24 h at 35 ± 1°C with inoculums of *E. coli* and *S. aureus*. After incubation, the TPE samples were immersed in a glutaraldehyde buffer (1.2 mL glutaraldehyde 25%, 5.0 mL 0.2 M PO_4^{3-} buffer and 3.8 mL H_2O). The fixed samples were rinsed three times with phosphate buffer (0.2 M in distillated water 1:1) to remove any traces of glutaraldehyde. The samples were dehydrated through a series of dehydrating solutions (30, 50, 70, and 90% acetone for 10 min each; 90 and 100% acetone for 20 min) and then subjected to critical point drying. TPE samples were deposited in a carbon type stuck to stub, metalized with gold. For image acquisition, a SEM of field

emission (SEM-FEG) (Inspect F50, FEI) was used with 20 kV, spot 3 and a working distance of 10 mm.

6.2.4.3 Analysis of fourier transform infrared spectroscopy

Fourier transform infrared spectroscopy attenuated total reflection (FTIR–ATR) was recorded on a PerkinElmer spectroscope (Frontier), on the side of the sample that was exposed to the weather. Each spectrum was recorded from a total of 8 scans at a resolution of 4 cm^{-1} at room temperature. The Spectrum software was used for spectra analysis. The carbonyl group index was calculated by the ratio of between 1850-1680 cm^{-1} by the area in the region of 1480-1400 cm^{-1}, corresponding to the characteristic bands of the carbonyl and CH_2 groups respectively.

6.2.4.4 Atomic force microscopy

Atomic force microscope (AFM) (Bruke, Dimension Icon® VT-1000, Santa Barbara, CA, USA) operated under ambient conditions was used to analyze the surface characteristics of polymeric plates in Peak Force Tapping® mode using an AFM Scanasyst-Air probe with a cantilever length of 115 µm and a width of 25 µm, drive frequency of 70 kHz. Changes in surface roughness were elucidated from the topography AFM images using Nanoscope Analysis (version 1.4, Bruker Corporation) software. To measure sample roughness (Ra), was calculated representing the average distance of the roughness profile from its imaginary center plane.

6.2.4.5 Surface wettability and surface free energy

Surface wettability and surface free energy (SFE) of the specimens were determined by contact angle measurement using deionized water, ethylene glycol, and hexane as reference liquids. The method consisted of applying a sessile drop of the reference liquid with a syringe onto a specimen and contact angles were measured at 2 seconds upon droplet application. The profile of the liquid drops was recorded using a contact angle analyzer (Labometric, LBDX) and measured using Image J (Version 1.40, National Institute of Health, USA) software. The surface free energies (γ) were then calculated by the three liquids phase method based on Van Oss–Chaundhury–Good theory of wettability. Total SFE consists of dispersive γ^D

(Lifshitz–Van der Waals) and polar γ^P (Lewis acid γ^+/base γ^-) forces, according to equation (1).

$$\gamma = \gamma^D + \gamma^P = \gamma^D + 2(\gamma^+\gamma^-)^{0.5} \quad (1)$$

When two phases, liquid and solid, are placed in close contact, the relationship of the adhesion to the contact angle of the liquid is presented with equation (2).

$$\gamma_L(1 - cos\Theta) = \gamma_L + \gamma_S - \gamma_{LS} \quad (2)$$

Where γ_L is the liquid surface tension, γ_S is the SFE to be determined; γ_{LS} presents interfacial free energy while Θ is liquid-solid contact angle. Furthermore, after replacing the value of interfacial free energy, equation (2) becomes equation (3).

$$\gamma_L(1 - cos\Theta) = 2[(\gamma_L^D\gamma_S^D)^{0.5} + (\gamma_L^+\gamma_S^-)^{0.5} + (\gamma_L^-\gamma_S^+)^{0.5}] \quad (3)$$

Unknown values of γ_S^D, γ_S^- and γ_S^+ could be found solving three linear equations when the values of SFE for reference liquids are replaced.

6.2.5 Statistical analysis

All data were expressed as means with standard deviations. The results were tested for normality of distribution by Shapiro-Wilk test. One-way Analysis Of Variance (ANOVA) or nonparametric alternative (Kruskal-Wallis) followed by Tukey or Dunn's multiple comparison tests were adopted for statistical analysis using PAST version 3.14 software (Natural History Museum, University of Oslo, Norway) [15]. The level of significance was set at 0.05.

6.3 RESULTS AND DISCUSSION

6.3.1 Bacterial development

Any given surface holds features that may influence on microbial attachment. To visualize biofilm formation on TPE surface, standard samples were analyzed by SEM after exposure to bacteria inoculums. As seen in Figure 6.2, SEBS-based TPE

compounds are prone to microbial growth when not loaded with antimicrobial substances. In Figure 6.2a it is noted that *S. aureus* population settled in a cavity and next to cracks on the TPE surface. To investigate which characteristics may affect the antimicrobial efficacy of loaded TPE compounds, surface properties of TPE such as wettability, free energy and topography were evaluated.

Figure 6.2 Growth of (a) *S. aureus* and (b) *E. coli* on SEBS-based TPE compounds

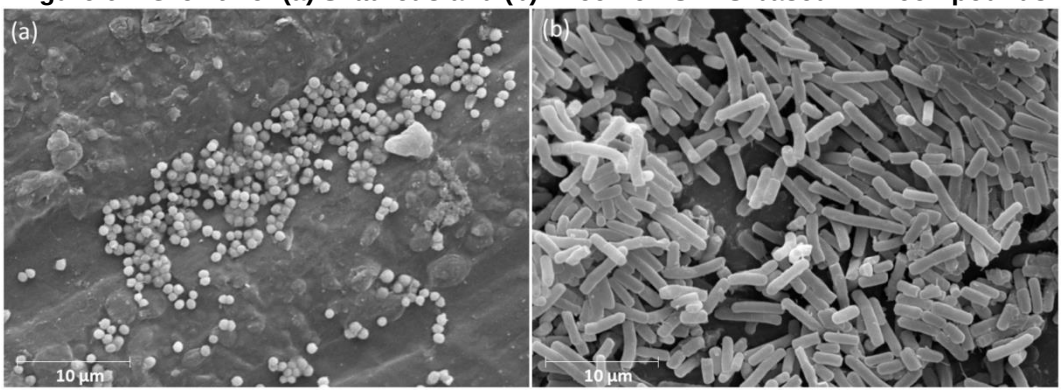

6.3.2 Antimicrobial properties

Figure 6.3 shows the antibacterial activity of TPE samples against *E. coli* and *S. aureus* strains at zero, three, six, and nine months of exposure to natural ageing. It was possible to verify a decrease in antibacterial efficacy along the time of exposure. After nine months of exposure, all samples showed *E. coli* proliferation, with an increase of around 200% in the bacteria population on the loaded sample, and around 600% on the Standard sample.

Figure 6.3 Antibacterial activity of loaded TPE samples against (a) *E. coli* and (b) *S. aureus* population after zero, three, six and nine months of natural ageing exposure. (-●-) Standard, (-♦-) Ag^+_bentonite, (-■-) Ag^+_phosphate, (-▲-) AgNp_silica

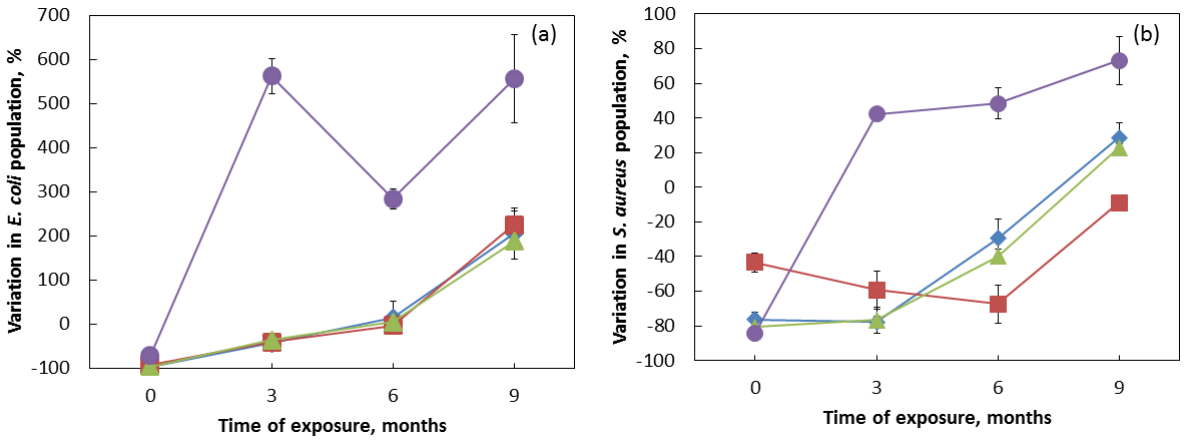

On the contrary, after nine months of exposure the samples loaded with Ag^+_phosphate maintained their antibacterial activity against *S. aureus*, eliminating 15% of the population after 24 h of incubation, while Ag^+_bentonite and AgNp_silica loaded samples provided a substrate to *S. aureus* with proliferation increasing by around 20%. The Standard sample presented an increase of 70% in the *S. aureus* population.

Fungal growth was not observed in samples exposed for three and six months, or in unexposed samples. However, after nine months of exposure all samples presented fungal growth (the percentages of surface recovery verified by stereoscopic microscope were 10% in Standard, 15% in Ag^+_bentonite, 10% in Ag^+_phosphate and 15% in AgNp_silica samples) as seen in Figure 6.4.

Study has been done to evaluate the growth of fungi in polymers blended with natural wood [16, 17], plasticized polyvinyl chloride [18, 19] and polyurethane [20]. Those studies showed that the growth of fungi in the polymer surface is variable and depends on the fungal species and substrate. Furthermore, comparisons between previous studies are hampered by the divergence in the experimental conditions and the different species of fungi.

Figure 6.4 Aged-TPE samples exposed to fungal growth

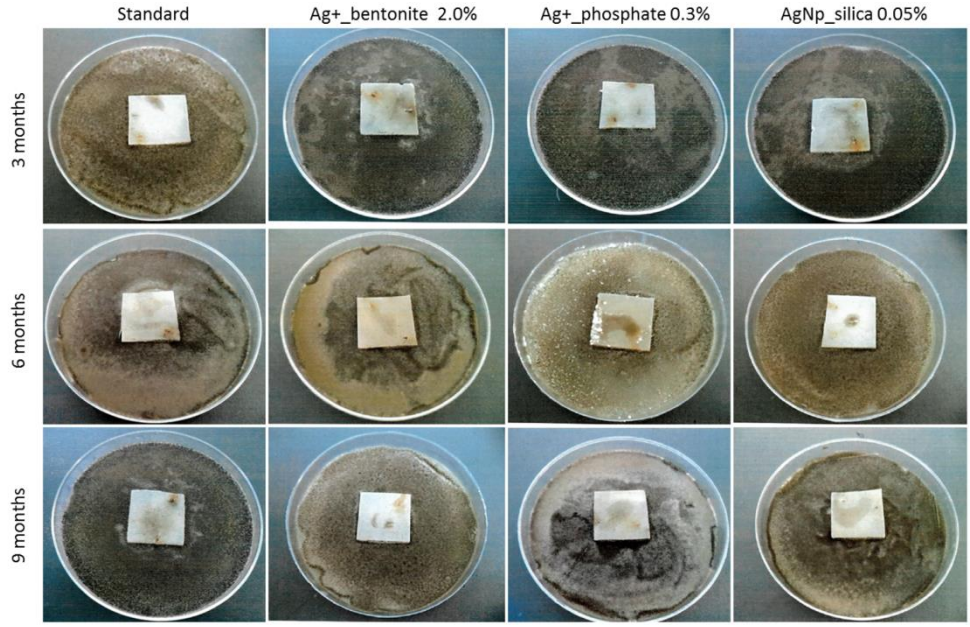

6.3.3 Modifications on the surface and their influence in antimicrobial properties

Figure 6.5 shows the carbonyl index throughout the assay. Formation of carbonyl groups on polymer surface is one of the main indicators of the extent of polymer degradation. The appearance of a peak in the region of 1800-1600 cm^{-1} is usually attributed to carbonyl groups from ketones, esters, lactones and others, originated from polymer chain cleavage and linkage with oxygen molecules, which is initiated by photodegradation due to UV radiation [21-23]. There was an increase in the carbonyl index only after six months of exposure. After nine months, the carbonyl indexes of Ag^{+}_bentonite and AgNp_silica were the highest, followed by the Standard and Ag^{+}_phosphate samples.

Figure 6.5 Carbonyl index (a, -●-) Standard, (b, -♦-) Ag^{+}_bentonite, (c, -■-) Ag^{+}_phosphate and (d, -▲-) AgNp_silica

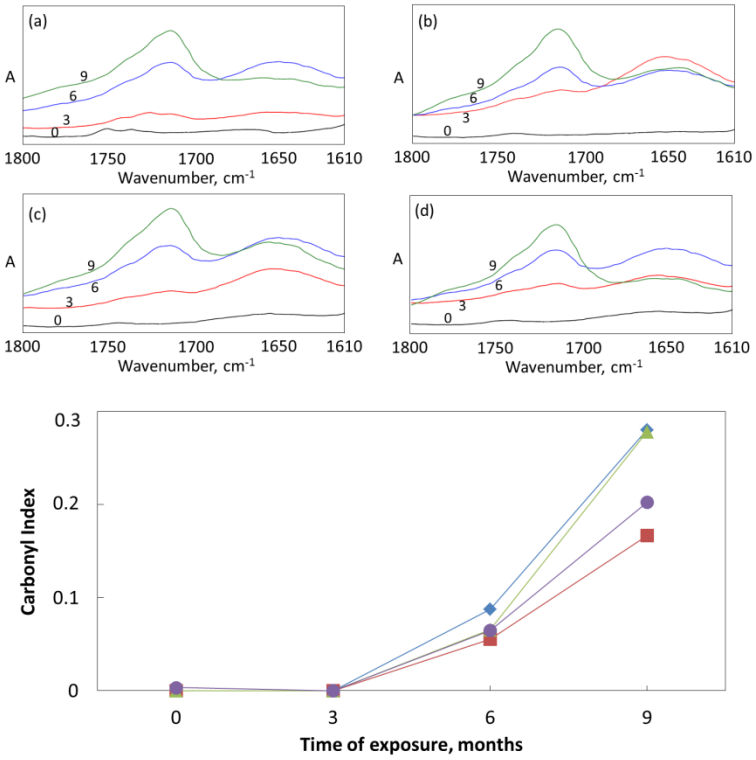

The degradation of polymer exposed to natural ageing can also be related to erosion and damage from acid precipitation [24, 25]. Inorganic fillers are hydrophilic and suffer more from acid precipitation than the polymer matrix [24]. This feature can explain why the carbonyl index was higher in compounds loaded with Ag^{+}_bentonite and AgNp_silica than in the Standard sample.

Figure 6.6 shows the modifications in sample wettability after nine months of exposure. It was noted that the water drops spread further after degradation, showing higher wettability.

Figure 6.6 Modifications in sample wettability before (right) and after (left) nine months of exposure: (a) Standard, (b) Ag^+_bentonite, (c) Ag^+_phosphate and (d) AgNp_silica

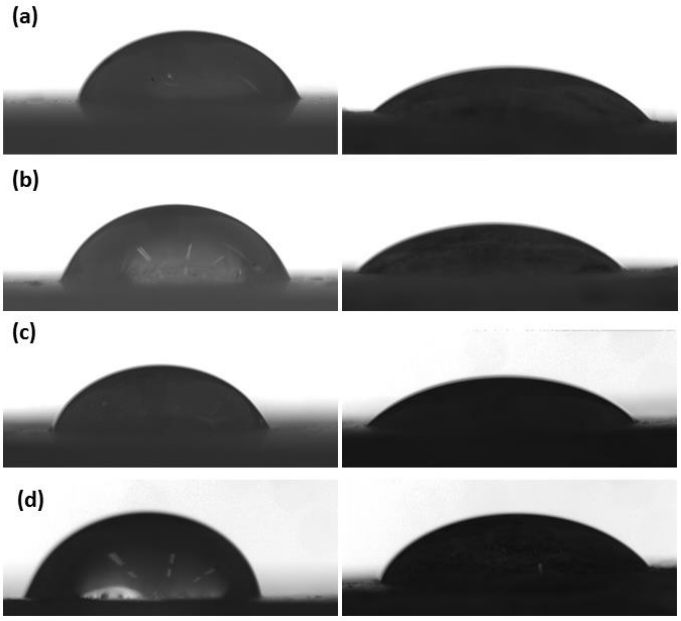

Numerical values of the water contact angle are show in Figure 6.7. The increase in wettability is correlated with modifications in surface chemistry due to the formation of oxygenated groups (verified in Figure 6.5), which improve surface polarity [26]. Also, the presence of a biofilm can change the contact angle of a surface and improve the wettability of hydrophilic surfaces or decrease that of hydrophobic ones [27].

Figure 6.7 Water contact angle (-●-) Standard, (-♦-) Ag^+_bentonite, (-■-) Ag^+_phosphate and (-▲-) AgNp_silica

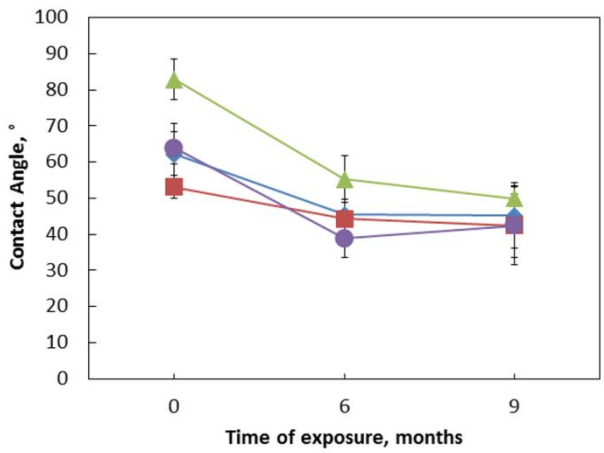

Biofilm formation occurs when proteins from microbial cells are absorbed into the substrate, promoting an interface for an initial connection. It is known that when in contact, the secretion of proteins reinforces adhesion and leads to bacterial fixation [28]. Besides that, the hydrophilic (low contact angle) and hydrophobic (contact angle higher than 90°) characteristics of surfaces may influence biofilm formation, since hydrophilic and hydrophobic surfaces accumulate a variety of proteins [29], which allows for the colonization of a diverse and complex microbial community.

Studies have been reported that highly hydrophobic surfaces are not prone to microbial attachment and biofouling [13]. Other studies suggest that hydrophilic surfaces have higher resistance to cell attachment than hydrophobic ones, since hydrophobic surfaces broaden protein contact to the polymeric substrate, which further assists biofilm formation [3, 11, 30].

This study found that the susceptibility of TPE samples to microbial attack increased as TPE wettability increased. These findings may be associated to the wettability features of the microorganism's external membrane, as well as specific groups on the polymer, surface roughness and charge [30]. Hydrophobic organisms prefer hydrophobic materials for adhesion and hydrophilic organism prefer hydrophilic surfaces [11]. Gram-positive bacteria (*S. aureus*) are more hydrophobic when compared to Gram-negative ones (*E. coli*) [11]. These relationships may explain the reason for greater development of the *E. coli* population on hydrophilic samples.

Biodegradation of some materials, such as polyurethane, by fungi has been achieved with the incorporation of hydrophilic polyols, such as poly (ethylene glycol) that decreased hydrophobicity and enabled the degradation rate by increasing water permeability [31, 32]. Moreover, as observed in polyvinyl chlorine formulations, the presence of ester groups from plasticizers can improve the biodegradation process through hydrolysis by fungal enzymes [19, 33-35]. In this study, the fungal development observed in TPE samples after nine months of weathering (Figure 6.4) can be explained by the increase in wettability (that improves fungal hydrolysis) and the formation of ester groups on the surface. In addition, an extensive chain scission could result in molecules that are small enough to be accessed by the fungi [36].

Table 6.1 shows the surface free energy (SFE) of samples after zero, six and nine months of ageing exposure. After nine months, there was an increase in SFE values for all samples, with higher values found in the Standard and Ag^{+}_phosphate.

The differences in SFE values may be related to differences in the particles' zeta potential (ZP) (Figure 6.1). The Ag^+_phosphate additive presented the highest ZP value, and the loaded compounds with this additive obtained high polar forces (Table 6.1).

Table 6.1 Surface free energy of samples before and after six and nine months of exposure

Compounds	Period of exposure	Surface Free Energy, mJ m^{-2}				
		Total (γ_S)	Dispersive (γ_S^D)	Polar (γ_S^P)	Lewis acid (γ_S^+)	Lewis base (γ_S^-)
Standard	**0**	$51.5 \pm 2.8^{a,1}$	18.4 ± 0.0	$33.1 \pm 2.8^{a,1}$	$8.4 \pm 0.5^{a,1}$	$32.8 \pm 6.8^{a,1}$
	6	$59.3 \pm 2.5^{a,1}$	18.4 ± 0.0	$40.9 \pm 2.5^{a,1}$	$5.1 \pm 1.3^{b,1}$	$83.7 \pm 12.9^{b,1}$
	9	$55.8 \pm 2.1^{a,1}$	18.4 ± 0.0	$37.4 \pm 2.1^{a,1}$	$5.3 \pm 1.3^{b,1}$	$67.6 \pm 13.5^{a,1}$
Ag^+_bentonite	**0**	$42.0 \pm 2.6^{a,1}$	18.4 ± 0.0	$23.6 \pm 2.6^{a,1}$	$4.6 \pm 1.2^{a,2}$	$32.3 \pm 12.8^{a,1}$
	6	$34.5 \pm 8.0^{a,2}$	18.4 ± 0.0	$16.1 \pm 8.0^{a,2}$	$1.1 \pm 0.8^{b,2}$	$67.7 \pm 5.7^{a,1}$
	9	$46.1 \pm 7.3^{a,1}$	18.4 ± 0.0	$27.7 \pm 7.3^{a,1}$	$2.9 \pm 1.0^{a,1}$	$66.1 \pm 12.6^{a,1}$
Ag^+_phosphate	**0**	$47.0 \pm 18.4^{a,1}$	18.4 ± 0.0	$28.6 \pm 18.7^{a,1}$	$6.7 \pm 1.9^{a,1}$	$34.0 \pm 4.6^{a,1}$
	6	$57.7 \pm 2.0^{a,1}$	18.4 ± 0.0	$39.3 \pm 2.0^{a,1}$	$6.0 \pm 0.^{a,1}$	$64.6 \pm 3.7^{a,1}$
	9	$56.5 \pm 4.4^{a,1}$	18.4 ± 0.0	$38.1 \pm 4^{a,1}$	$5.5 \pm 0.6^{a,1}$	$67.5 \pm 16.3^{a,1}$
AgNp_silica	**0**	$28.1 \pm 1.0^{a,2}$	18.4 ± 0.0	$9.7 \pm 1.0^{a,2}$	$2.2 \pm 0.5^{a,2}$	$10.9 \pm 2.3^{a,1}$
	6	$39.6 \pm 4.4^{a,2}$	18.4 ± 0.0	$21.2 \pm 4.4^{a,2}$	$2.5 \pm 0.6^{a,1}$	$44.1 \pm 8.2^{a,1}$
	9	$44.3 \pm 3.9^{a,1}$	18.4 ± 0.0	$25.9 \pm 3.9^{a,1}$	$2.9 \pm 0.9^{a,1}$	$59.4 \pm 5.4^{b,1}$

Note: The values are presented as the mean ±SD. For each compound values in the same column sharing identical superscript letter showed no significant differences between the periods of exposure ($p > 0.05$). For different compounds, values in the same column sharing identical superscript number showed no significant differences between the periods of exposure ($p > 0.05$).

The increase in the polar component over the exposure period, suggest the presence of polar groups (known to increase wettability) [7]. Additionally, the polar component could be associated with the formation of ester groups [7] and is in agreement with the carbonyl index found in this study (Figure 6.5). According to Brajkovic et al. [12], a higher polar component is prone to bacterial adhesion. Carvalho et al. [8] attributed the antibacterial properties of surfaces with high surface energy and reactivity to the difficulty of interactions between polymer and bacteria due to charge repulsion. On the contrary, and as observed in this study, several authors reported that samples with high surface free energy present an elevated percentage of bacterial adherences [12, 37].

Shao and Zhao [38] found that bacterial adhesion may decrease or increase with improved substrates surface energy, depending on the physical and chemical properties of the bacteria and substrates. However, in the case of chemical properties of bacteria, such as the values of bacterial membrane hydrophobicity–

hydrophilicity [7, 39] the predictions about bacterial attachment are complicated by the fact that these characteristics may vary within the same bacterial genus [40].

According to Knorr et al. [41] the difference in y_S^- components of SFE represents an important parameter in predicting bacterial adhesion; a surface with a high Lewis base component may attract bacteria more than that with a low Lewis base component. The Lewis acid component (γ_S^+) of the Ag^+_phosphate sample was higher than that of other samples. This factor may be related to the best antibacterial property of this sample, since the bacterial cell wall has a negative charge [42], which can cause a destructive attraction between sample surface and bacterial cell. Moreover, the Ag^+_phosphate and Ag^+_bentonite samples had similar values of Lewis base components and a different degree of *S. aureus* growth, which reinforces the importance of Lewis acid for antibacterial properties.

The modifications in antimicrobial properties of all samples seem to be related to a decrease in the Lewis acid component (γ_S^+) and increase in the Lewis base component (γ_S^-). Considering that similar polar values were found between the Standard and Ag^+_phosphate samples, we can infer that modifications in the polymer surface depicted by the presence of oxygenated groups can hamper the antibacterial activity of Ag^+_bentonite and AgNp_silica and otherwise assist its activity in the compound Ag^+_phosphate.

The dot out of line observed in Standard sample tested against *E. coli* population (after 6 months of exposure, Figure 6.3) matches with a higher Lewis base force value (Table 6.1) noted in the same sample. Once that TPE samples were exposed to weathering, over the exposure time, dirt may have accumulated unevenly on the surface of the samples, affecting the variables of adhesion and wetting of this surface and, consequently the adherence of bacteria.

Figure 6.8 shows the values of sample surface roughness, expressed as Ra and 3-D images. The alterations in sample roughness may be related to differences in size and format of the additives (as shown in Figure 6.1). With the exclusion of the Ag^+_bentonite sample that maintained constant roughness values (Ra_I = 88 and Ra_F = 88 nm), the other samples showed a decrease in Ra values - Standard (Ra_I =150 and Ra_F = 110 nm), Ag^+_phosphate (Ra_I =105 and Ra_F = 78 nm) and AgNp_silica (Ra_I = 149 and Ra_F = 100 nm). According to Ting et al. [43], the decrease in polymer roughness occurs at a high degree of cross-linking. The explanation is that for high levels of cross-linking a lasting surface layer is created and quash roughness

formation. The modification in polymer roughness is dependent on the kind of polymer and on the main cause of degradation (radiation, temperature, and rainfall, stress-cracking) [43, 44]. Decrease in roughness can also be related to erosion and attack by acid precipitation [24].

Figure 6.8 Representative 20 µm x 20 µm AFM 3-D images of (a) Standard initial; (b) Standard after nine months; (c) Ag^+_bentonite initial; (d) Ag^+_bentonite after nine months; (e) Ag^+_phosphate initial; (f) Ag^+_phosphate after nine months; (g) AgNp_silica initial and (h) AgNp_silica after nine months

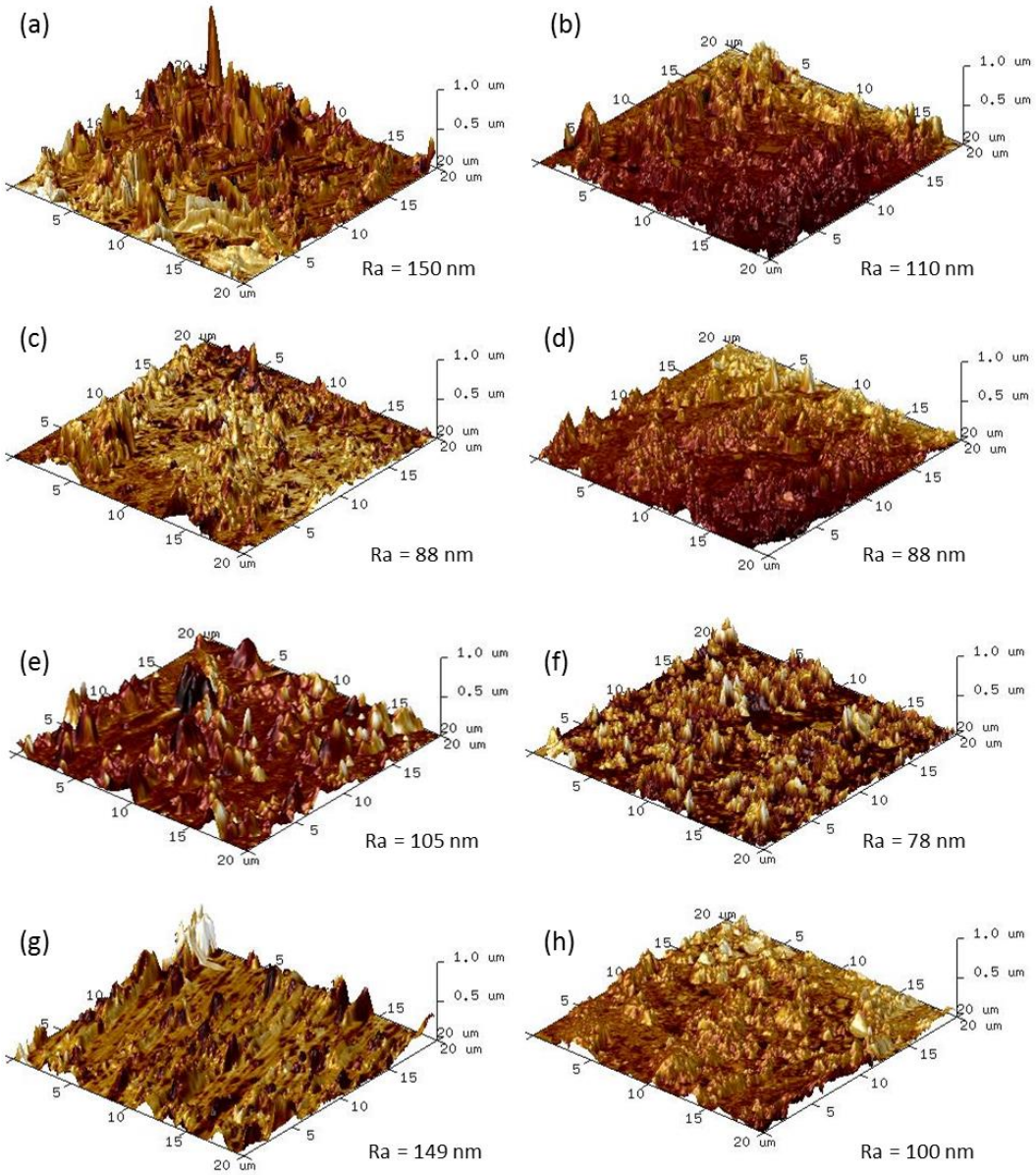

Sivakumar et al. [11] and Liu et al. [45] report that an increase in surface roughness can lead to a decrease in the contact angle. On the other hand, Al Radha and coworkers [37] could not relate the contact angle to surface roughness. According to Busscher et al. [46], if the Ra value of a solid surface is less than 100

nm, the contact angle is not influenced by roughness. Finally, in smooth surfaces with contact angle between 60° and 86°, surface roughening did not influence the contact angle. These studies reported that there are no consensuses on the relationship between roughness and contact angle.

It is difficult to correlate surface roughness and bacterial adhesion. Some studies report that rougher surfaces promote bacterial adhesion by increasing surface irregularities, which foment the substrate for bacterial adhesion [11, 38, 47]. Thus, the smooth surface of the Ag^+_phosphate sample (Ra_F = 78 nm) could contribute to the low bacterial development observed in this sample.

6.4 CONCLUSIONS

In the present study it was possible to conclude that modifications in silver loaded TPE surface, throughout the sample degradation, made the polymer prone to bacterial colonization and fungal growth. After weathering exposure, TPE increased its wettability and surface free energy raising its susceptibility to microbial development. However, the Ag^+_phosphate loaded sample maintained its antibacterial activity against *S. aureus* population after weathering exposure. The better performance of sample loaded with Ag^+_phosphate can be related to its high Lewis acid (γ_S^+) component of surface free energy, low carbonyl index and a surface more smoother than the other loaded compounds. Based on these facts we conclude that the loss of antimicrobial efficacy is a response to a group of modifications, as the reduction in hydrophobicity and decrease in Lewis acid (γ_S^+) component of the TPE samples.

6.5 REFERENCES

1. BARBES, L.; RĂDULESCU, C.; STIHI, C.; ATR-FTIR spectrometry characterization of polymeric materials. **Romanian Reports in Physics**, v. 66, n. 3, p. 765–777, 2014.
2. EGGINS, H. O. W.; MILLS, J.; HOLT, A.; SCOTT, G. Biodeterioration and biodegradation of synthetic polymers. IN: SYKES, G.; SKINNER, F. A. (Ed.). **Microbial aspects of pollution**. London: Academic Press, 1971. p. 267–277. ISBN: 0-12-648050-8
3. TRIBEDI, P.; SIL, A. K. Cell surface hydrophobicity: a key component in the degradation of polyethylene succinate by *Pseudomonas sp*. AKS2. **Journal of**

Applied Microbiology, v. 116, p. 295-303, 2013. Doi: 10.1111/jam.12375

4. CAPPITELLI, F.; POLO, A.; VILLA, F. Biofilm formation in food processing environments is still poorly understood and controlled. **Journal of Food Engineering**, v. 6, p. 29–42, 2014. Doi: 10.1007/s12393-014-9077-8
5. PALZA, H.; QUIJADA, R.; DELGADO, K. Antimicrobial polymer composites with copper micro and nanoparticles: Effect of particle size and polymer matrix. **Journal of Bioactive and Compatible Polymers**, p. 1–15, 2015. Doi: 10.1177/0883911515578870
6. TOMACHESKI, D.; PITTOL, M.; RIBEIRO, V.F.; SANTANA, R.M.C.; Efficiency of silver-based antibacterial additives and its influence in thermoplastic elastomers. **Journal of Applied Polymer Science**, v. 133, p. 43956, 2016. Doi: 10.1002/app.43956
7. MAHFOUDH, A.; PONCIN-ÉPAILLARD, F.; MOISAN, M.; BARBEAU, J. Effect of dry-ozone exposure on different polymer surfaces and their resulting biocidal action on sporulated bacteria. **Surface Science**, v. 604, p. 1487–1493, 2010. Doi: 10.1016/j.susc.2010.05.013
8. CARVALHO, D.; SOUSA, T.; MORAIS, P. .; PIEDADE, A. P. Polymer/metal nanocomposite coating with antimicrobial activity against hospital isolated pathogen. **Applied Surface Science**, v. 379, p. 489–496, 2016. Doi: 10.1016/j.apsusc.2016.04.109
9. BASTARRACHEA, L. J.; GODDARD, J. M. Self-healing antimicrobial polymer coating with efficacy in the presence of organic matter. **Applied Surface Science**, v. 378, p. 479–488, 2016. Doi: 10.1016/j.apsusc.2016.03.198
10. TOMACHESKI, D.; PITTOL, M.; LOPES, A. P. M.; SIMÕES, D. N.; RIBEIRO, V. F.; SANTANA, R. M. C. Effects of weathering on mechanical, antimicrobial properties and biodegradation process of silver loaded TPE compounds. **Journal of Polymer and the Environment**, 2017. Doi: 10.1007/s10924-016-0927-8
11. SIVAKUMAR, P. M.; IYER, G.; NATESAN, L.; DOBLE, M. 3-Hydroxy-4-methoxychalcone as a potential antibacterial coating on polymeric biomaterials, **Applied Surface Science**, v. 256, p. 6018–6024, 2010. Doi: 10.1016/j.apsusc.2010.03.112
12. BRAJKOVIC, D.; ANTONIJEVIC, D.; MILOVANOVIC, P.; KISIC, D.; ZELIC, K.; DJURIC, M.; RAKOCEVIC, Z. Surface characterization of the cement for retention of implant supported dental prostheses: In vitro evaluation of cement roughness and surface free energy. **Applied Surface Science**, v. 311, p. 131–138, 2014. Doi: 10.1016/j.apsusc.2014.05.027
13. LOBELLE, D.; CUNLIFFE, M. Early microbial biofilm formation on marine plastic debris. **Marine Pollution Bulletin**, v. 62, p. 197–200, 2011. Doi: 10.1016/j.marpolbul.2010.10.013
14. TOMACHESKI, D.; PITTOL, M.; SIMÕES, D. N.; RIBEIRO, V. F.; SANTANA, R.M.C. Effects of silver adsorbed on fumed silica, silver phosphate glass, bentonite organomodified with silver and titanium dioxide in aquatic indicator organisms. **Journal of Environment Science**, 2017. Doi: 10.1016/j.jes.2016.07.018

15. HAMMER, Ø.; HARPER, D. A. T.; RYAN, P. D. PAST: Paleontological statistics software package for education and data analysis. **Palaeontologia Electronica**, v. 4, n. 1, p. 1-9, 2001.

16. SUDÁR, A.; LÓPEZ, M. J.; KELEDI, G.; VARGAS-GARCÍA, M. C.; SUÁREZ-ESTRELLA, F.; MORENO, J.; BURGSTALLER, C.; PUKÁNSZKY, B. Ecotoxicity and fungal deterioration of recycled polypropylene/wood composites: Effect of wood content and coupling. **Chemosphere**, v. 93, p. 408–414, 2013. Doi: 10.1016/j.chemosphere.2013.05.019

17. CATTO, A. L.; ROSSETO, E. S.; RECK, M. A.; ROSSINI, K.; SILVEIRA, R. M. B.;. SANTANA, R. M. C. Growth of white rot fungi in composites produced from urban plastic waste and wood. **Macromolecular Symposia**, v. 344, p. 33–38, 2014. Doi: 10.1002/masy.201300216

18. WEBB, J. S.; NIXON, M.; EASTWOOD, I. M.; GREENHALGH, M.; ROBSON, G. D.; HANDLEY, P.S. Fungal colonization and biodeterioration of plasticized polyvinyl chloride. **Applied and Environmental Microbiology**, v. 66, n. 8, p. 3194–3200, 2000.

19. SABEV, H. A.; HANDLEY, P. S.; ROBSON, G.D. Fungal colonization of soil buried plasticized polyvinyl chloride (pPVC) and the impact of incorporated biocides. **Microbiology**, v. 152, p. 1731–1739, 2006. Doi: 10.1099/mic.0.28569-0

20. OPREA, S.; GRADINARIU, P.; JOGA, A.; ZORLESCU, B.; OPREA, V.; POTOLINCA, V. O. Fungal degradation behavior of two series of polyurethane urea composites obtained by different silver incorporation methods. **Journal of Elastomers and Plastics**, p. 1-12, 2016. Doi: 10.1177/0095244316639636.

21. ALLEN, N. S.; EDGE, M.; WILKINSON, A.; LIAUW, C.; MOURELATOU, D.; BARRIO, J.; MARTÍNEZ-ZAPORTA, M. A. Degradation and stabilisation of styrene-ethylene-butadiene-styrene (SEBS) block copolymer. **Polymer Degradation and Stability**, v. 71, p. 113-122, 2001.

22. GULMINE, J. V.; AKCELRUD, L. FTIR characterization of aged XLPE. **Polymer Testing**, v. 25, p. 932–942, 2006.

23. LV, Y.; HUANG, Y.; YANG, J.; KONG, M.; YANG, H.; ZHAO, J.; LI, G. Outdoor and accelerated laboratory weathering of polypropylene: A comparison and correlation study. **Polymer Degradation and Stability**, v. 112, p. 145-159, 2015. Doi: 10.1016/j.polymdegradstab.2014.12.023

24. WANG, X.; KUMAGAI, S.; YOSHIMURA, N. Contamination performances of silicone rubber insulator subjected to acid rain. **IEEE Transactions on Dielectrics and Electrical Insulation**, v. 5, n. 6, p. 909-916, 1998.

25. AZUMA, Y.; TAKEDA, H.; WATANABE, S.; NAKATANI, H. Outdoor and accelerated weathering tests for polypropylene and polypropylene/talc composites: A comparative study of their weathering behavior. **Polymer Degradation and Stability**, v. 94, p. 2267–2274, 2009. Doi: 10.1016/j.polymdegradstab.2009.08.008

26. SLEPICKA, P.; KASÁLKOVÁ, N. S; STRÁNSKÁ, E.; BACÁKOVÁ, L.; SVORCÍK, V. Surface characterization of plasma treated polymers for applications as biocompatible carriers. **eXPRESS Polymer Letters**, v. 7, n. 6,

p. 535–545, 2013. Doi: 10.3144/expresspolymlett.2013.50

27. SCHNEIDER, R. C. P.; MARSHALL, K. C. Retention of the Gram-negative marine bacterium SW8 on surfaces - effects of microbial physiology, substratum nature and conditioning films. **Colloids and Surfaces B: Biointerfaces**, v. 2, p. 387-396, 1994.
28. DUFRENE, Y. F.; BOONAERT, C. J.-P.; ROUXHET, P. G. Adhesion of *Azospirillum brasilense*: role of proteins at the cell-support interface. **Colloids and Surfaces B: Biointerfaces**, v. 7, p. 113-128, 1996.
29. BRUINSMA, G.M.; VAN DER MEI, H.C.; BUSSCHER; H.J. Bacterial adhesion to surface hydrophilic and hydrophobic contact lenses. **Biomaterials**, v. 22 p. 3217–3224, 2001.
30. CUNLIFFE, D.; SMART, C. A.; ALEXANDER, C.; VULFSON, E. N. Bacterial adhesion at synthetic surfaces. **Applied and Environmental Microbiology**, v. 65, n. 11, p. 4995–5002, 1999.
31. YEGANEH, H.; HOJATI-TALEMI, P.; Preparation and properties of novel biodegradable polyurethane networks based on castor oil and poly(ethylene glycol). **Polymer Degradation and Stability**, v. 92, p. 480-489, 2007. Doi: 10.1016/j.polymdegradstab.2006.10.011
32. OPREA, S. Dependence of fungal biodegradation of PEG/castor oil-based polyurethane elastomers on the hard-segment structure. **Polymer Degradation and Stability**, v. 95, p. 2396-2404, 2010. Doi: 10.1016/j.polymdegradstab.2010.08.013
33. GUMARGALIEVA, K.Z.; ZAIKOV, G.E.; SEMENOV, S.A.; ZHDANOVA, O.A. The influence of biodegradation on the loss of a plasticiser from poly(vinyl chloride). **Polymer Degradation and Stability**, v. 63, p. 111-112, 1999.
34. EL-AGHOURY, A.; VASUDEVA. R. K.; BANU, D.; ELEKTOROWIC, M.; FELDMAN, D. Contribution to the study of fungal attack on some plasticized vinyl formulations. **Journal of Polymer and the Environment**, v. 14, p. 135–147, 2006. Doi: 10.1007/s10924-006-0004-9
35. PRADEEP, S.; FASEELA, P.; JOSH, M. K. S.; BALACHANDRAN, S.; DEVI, R. S.; BENJAMIN, S. Fungal biodegradation of phthalate plasticizer in situ, **Biodegradation**, v. 24, p. 257–267, 2013. Doi: 10.1007/s10532-012-9584-3
36. ZAHRA, S.; ABBAS, S. S.; MAHSA, M-T; MOHSEN, N. Biodegradation of low-density polyethylene (LDPE) by isolated fungi in solid waste medium. **Waste Management**, v. 30, p. 396–401, 2010. Doi: 10.1016/j.wasman.2009.09.027
37. AL-RADHA, A. S. D.; DYMOCK, D.; YOUNES, C.; O'SULLIVAN, D. Surface properties of titanium and zirconia dental implant materials and their effect on bacterial adhesion. **Journal of Dentistry**, v. 40, p. 146–153, 2012. Doi: 10.1016/j.jdent.2011.12.006
38. SHAO, W.; ZHAO, Q. Influence of reducers on nanostructure and surface energy of silver coatings and bacterial adhesion. **Surface and Coatings Technology**, v. 204, p. 1288–1294, 2010. Doi: 10.1016/j.surfcoat.2009.10.015
39. FENG, G.; CHENG, Y.; WANG, S-Y.; BORCA-TASCIUC, D. A.; WOROBO, R. W.; MORARU C.I. Bacterial attachment and biofilm formation on surfaces are

reduced by small-diameter nanoscale pores: how small is small enough? **NPJ Biofilms Microbiomes**, v. 1, p. 15022, 2015. Doi:10.1038/npjbiofilms.2015.22

40. LUO, G.; SAMARANAYAKE, L. P. *Candida glabrata*, an emerging fungal pathogen, exhibits superior relative cell surface hydrophobicity and adhesion to denture acrylic surfaces compared with *Candida albicans*. **APMIS**, v. 110, p. 601–10, 2002.

41. KNORR, S. D.; COMBEA, E. C.; WOLFF, L. F.; HODGES, J. S. The surface free energy of dental gold-based materials. **Dental Materials**, v. 21, p. 272–277, 2005. Doi: 10.1016/j.dental.2004.06.002

42. EGGER, S.; LEHMANN, R. P.; HEIGHT, M. J.; LOESSNER, M. J.; SCHUPPLER, M. Antimicrobial properties of a novel silver-silica nanocomposite material. **Applied and Environmental Microbiology**, v. 75, p. 2973–2976, 2009. Doi: 10.1128/AEM.01658-08.

43. TING, Y-H.; LIU, C.-C.; PARK, S-M.; JIANG, H.; NEALEY, P. F; WENDT, A. E. Surface roughening of polystyrene and poly(methyl methacrylate) in Ar/O_2 plasma etching. **Polymers**, v. 2, p. 649-663, 2010. Doi:10.3390/polym2040649

44. CHEN, Y.; CHOU, I-N.; TSAI, Y-H.; WU, H-S. Thermal degradation of poly(3-hydroxybutyrate) and poly(3-hydroxybutyrate-co-3-hydroxyvalerate) in drying treatment. **Journal of Applied Polymer Science**, v. 130, p. 3659–3667, 2013. Doi: 10.1002/app.39616

45. LIU, Y.; WU, N.; WEI, Q.; CAI, Y.; WEI, A. Wetting behavior of electrospun poly(l-lactic acid)/ poly(vinyl alcohol) composite nonwovens. **Journal of Applied Polymer Science**, v. 110, p. 3172–3177, 2008. Doi: 10.1002/app.28904

46. BUSSCHER, H. J.; VAN PELT, A. W. J.; DE BOER, P.; DE JONG, H. P.; ARENDS, J. The effect of surface roughening of polymers on measured contact angles of liquids. **Colloids and Surfaces A**, v. 9, p. 319-331, 1984.

47. YODA, I.; KOSEKI, H.; TOMITA, M.; SHIDA, T.; HORIUCHI, H.; SAKODA, H.; OSAKI, M. Effect of surface roughness of biomaterials on *Staphylococcus epidermidis* adhesion. **BMC Microbiology**, v.14, p. 234, 2014. Doi: 10.1186/s12866-014-0234-2

7 EFFECTS OF SILVER ADSORBED ON FUMED SILICA, SILVER PHOSPHATE GLASS, BENTONITE ORGANOMODIFIED WITH SILVER AND TITANIUM DIOXIDE IN AQUATIC INDICATOR ORGANISMS[4]

Abstract

In order to reduce the level of transmission of diseases caused by bacteria and fungi, the development of antimicrobial additives for use in personal care, hygiene products, clothing and others has increased. Many of these additives are based on metals such as silver and titanium. The disposal of these products in the environment has raised concerns pertaining to their potential harmfulness for beneficial organisms. The objective of this study was to evaluate the influence of the shape, surface chemistry, size and carrier of three additives containing silver and one with titanium dioxide (TiO_2) on microcrustacean survival. Daphnia magna was used as a bioindicator for acute exposure test in suspensions from 0.0001 to 10000 mg L^{-1}. Ceriodaphnia dubia was used for chronic test in TiO_2 suspensions from 0.001 to 100 mg L^{-1}. Daphnia magna populations presented high susceptibility to all silver based additives, with 100% mortality after 24 h of exposure. A different result was found in the acute experiments containing TiO_2 suspensions, with mortality rates only after 48 h of incubation. Even on acute and chronic tests, TiO_2 did not reach a linear concentration-response versus mortality, with 1 mg L^{-1} being more toxic than 10000 mg L^{-1} on acute test and 0.001 mg L^{-1} more toxic than 0.01 mg L^{-1} m on chronic assay. Silver based materials toxicity was attributed to silver itself, and had no relation to either form (nano or ion) or carrier (silica, phosphate glass or bentonite). TiO_2 demonstrated to have a low acute toxicity against D. magna.

Keywords: *Daphnia magna; Ceriodaphnia dubia*; Titanium dioxide; Silver ion; Nanosilver.

7.1 INTRODUCTION

Due to the known antimicrobial characteristics of silver (Ag) and titanium dioxide (TiO_2), the use of these elements is increasing in many industrial fields and consumer use materials (e.g., surface coating, electronics, clothes, cosmetics, shoes, keyboards, toothpaste, sunscreen, etc.) [1, 2]. However, while these elements may provide a manner to prevent infections by interfering in pathogenic microorganism proliferation, they may potentially impact the environment when released and transported into air, water, and soil ecosystems during their product life-cycle [3]. In

[4] Publicado como: TOMACHESKI, D.; PITTOL, M.; SIMÕES, D. N.; FERREIRA, V. F.; SANTANA, R. M. C. Effects of silver adsorbed on fumed silica, silver phosphate glass, bentonite organomodified with silver and titanium dioxide in aquatic indicator organisms. **Journal of Environmental Sciences**, 2016. Doi: 10.1016/j.jes.2016.07.018

this respect, an assessment of metal particles regarding their effects on human health and environmental is necessary [4].

In the aquatic environment, organisms can come into contact with substances that cause chromosomal aberrations, leading to impairment of cell division and tumor formation [5]. The researches have focused on the toxicity of Ag and TiO_2 particles to organisms, including algae [6, 7], bacteria [8, 9], invertebrates such as cladocerans [9, 10] and vertebrates such as fish [11-13]). *Daphnia magna* (*D. magna*) is recognized as a key organism in freshwater ecosystems by being important phytoplankton consumer, while they are preferentially preyed upon by fish [14]. Also, because their filter feeding mechanisms [15, 16], sensitivity to environmental pollution, small body size and short life spans, *D. magna* is considered the most sensitive organism in the food web [17, 18], being used to assess the health of environments in ecotoxicological investigations [19-21].

A wide range of silver modifications have been employed to improve silver antimicrobial capacity, like carbon nanotubes with silver [22], silver/silica nanocomposites [23], zeolites doped with silver [24], and silver nanoparticles [25]. The mechanisms reported about metal particles' toxicity have been variable depending on the carrier, surface coatings, size and system [26]. Since nanoparticles (Nps) can interact in unpredicted ways with biological systems, a better understanding of the behavior of metal particles with different characteristics and interactions with key aquatic species is required [27]. Ag can be ranked after Hg (mercury) as having a high potential cumulative into daphnid bodies [19]. Also, the ionic form Ag^+ is described as being the most harmful to aquatic organisms [28]. Silver nanoparticles (AgNp) are reported as more highly reactive and toxic [29]. On the other hand, TiO_2 microparticles have been reported as being inert, non-toxic and non-migratory [30], with a lethal concentration (LC_{50}) higher than 100 mg L^{-1} for nanoform and non-nanoform TiO_2 [31]. Though, studies with nano TiO_2 have described EC_{50}-48h around 8 mg L^{-1} in acute test [32] and LC_{50}-48 h of 7.75 mg L^{-1} [33].

Reckoning with this fact, this study aims to investigate the toxicity effects of nanosilver, silver ions and titanium dioxide (TiO_2) particles toward aquatic crustaceans *Daphnia magna (D. magna*) and *Ceriodaphnia dubia* (*C. dubia*). The silver additives tested have three different forms: silver nanoparticles on fumed silica (AgNp_silica), silver phosphate glass (Ag^+_phosphate) and bentonite organomodified

with silver (Ag^+_bentonite). The goal of comparing Ag and TiO_2 was to reveal potential differences in toxic mechanisms between these elements. Additionally, *C. dubia* reproduction was investigated after the exposition to TiO_2.

7.2 MATERIAL AND METHODS

7.2.1 Characterization of the particles

Four additives were tested; nanosilver adsorbed on fumed silica ("AgNp_silica"), silver ions supported in phosphate glass ("Ag^+_phosphate"), bentonite organomodified with silver ("Ag^+_bentonite") and a commercial rutile titanium dioxide ("TiO_2").

Determination of mineral composition was held by qualitative analysis by X-ray diffraction, in a PanAnalytical X'pert PRO (PanAnalytical, The Netherlands) and software X'PertHighScore (PanAnalytical, The Netherlands). Particle size distribution was determined by laser diffraction, the equipment used was a CILAS 1180 (Cilas, Orleans, France) particle size analyzer, with scanning range between 0.04 µm and 2500 µm. AgNp_silica, Ag^+_phosphate and TiO_2 were predispersed in deionized water using ultrasound (60 s), Ag^+_bentonite was predispersed in isopropyl alcohol.

For transmission electron microscopy (TEM) G2 T20 (Tecnai), samples were dispersed in ethanol by ultrasound for 30 min. The samples were prepared by mounting a drop of the ethanol suspension containing the particles on a 300 mesh copper grid carbon film. Image acquisition was through acceleration voltage of 200 kV. The average particle diameter and scale distribution were calculated using ImageJ version 1.40g software.

The specific surface area (SSA) was measured by nitrogen adsorption using BET method. Measurements were performed by a Quantachrome Nova 1000 (Quantachrome Instruments, Boynton Beach, FL, USA) and surface area analyzer. Samples were dried in an oven at 110°C for 24 h and then vacuum at 200°C for 3 h.

The zeta potential (ZP) measurements were carried out using a zeta scaler Zetasizer NanoZ, (Malvern Instruments, Malvern, UK). Each sample was dispersed in deionized water to obtain suspensions at 1%. Suspension pH was adjusted to 3, 5, 7, 9 and 11 using NaOH 0.1 M or HCl 0.1 M.

7.2.2 *Daphnia magna* preparation to the acute toxicity assays

Acute toxicity tests were conducted according to ABNT NBR 12713 [34]. The acute 24 h and 48 h toxicity tests were performed using neonate (2 h and 26 h old) *D. magna* (Landesamt Für Wasser und Abfall (LWA), Nordrhein-Westfalen, Düsseldorf, Germany). The animals were derived from the laboratory stock culture at the test facility, where they were reared in artificial fully defined M4 medium at 20°C. Culture medium was renewed twice weekly and the daphnids were fed with a suspension of the unicellular green algae *Desmodesmus subspicatus* and fish-yeast compost.

7.2.3 Preparation of solutions

For stock suspension preparation, appropriate amounts of Ag and TiO_2 particles were suspended in sterilized double distilled water and dispersed by shaking for 30 min (1500 r min^{-1} at 25°C) in a magnetic stirrer-SP-160 (Advantec MFS, Inc., Dublin, CA, USA). Working suspensions were made through serial dilution followed by vigorous vortexing when required. During testing the suspensions were not shaken in order to avoid physically damaging the organisms. In the TiO_2 suspensions, further sedimentation of particles was visually observed.

7.2.4 Exposure

The test suspensions were prepared immediately before use by diluting the particle powder in eight different concentrations (0.001; 0.01; 0.1; 1; 10; 100; 1000; 10000 mg L^{-1}). Four replicates per concentration were used. A control test, without the added metal, was included for each treatment. The neonates were exposed to each particle/concentration in four replicates with five daphnids per replicate. A total of 32 acute tests were run. Tests were performed according to ABNT NBR 12713 in a photoperiod of 16 h under light (PHILIPS TLD 100-1000 lux 16w/840-NG) and 8 h in the dark at a temperature of 20 ± 2°C.

D. magna was not fed during the testing period. Mortality status for the individuals in each container was checked after 24 h and 48 h of exposure. After an incubation period of 48 h, immobilization of the daphnids was determined. The assay endpoint was death/immobilization. Oxygen content, temperature and pH of the control, first and last test dilutions were measured.

7.2.5 *Ceriodaphnia dubia* preparation to the chronic assay

Chronic toxicity test with the TiO_2 particle was conducted based on the ABNT NBR 13373 [35]. The chronic seven-day test was performed using neonates of *C. dubia* (6–24 h old at the start of the test) (Aplysia Soluções Ambientais LTDA, Vitória, Espírito Santo, Brazil), individually exposed per concentration. The animals were fed with the green algae *Desmodesmus subspicatus* and a compost of fish and yeast, reared in artificial medium - Standard Methods for the Examination of Water and Wastewater.

7.2.6 Exposure

The test suspensions were prepared immediately before use by diluting appropriate amounts of the particle powder in six different concentrations (0.001; 0.01; 0.1; 1; 10; 100 mg L^{-1}). A control test, without the added metal, was included for each treatment. The neonates were exposed to each particle/concentration in ten replicates with one daphnids per replicate. In total, 60 chronic tests were run. Chronic seven days test was performed in a photoperiod of 16 h under light (PHILIPS TLD 100-1000 lux 16w/840-NG) and 8 h in the dark at a temperature of 25 ± 2°C. Culture medium was renewed in an interval of 3 day. After the incubation period of 7 days, survival rate and the number of neonates produced by each female (reproduction) was recorded. Oxygen content and pH of the control, first and last test dilutions were measured.

7.2.7 Data analysis

Effective concentrations (EC) that cause an effect in 0 or 50% of test organisms (EC_0, EC_{50}) and no-observed-effect concentration (NOEC) were calculated with the help of the results obtained from the 7-day chronic toxicity tests.

Treatments were conducted with four (acute) and ten (chronic) replicates, and the results were presented as mean ± SD (standard deviation). All calculations were done with the aid of Microsoft Excel 2007.

7.3 RESULTS

7.3.1 Particles characterization

Figure 7.1 summarizes the characteristics of the different particles tested in this study, characterized by X-ray diffraction, transmission electronic micrograph, laser diffraction, specific surface area and zeta potential analyses. Diffraction X-ray analyses detected the presence of SiO_2 and Ag in the AgNp_silica (Figure 7.1a) sample. The Ag^+_phosphate (Figure 7.1b) sample featured an amorphous structure, not being possible to characterize its composition through this method. Ag^+_bentonite (Figure 7.1c) sample was compounded by Montmorillonite-22A and cristobalite. TiO_2 (Figure 7.1d) sample was characterized as pure rutile.

Figure 7.1 Micrographs obtained by TEM, diameter, specific surface area (SSA) and zeta potential of the additives: (a) AgNp_silica, (b) Ag^+_phosphate, (c) Ag^+_bentonite and (d) TiO_2

	Micrographs obtained by TEM	Average diameter by TEM, µm	Diameter by laser diffraction, µm		SSA, $m^2\ g^{-1}$	Zeta potential at pH 5, mV	X-Ray diffraction graphics
(a)	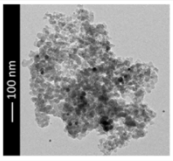	0.02	D_{10}	4.70	293.90	-6.48	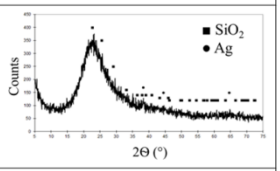
			D_{50}	9.20			
			D_{90}	28.99			
			Average	12.97			
(b)	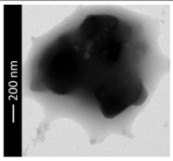	1.0	D_{10}	0.86	6.16	6.82	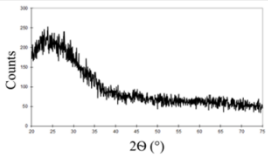
			D_{50}	1.50			
			D_{90}	2.49			
			Average	1.61			
(c)	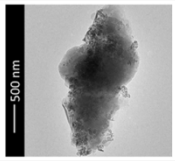	overlapping sheets	D_{10}	2.08	36.73	3.77	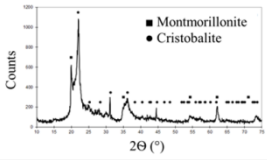
			D_{50}	6.32			
			D_{90}	13.92			
			Average	7.30			
(d)	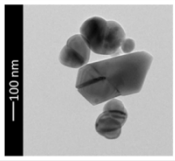	0.09	D_{10}	0.08	12.16	0.87	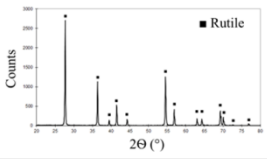
			D_{50}	0.25			
			D_{90}	0.54			
			Average	0.29			

Figure 7.1a indicates nanoparticles of silica (20 nm) and silver (10 nm). Composition was confirmed by energy dispersive X-ray (EDS) assay (result not shown). Laser diffraction assay determined an average size of 12.97 µm in the AgNp_silica sample. The size difference determined on TEM images and laser diffraction shows that particles have a high tendency to agglomeration. The SSA values found suggest that nanoparticles of silver and silica are irregular, which provides a high surface contact (Figure 7.1a). In Figure 7.1b it can be seen that it is

possible to see that the Ag^+_phosphate sample presents a planar form. The planar form found in Ag^+_phosphate and its non-crystalline shape characterized in the x-ray diffraction can be related to the preferences of silver ions for a tetrahedral molecular configuration, and creates a two-dimensional sheet composition including dimeric units [36]. In TEM image the particles are 1 µm, similar to that determined by granulometric assay. The SSA value of Ag^+_phosphate was 6.16 $m^2\ g^{-1}$.

Ag^+_bentonite sample, showed in Figure 7.1c, presents a typical platelet form found in montmorillonite clay [37]. The same size difference occurred with this sample, according to the laser diffraction assay, with an average size of 7.3 µm being observed, while in TEM the 1 µm size showed an agglomeration tendency. The SSA of 36.73 $m^2\ g^{-1}$ was in agreement with the literature (20-90 $m^2\ g^{-1}$) [38, 39]. The measure of SSA of montmorilonite by BET method was reported as non-effective, since nitrogen does not access the interlayer space [40]. As seen in Figure 7.1d**,** the TiO_2 sample features a spherical form, average size of 90 nm, lower than that determined by laser diffraction assay (0.29 µm), showing a low tendency to agglomeration.

The knowledge of the surface characteristic of the nanoparticles (NPs) is a pre-requisite to predict its stability in colloidal systems, and consequently its toxicity [41]. In that way, zeta potential (ZP) values, gives an indication about the NPs stability [42]. The amount of ZP provides a clue of potential stability of the particle, since particles with ZP below 30 mV or above -30 mV are deemed with high potential to form aggregates [43, 44]. ZP value from particles is not absolute and is dependent on the medium in which the particles are embedded, for example the substances present in the medium [42, 45, 46] and its pH [41].

To verify sample stability, the zeta potential of particles in different pH ranges was investigated and shown in Figure 7.2. Except for the TiO_2 sample, the ZP value was between -30 and +30 mV in a wide range of pH, and was considered unstable with high tendency to agglomerate, in agreement with discrepancies of size determined by laser diffraction and TEM images (Figure 7.1).

Figure 7.2 Zeta potential of (-▲-) AgNp_silica; (-■-) Ag^+_phosphate; (-♦-) Ag^+_bentonite and (-x-) TiO_2

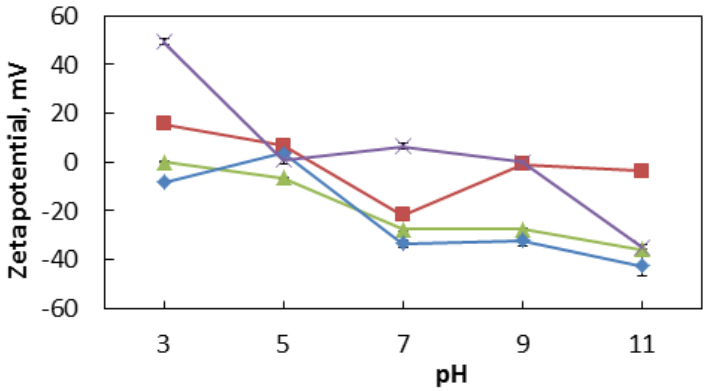

7.3.2 Abiotic variables

According to Ratte [47], pH, organic carbon, cation exchange quality and the levels of silt and clay may be responsible for transforming the toxicity behavior of a determined substance. During all acute toxicity tests, the pH value remained within the range of 5.0 and did not vary by more than 6.2 units in any given test. The mean oxygen content of the test dispersions in acute toxicity tests was 5.96 mg L^{-1}. During the chronic toxicity study the oxygen and pH content were 4.42 and 7.98 mg L^{-1}, respectively (Table 7.1).

Table 7.1. Mean values of the aqueous suspensions parameters

Aqueous suspensions	24-48 h *Daphnia magna*		7-days *Ceriodaphnia dubia*	
	Dissolved Oxygen, mg L^{-1}	pH	Dissolved Oxygen, mg L^{-1}	pH
AgNp_silica	5.76	5.00	-	-
Ag^+_phosphate	6.18	5.50	-	-
Ag^+_bentonite	5.71	6.00	-	-
TiO_2	6.20	5.00	4.42	7.98

7.3.3 Acute toxicity

The results from the acute toxicity tests performed with AgNp_silica, Ag^+_phosphate and Ag^+_bentonite are summarized in Table 7.2. TiO_2 results are shown in Figure 7.3. *D. magna* was found to be very sensitive to Ag based additives (AgNp_silica, Ag^+_phosphate, Ag^+_bentonite - 24 h, 100% mortality), even at the low concentration of 0.0001 mg L^{-1}.

Table 7.2. Evaluation of metal aqueous suspensions (AgNp_silica, Ag^+_phosphate and Ag^+_bentonite) to *Daphnia magna*

Aqueous suspensions		Treatments, mg L^{-1}								
		Control	0.0001	0.001	0.01	1	10	100	1000	10000
AgNp_silica	Total individuals dead	0	20	20	20	20	20	20	20	20
	Mortality (%) after 24h	0	100	100	100	100	100	100	100	100
	Mortality (%) after 48h	-	-	-	-	-	-	-	-	-
Ag^+_phosphate	Total individuals dead	0	20	20	20	20	20	20	20	20
	Mortality (%) after 24h	0	100	100	100	100	100	100	100	100
	Mortality (%) after 48h	-	-	-	-	-	-	-	-	-
Ag^+_bentonite	Total individuals dead	0	20	20	20	20	20	20	20	20
	Mortality (%) after 24h	0	100	100	100	100	100	100	100	100
	Mortality (%) after 48h	-	-	-	-	-	-	-	-	-

In all acute toxicity tests, the survival in the controls was 100%. This confirms that the validity criteria were fulfilled. In the acute assays from TiO_2 sample, 1 mg L^{-1} caused the high mortality percentage (75%) and 0.0001 mg L^{-1} caused the low mortality percentage (0%) (Figure 7.3). Calculation of EC_{50}-48 h for TiO_2 was not possible due the non-homogeneity of the results through the Trimmed Spearman-Karber method.

Figure 7.3 Total of dead *Daphnia magna* after 48 h in contact with TiO_2 suspensions

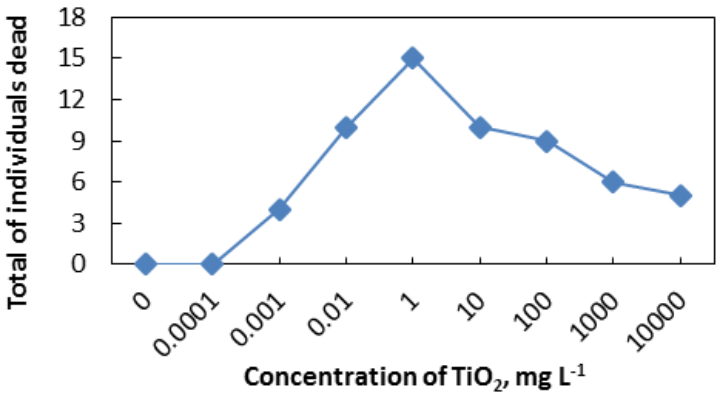

7.3.4 Chronic toxicity

The chronic toxicity test (*C. dubia* reproduction) with TiO_2 showed the biggest neonates number with 0.01 mg L^{-1}. Reproduction numbers decreased as the TiO_2 ratio increased (Figure 7.4).

Figure 7.4 *Ceriodaphnia dubia* neonates produced during the 7-days in contact with TiO_2 suspensions

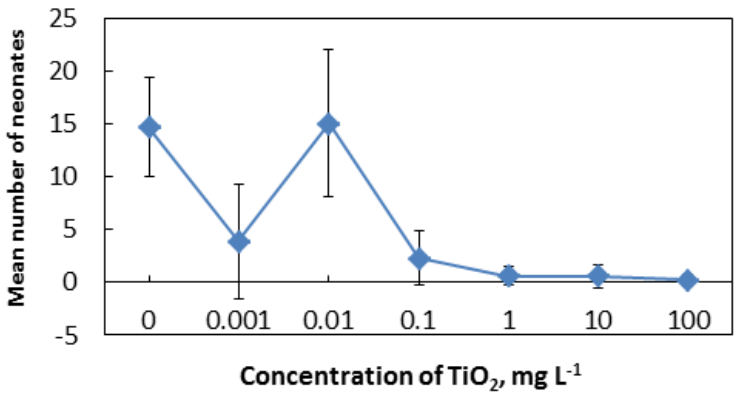

The chronic toxicity test (*C. dubia* reproduction) with TiO_2 showed the biggest neonates number with 0.01 mg L^{-1}. Starting from 0.1 mg L^{-1} the reproduction numbers decreased as the TiO_2 ratio increased (Figure 7.4).

The highest concentration of TiO_2 that caused no observed deleterious effect (NOEC) in the *C. dubia* reproduction after 7-day chronic toxicity tests was 0.01 mg L^{-1}. The effective concentration of TiO_2 that produces an effect in 0% (EC_0) and 50% (EC_{50}) of the tested organisms were 0.10 mg L^{-1} and 0.063 mg L^{-1}, respectively.

7.4 DISCUSSION

In this study we assessed issues pertaining to the physic-chemical properties of four samples of metal particles and their relation to daphnids toxicity. Toxicity was observed in all Ag based acute assays (24 h). On the other hand, TiO_2 was less toxic, leading to daphnia death only after 48 h of the assay.

Below are some of the characteristics of the particles addressed in toxicological research and that can explain the differences in toxicity observed in the present study.

7.4.1 Size dependent toxicity

The first point of discussion about particle toxicity is their size. These concerns are related to the fact that small sized particles have the ability to traverse biological membranes [48, 49]. Moreover, the nano design provides physical and chemical characteristics that differ from the bulk materials of same chemical structure [50]. In this way, nanoparticles may lead to the death of aquatic organisms due to accumulation of nanoparticles in the gut and disturbance of food intake [51, 52]. In the case of daphnids, the activity of thoracic segments promotes a current of water, whereas particles (< 50 µm in diameter) are directed to the mouth without any selective process [51, 53], which is compounded by the difficulty in excreting the particulates [54]. In a study performed by Zhao and Wang [55] more than 60% of AgNp was present in the gut of daphnids, indicating that ingestion was the prevalent route of consumption. Petersen et al. [54] demonstrated that the carbon nanotubes captured by the daphnids remain mostly in the gut and were not incorporated by cell tissue. Once that nanoparticle is taken up by the cells, they may cause disorder in the protein structure [56] and DNA damage [11] with the production of reactive oxygen species [32, 56]. Fabrega et al. [57] reviewed the effects of silver nanoparticles on algae, invertebrate, and fish species. Those authors support the idea that concentration as low as a few mg L^{-1} of AgNp can be harmful to various aquatic species.

According to micrograph images, AgNp_silica and TiO_2 feature a nanoform, and both particles presented a different pattern of toxicity. In this way, the toxicity observed does not appear to be a response to exposure to nanoform particles; rather, it may be explained by the intrinsic metal properties [16].

7.4.2 Metal ion release and associated damage

Although the metal ion release from silver-based particles was not addressed in this study, this matter related to the metal toxicity is subject to discussion. There is no consensus as to which degree the AgNp toxicity originates from released silver ions and how much toxicity is related to AgNp per se [58]. Nanoparticles require special attention because tiny particles have characteristics that increases metal ion release [59]. However, this release process can potentially be affected by the particles' agglomeration behavior [29]. To some authors, the antimicrobial

mechanism of silver loaded materials results from a long term release of the dissolved ion by oxidation of metallic silver in contact with water [29, 60]. In this case, for aquatic organisms such as *D. magna*, the ion regular release is the most widely accepted mechanism to explain Ag toxicity [61, 62]. Asharani et al. [11] observed a higher toxicity of AgNp in the development of zebrafish (*Danio rerio*) embryos when compared to the Ag ions. The authors suggest that the penetration of nanoparticles through the skin and their interactions with tissues may have caused phenotypic defects in the treated embryos. Otherwise, Zhao and Wang [63] observed no mortality in 48 h when the daphnids were exposed up to 500 µg L^{-1} of AgNp, but harmful effects were detected when the substance of exposition was silver nitrate. Navarro et al. [6] evaluated the toxic effect of AgNp and ionic Ag ($AgNO_3$) to photosynthesis process of *Chlamydomonas reinhardtii* and concluded that the inhibition on photosynthesis was mediated by the release of Ag ions. Zhang et al. [64] also found that sunlight drive the reduction of Ag^+ to AgNp, decreasing acute toxicity of silver to *D. magna*, linking toxicity of silver to Ag^+ instead of AgNp or total silver.

7.4.3 Metal binding process and toxicity

Ag ions may be the highest risk factor from AgNp to aquatic organisms, and these ions have the binding ability with multiple substances, such as silver sulfide, silver chloride [65], cysteine [6] and dissolved organic carbon (DOC) [21]. These interactions between oxidized AgNp and ligants can modify the metal bioavailability and influence the toxicity of particles in natural aquatic environments [21, 29]. Also, the increase in organic matter (OM) concentration, can lead to a decrease in toxicity of the AgNp to daphnids [66, 67]. In *D. magna* Ag and TiO_2 Np assimilation and depuration appeared to be more affected by the food concentration [19, 51]. Ag can bind to OM from food residues or excreted by animals, and become less available to *D. magna* [66]. According to the standard protocol used it this study, *D. magna* was not fed during the acute toxic assays and no organic matter was added in the test suspensions. Also, other methods, such as the ISO 6341 and OECD 202 follow the same standard. Therefore, we did not take into account this factor when evaluating the results.

In the present study, as all silver based additives with different physic-chemical properties were harmful to the microcrustaceans, the toxicity effect was linked to the silver itself, and not its form, size or characteristics of the carrier. In a broad view, the same pattern was reported by Carlson et al. [4] who demonstrate that the toxicity of Ag may be connected to the material composition and not intrinsic to the nano size. Also, Griffitt et al. [16] reported that Ag^{+} did not explain all toxicity observed for AgNp exposure to *Danio rerio, Daphnia pulex* and *C. dubia*, and suggested that within the metals tested (silver, copper, aluminum, nickel, cobalt), some of them (copper and silver) had an intrinsic toxic characteristic.

7.4.4 TiO_2 properties and its toxic behavior

The acute assay with TiO_2 performed here showed heterogeneity in concentration–response, with 0.1 mg L^{-1} being more toxic than 10000 mg L^{-1}. Hartmann et al. [7] also reported a nonlinear characteristic in TiO_2 suspensions toward a freshwater green alga. Those authors observed that agglomerates in the suspension of 250 mg L^{-1} were smaller than in 2 mg L^{-1} dilution. This aggregate arrangement could be explained by the alterations in electrostatic repulsion or interactions with other materials with the dilution, which leads to the formation of larger and settleable agglomerates [49, 68].

During the toxicological experiments, agglomerated particles do not become readily available to the organisms contact and absorption, which lead to a less reactivity, and consequently, a less toxicity [15]. Also, the agglomeration of nanoparticles reduces the surface area in which the metal oxidation reactions takes place [29]. Dalai et al. [32] reported a nonlinear result on *C. dubia* acute assay due to the agglomeration and sedimentation of TiO_2 nanoparticles at high concentration, which produced a lower bioavailability of the metal. However, the OECD (Organization for Economic Co-operation and Development), proposed finding the CL_{50} up to the concentration of 100 mg L^{-1} of TiO_2 Np, but this value was described as difficult to be dispersed [31].

The evaluation of the effects of filtered and unfiltered but sonicated suspensions of TiO_2 was performed by Lovern and Kapler [15]. They found that the unfiltered/sonicated sample did not promote good dispersion of particles leading to less severe toxicity of TiO_2 (100-500 nm) to *D. magna* even at concentrations as high

as 500 mg L^{-1}. Hund-Rinke and Simon [53] also observed the influence of sedimentation on low TiO_2 toxicity. For AgNp, the filtered suspensions were also more toxic than the unfiltered equivalent [29]. In the acute tests, calculation of TiO_2 EC_{50}-48h was not possible due the heterogeneity of dose response values. The lower negative consequences observed in the TiO_2 acute test performed here, may be explained, at least in part, by the sedimentation of TiO_2 during the assay, which may have provided a low availability of particles in suspension and ultimately reduced releases of metal. In the chronic assay, the concentrations that caused an effect of 0 or 50% in test organisms were EC_0 (0.10 mg L^{-1}) and EC_{50} (0.063 mg L^{-1}), respectively.

No appreciable effects of TiO_2 Np (100 mg L^{-1}) were observed in *Chydorus sphaericus*, *Pseudokirchneriella subcapitata* and *Vibrio fischeri* (Velzeboer et al. 2008). A study using *Danio rerio* embryos, in which TiO_2 Np was set at concentrations as high as 500 mg L^{-1} also did not show any toxic effects, but, instead provided a high hatching rate [13]. According to the previous studies, TiO_2 Np appears to exert a wide range of toxicological effects in bioindicator species. However, the non toxic effect of TiO_2 found in short assays (48 h and 7 days) cannot be repeated in an extended period of exposition. Wiench et al. [31] and Zhu et al. [50] performed a long term, acute (48 h and 72 h) and chronic (21 days) experiments, for analyze the *D. magna* response when exposed to nano and non-nano form of TiO_2. Those authors observed no particle size dependence and low acute toxicity with an EC_{50} – 48h > 100 mg L^{-1}. However, in the acute test (72 h) the EC_{50} was 1.62 mg L^{-1} and in the chronic test (21 days) the EC_{50} was 0.46 [50] and 26.6 mg L^{-1} [31]. Ribeiro et al. [3], when exposing *D. magna* to a 21-day test reported an EC_{50} of 0.38 µg L^{-1} and 1.0 µg L^{-1} for $AgNO_3$ and AgNp, respectively. It could be noted that the concentrations required to cause any damage to the *D. magna* health in the long term were much lower than that in the short (48 h) acute test.

Anatase and rutile are two crystalline structures of TiO_2, with anatase being more chemically reactive [69] and toxic [17]. The photocatalyst properties of TiO_2 are related to its toxicity due the reactive oxygen species (ROS) production [70]. Thus, the rutile structure is described as the less photocatalyst [71] and non-cytotoxic form of TiO_2 crystal [72, 73]. In the present study, TiO_2 features the rutile form that may be related to the non-acute toxicity.

In chronic toxicity experiments performed here, TiO_2 showed a reduction on neonate numbers with the increase in TiO_2 concentration (Figure 7.4). Hund-Rinke and Simon [53] found a TiO_2 NP dose-dependent toxicity to algae (*Desmodesmus subspicatus*) (EC_{50} = 44 mg L^{-1}), but the effects to *D. magna* were less strong. In a toxicological study with TiO_2 nanoparticles towards *C. dubia*, Dalai et al. [32] reported an EC_{50} on acute test of around 8.26 mg L^{-1} in experiments realized under photoperiod and 27.45 mg L^{-1} in the dark. Oxidative stress was the main factor related to the toxicity action under both dark and light situations.

In the present study, no relationship was apparent between the physical-chemical characteristics of the particles evaluated and toxicity. For example, sample Ag^+_phosphate featured a specific surface area (SSA) close to that of TiO_2 and high toxic effects were observed even at a low concentration of Ag^+_phosphate. On the other hand, AgNp_silica showed a nano scale similar to that of TiO_2, and it was even more toxic. Particles with high and low SSA values (AgNp_silica – 293.9 m^2 g^{-1}) (Ag^+_phosphate – 6.16 m^2 g^{-1}) respectively, produced the same toxicity results (100% mortality). Ag^+_bentonite have intermediate physical-chemical characteristics compared to the other analyzed particles, but also presented a high toxic behavior. Upon observation, the zeta potential (ZP) from TiO_2 presented the ZP value next to zero in the pH used in acute assay (0.87 mV in pH 5.0), and it was much less toxic than AgNp_silica (-6.48 mV in pH 5.0), Ag^+_phosphate (~7.0 mV in pH 5.5) and Ag^+_bentonite (~ -20mV in pH 6.0). Tavares et al. [44] attributed the toxicity of Cr_2O_3 (15-30 nm) to *Daphnia similis* to the small particle sizes combined with the higher zeta potential value (-19.65 mV in pH 6.87). The more negative was the zeta potential values of carboxyl quantum dots, the greater the toxicity toward mice [74]. Still, Arndt et al. [75] could not find a relation between the zeta potential and toxicity, after the study of carbon nanotubes with all charge types (positive, negative and neutral) which showed toxicity toward *D. magna*. Sha and coworkers [76], following an extensive review, could not understand the pattern of toxicity from TiO_2 Np due to the lack of information about particle characteristics in the previous studies. In this study, considering that the TiO_2 ZP value was near zero and this sample presented no harmful effects against *D. magna*, assumptions can be made on the possibility of the low rate of electrons on the particle surface exerting an influence on the mode of interaction between TiO_2 and the daphnids.

The reported results indicate that undetermined processes are responsible for the toxic effects. In this regard, further studies are needed to verify the relation between the physical-chemical properties of particles and their toxic consequences.

7.5 CONCLUSIONS

The knowledge of the effects of novel particles to plants and animals is required in order to identify the most appropriate engineering to promote environmental preservation along with technological advance.

The present study considered four samples; three containing silver and one commercial titanium dioxide that can be used as antimicrobial additives. The objective was to investigate the toxicity effects of metal particles with different characteristics to daphnids. All silver samples were toxic to daphnids, even at a low concentration (0.0001 mg L^{-1}), and was not possible to find a relation between the characteristics of the particles analyzed and its toxicity. On the other hand, TiO_2 showed little acute effect on *D. magna* and a dose-dependent response on *C. dubia*.

Despite no apparent relationship between the physical-chemical characteristics of the particles evaluated and toxicity, the TiO_2 zeta potential value next to zero may have influenced its biological response due to the low rate of particle surface electrons, on which can alter the interaction between TiO_2 particles and the daphnids.

Since there is a great variation between the encapsulation system, size, shape, and chemical composition of particles being used in materials; the heterogeneity of the new metal particles, hinders the comparison between our results and others studies. In this way, future investigations are needed to explain the toxic mechanism of silver and titanium, in a variety of particles features in a long-term assay.

7.6 REFERENCES

1. DANKOVIC, D.; KUEMPEL, E.; WHEELER, M. An approach to risk assessment for TiO_2. **Inhalation Toxicology**, v. 19, Suppl. 1, p. 205–212, 2007. Doi: 10.1080/08958370701497754
2. KALBASSI, M. R.; SALARI-JOO H.; JOHARI, A. Toxicity of silver nanoparticles in aquatic ecosystems: salinity as the main cause in reducing toxicity. **Iranian Journal of Toxicology**, v. 5, n. 1&2, p. 436-443, 2011.

3. RIBEIRO, F.; GALLEGO-URREA, J. A.; JURKSCHAT, K.; CROSSLEY, A.; HASSELLÖV, M.; TAYLOR, C.; SOARES, A.M.V.M.; LOUREIRO, S. Silver nanoparticles and silver nitrate induce high toxicity to *Pseudokirchneriella subcapitata*, *Daphnia magna* and *Danio rerio.* **Science of the Total Environment**, v. 466–467, p. 232–241, 2014. Doi: 10.1016/j.scitotenv.2013.06.101

4. CARLSON, C.; HUSSAIN, S. M.; SCHRAND, A. M. Unique cellular interaction of silver nanoparticles: size-dependent generation of reactive oxygen species. **Journal of Physical Chemistry B**, v. 112, p. 13608–13619, 2008. Doi: 10.1021/jp712087m

5. BUZEA, C.; BLANDINO, I. I. P.; ROBBIE K. Nanomaterials and nanoparticles: Sources and toxicity. **Biointerphases**, v. 2, n. 4, p. MR17 - MR172, 2007.

6. NAVARRO, H.; CAPIETRA, F.; WAGNER, B.; MARCONI , F.; KAEGI, R.; ODZAK, N.; SIGG, L.; BEHRA, R. Toxicity of silver nanoparticles to *Chlamydomonas reinhardtii.* **Environmental Science and Technology**, v. 42, p. 8959–8964, 2008. Doi: 10.1021/es801785m

7. HARTMANN, N. B.; VON DER KAMMER, F.; HOFMANN, T.; BAALOUSHA, M.; OTTOFUELLING, S.; BAUN, A. Algal testing of titanium dioxide nanoparticles — Testing considerations, inhibitory effects and modification of cadmium bioavailability. **Toxicology**, v. 269, p. 190–197, 2010. Doi: 10.1016/j.tox.2009.08.008

8. BINAEIAN, E.; RASHIDI, A. M.; ATTAR, H. Toxicity study of two different synthesized silver nanoparticles on bacteria *Vibrio fischeri.* **World Academy of Science, Engineering and Technology**, v. 6, p. 07-26, 2012.

9. HEINLAAN, M.; IVASK, A.; BLINOVA, I.; DUBOURGUIER, H-C.; KAHRU, A. Toxicity of nanosized and bulk ZnO, CuO and TiO_2 to bacteria *Vibrio fischeri* and crustaceans *Daphnia magna* and *Thamnocephalus platyurus*. **Chemosphere**, v. 71, p. 1308–1316, 2008. Doi: 10.1016/j.chemosphere.2007.11.047

10. SAKAMOTO, M.; HA, J-Y.; YONESHIMA, S.; KATAOKA, C.; TATSUTA, H.; KASHIWADA, S. Free silver ion as the main cause of acute and chronic toxicity of silver nanoparticles to cladocerans. **Archives of Environmental Contamination and Toxicology**, v. 68, p. 500–509, 2015. Doi: 10.1007/s00244-014-0091-x

11. ASHARANI, P. V.; WU, Y.L.; GONG Z.; VALIYAVEETTIL, S. Toxicity of silver nanoparticles in zebrafish models. **Nanotechnology**, v. 19, p. 255102-255110, 2008. Doi: 10.1088/0957-4484/19/25/255102

12. WEHMAS, L. C.; ANDERS C.; CHESS J.; PUNNOOSE, A.; PEREIRA, C. B.; GREENWOOD, J. A.; TANGUAYA, R. L. Comparative metal oxide nanoparticle toxicity using embryonic zebrafish. **Toxicology Reports**, v. 22, p. 702–715, 2015. Doi: 10.1016/j.toxrep.2015.03.015

13. ZHU, X.; ZHU, L.; DUAN, Z. QI, R.; LI, Y.; LANG, Y. Comparative toxicity of several metal oxide nanoparticle aqueous suspensions to Zebrafish (*Danio rerio*) early developmental stage. **Journal of Environmental Science and Health Part A**, v. 43, p. 278-284, 2008. Doi: 10.1080/10934520701792779

14. PERSSON, J.; BRETT, M. T.; VREDE, T.; RAVET, J. L. Food quantity and quality regulation of trophic transfer between primary producers and a keystone grazer (*Daphnia*) in pelagic freshwater food webs. **Oikos**, v. 116, p. 1152-1163, 2007. Doi: 10.1111/j.2007.0030-1299.15639.x

15. LOVERN, S. B.; KLAPER, R. *Daphnia magna* mortality when exposed to titanium dioxide and fullerene (C_{60}) nanoparticles. **Environmental Toxicology and Chemistry**, v. 25, n. 4, p. 1132–1137, 2006.

16. GRIFFITT, R. J.; LUO, J.; GAO, J.; BONZONGO, J-C.; BARBER, D. S. Effects of particle composition and species on toxicity of metallic nanomaterials in aquatic organisms. **Environmental Toxicology and Chemistry**, v. 27, n. 9, p. 1972–1978, 2008.

17. CLÉMENT, L.; HUREL, C.; MARMIER, N. Toxicity of TiO_2 nanoparticles to cladocerans, algae, rotifers and plants – Effects of size and crystalline structure. **Chemosphere**, v. 90, p. 1083–1090, 2013. Doi: 10.1016/j.chemosphere.2012.09.013

18. BONDARENKO, O.; JUGANSON, K.; IVASK, A.; KASEMETS, K.; MORTIMER, M.; KAHRU, A. Toxicity of Ag, CuO and ZnO nanoparticles to selected environmentally relevant test organisms and mammalian cells in vitro: a critical review. **Archives of Toxicology**, v. 87, p. 1181–1200, 2013. Doi: 10.1007/s00204-013-1079-4

19. LAM, I. K. S.; WANG, W-X. Accumulation and elimination of aqueous and dietary silver in *Daphnia magna*. **Chemosphere**, v. 64, p. 26–35, 2006. Doi: 10.1016/j.chemosphere.2005.12.023

20. FLOHR, L.; CASTILHOS JÚNIOR, A. B. DE; MATIAS, W. G. Acute and chronic toxicity of soluble fractions of industrial solid wastes on *Daphnia magna* and *Vibrio fischeri*. **The Scientific World Journal**, 2012. Doi: 10.1100/2012/643904

21. NEWTON, K. M.; PUPPALA, H. L.; KITCHENS C. L.; COLVIN, V. L.; KLAINE S. J.. Silver nanoparticle toxicity to *Daphnia magna* is a function of dissolved silver concentration. **Environmental Toxicology and Chemistry**, v. 32, n. 10, p. 2356–2364, 2013. Doi: 10.1002/etc.2300

22. RANGARI, V. K.; MOHAMMAD, G. M.; JEELANI, S.; HUNDLEY, A.; VIG, K.L; SINGH, S. R.; PILLAI, S. Synthesis of Ag/CNT hybrid nanoparticles and fabrication of their Nylon-6 polymer nanocomposite fibers for antimicrobial applications. **Nanotechnology**, 21, p. 095102-095113, 2010. Doi: 10.1088/0957-4484/21/9/095102

23. EGGER, S.; LEHMANN, R. P.; HEIGHT, M. J.; LOESSNER, M. J.; SCHUPPLER, M. Antimicrobial properties of a novel silver-silica nanocomposite material. **Applied and Environmental Microbiology**, v. 75, p. 2973–2976, 2009. Doi: 10.1128/AEM.01658-08

24. FERREIRA, L.; FONSECA, A. M.; BOTELHO, G.; ALMEIDA- AGUIAR, C.; NEVES, I.C. Antimicrobial activity of faujasite zeolites doped with silver**. Microporous and Mesoporous Materials**, v. 160, p. 126–132, 2012. Doi: 10.1016/j.micromeso.2012.05.006.

25. KONG, H.; JANG, J. Antibacterial properties of novel poly(methyl methacrylate)

nanofiber containing silver nanoparticles. **Langmuir**, v. 24, p. 2051-2056, 2008.

26. GATOO, M. A.; NASEEM, S.; ARFAT, M. Y.; DAR, A. M.; QASIM, K.; ZUBAIR, S. Physicochemical properties of nanomaterials: implication in associated toxic manifestations. **BioMed Research International**, 2014. Doi: 10.1155/2014/498420.

27. ALBANESE, A.; TANG, P. S.; CHAN, W. C. W. The effect of nanoparticle size, shape, and surface chemistry on biological systems. **Annual Review of Biomedical Engineering**, v. 14, p. 1–16, 2012. Doi: 10.1146/annurev-bioeng-071811-150124

28. BENN, T. M.; WESTERHOFF, P. Nanoparticle silver released into water from commercially available sock fabrics. **Environmental Science Technology**, v. 42, p. 4133–4139, 2008. Doi: 10.1021/es7032718

29. ALLEN, H. J.; IMPELLITTERI, C. A.; MACKE, D. A.; HECKMAN, J.L.; POYNTON, H. C.; LAZORCHAK, J. M.; GOVINDASWAMY, S.; ROOSE, D. L.; NADAGOUDAK, M. N. Effects from filtration, capping agents, and presence/absence of food on the toxicity of silver nanoparticles to *Daphnia magna*. **Environmental Toxicology and Chemistry**, v. 29, p. 2742–2750, 2010. Doi: 10.1002/etc.329

30. ROSA, E. L. S. Kinetic effects of TiO_2 fine particles and nanoparticles aggregates on the nanomechanical properties of human neutrophils assessed by force spectroscopy. **BMC Biophysics**, v. 6, n. 11, p. 1-10, 2013. Doi: 10.1186/2046-1682-6-11

31. WIENCH, K.; WOHLLEBEN, W.; HISGEN, V.; RADKE, K..; SALINAS, E.; ZOK, S.; LANDSIEDEL, R. Acute and chronic effects of nano- and non-nano-scale TiO2 and ZnO particles on mobility and reproduction of the freshwater invertebrate *Daphnia magna*. **Chemosphere**, v. 76, p. 1356–1365, 2009. Doi: 10.1016/j.chemosphere.2009.06.025

32. DALAI, S.; PAKRASHI, S.; CHANDRASEKARAN, N.; MUKHERJEE, A. Acute toxicity of TiO_2 nanoparticles to *Ceriodaphnia dubia* under visible light and dark conditions in a freshwater system. **Plos One**, v.8, n. 4, p. e62970, 2013. Doi: 10.1371/journal.pone.0062970

33. DAS, P.; XENOPOULOS, M. A.; METCALFE, C. D. Toxicity of silver and titanium dioxide nanoparticle suspensions to the aquatic invertebrate, *Daphnia magna*. **Bulletin of Environmental Contamination and Toxicology**, v. 91, p. 76–82, 2013. Doi: 10.1007/s00128-013-1015-6

34. ASSOCIAÇÃO BRASILEIRA DE NORMAS TÉCNICAS. **NBR 12713**: Ecotoxicologia aquática – Toxicidade Aguda – Teste com *Daphnia spp* (*Cladocera, Crustacea*). 23 p., 2009.

35. ASSOCIAÇÃO BRASILEIRA DE NORMAS TÉCNICAS. **NBR 13373**: Aquatic exotoxicology - Chronic toxicity - Test with *Ceriodaphnia spp*. (*Crustacea, Cladrocera*). 19 p., 2010.

36. SUENAGA, Y.; KONAKA, H.; SUGIMOTO T.; KURODA-SOWA, T.; MAEKAWA, M.; MUNAKATA, M.; Crystal structure and photo-induced property of two-dimensional silver(I) complex with 1,3,5-tris(benzylsulfanyl)benzene.

Inorganic Chemistry Communications, v. 6, p. 389–393, 2003.

37. KAMENA, K. Nanoclays and their emerging markets. In: In: XANTHOS, M. (ed). **Functional Fillers for Plastics**, 2ª ed. Wiley-VCH Verlag GmbH & Co. KGaA, Weinheim, 2010. p. 177-187. ISBN 978-3-527-60442-5
38. PRAUS, P.; TURICOVÁ, M.; MACHOVIČ, V.; ŠTUDENTOVÁ, S.; KLEMENTOVÁ, M. Characterization of silver nanoparticles deposited on montmorillonite. **Applied Clay Science**, v. 49, p. 341–345, 2010. Doi: 10.1016/j.clay.2010.06.009
39. TIAN, L.; OULIAN, L.; ZHIYUAN, L.; LIUIMEI, H.; XIAOSHENG, W. Preparation and characterization of silver loaded montmorillonite modified with sulfur amino acid. **Applied Surface Science**, v. 305, p. 386–395, 2014. Doi: 10.1016/j.apsusc.2014.03.098
40. PRAUS, P.; TURICOVÁ, M.; KARLÍKOVÁ, M.; KVÍTEK, L.; DVORSKÝ, R. Nanocomposite of montmorillonite and silver nanoparticles: Characterization and application in catalytic reduction of 4-nitrophenol. **Materials Chemistry and Physics**, v. 140, p. 493-498, 2013. Doi: 10.1016/j.matchemphys.2013.03.059
41. PRATHNA, T. V.; CHANDRASEKARAN, N.; MUKHERJEE, A. Studies on aggregation behaviour of silver nanoparticles in aqueous matrices: Effect of surface functionalization and matrix composition. **Colloids and Surfaces A: Physicochemical and Engineering Aspects**, v. 390, p. 216–224, 2011. Doi: 10.1016/j.colsurfa.2011.09.047
42. BARRENA, R.; CASALS, E.; COLÓN, J.; FONT, X.; SÁNCHEZ, A.; PUNTES, V. Evaluation of the ecotoxicity of model nanoparticles. **Chemosphere**, v. 75, p. 850–857, 2009. Doi: 10.1016/j.chemosphere.2009.01.078
43. SHIEH, Y-T.; CHEN, J-Y.; TWU, Y-K.; CHEN, W-J. The effect of pH and ionic strength on the dispersion of carbon nanotubes in poly(acrylic acid) solutions. **Polymer Internatioal**, v. 61, p. 554–559, 2012. Doi: 10.1002/pi.3203
44. TAVARES, K. P.; CALOTO-OLIVEIRA, Á.; VICENTINI, D. S.; MELEGARI, S. .; MATIAS, W. G.; BARBOSA, S.; KUMMROW, F. Acute toxicity of copper and chromium oxide nanoparticles to *Daphnia similis.* **Ecotoxicology and Environmental Contamination**, v. 9, n. 1, p. 43-50, 2014. Doi: 10.5132/eec.2014.01.006
45. ORTS-GIL, G.; NATTE K.; DRESCHER D.; BRESCH, H.; MANTION, A.; KNEIPP, J.; ÖSTERLE, W. Characterisation of silica nanoparticles prior to in vitro studies: from primary particles to agglomerates. **Journal of Nanoparticle Research**, v. 13, p. 1593–1604, 2011. Doi: 10.1007/s11051-010-9910-9
46. GIOVANNI, M.; TAY, C. Y.; SETYAWATI, M. I.; XIE, J.; ONG, C. N.; FAN, R.; YUE, J.; ZHANG, L.; LEONG, D. T. Toxicity profiling of water contextual zinc oxide, silver, and titanium dioxide nanoparticles in human oral and gastrointestinal cell systems. **Environmental Toxicology**, v. 30, p. 1459–1469, 2015. Doi: 10.1002/tox.22015
47. RATTE, H. T. Bioaccumulation and toxicity of silver compounds: A review. **Environmental Toxicology and Chemistry**, v. 18, n. 1, p. 89–108, 1999.

48. OBERDORSTER, G.; SHARP, Z.; ATUDOREI, V.; KREYLING, W.; COX, C. Translocation of inhaled ultrafine particles to the brain**. Inhalation Toxicology**, v. 16, p. 437–445, 2004. Doi: 10.1080/08958370490439597

49. VELZEBOER, I.; HENDRIKS, A. J.; RAGAS, A. D. M. J.; MEENT, D. V. Aquatic ecotoxicity tests of some nanomaterials. **Environmental Toxicology and Chemistry**, v. 27, n. 9, p. 1942–1947, 2008.

50. SCHWIRN, K.; TIETJEN, L.; BEER, I. Why are nanomaterials different and how can they be appropriately regulated under REACH? **Environmental Sciences Europe**, v. 26, n.4, p. 1-9, 2014. Doi: 10.1186/2190-4715-26-4

51. ZHU, X.; CHANG, Y.; CHEN, Y. Toxicity and bioaccumulation of TiO_2 nanoparticle aggregates in *Daphnia magna*. **Chemosphere**, v. 78, p. 209–215, 2010. Doi: 10.1016/j.chemosphere.2009.11.013

52. ATES, M.; DANIELS, J.; ARSLAN, Z.; FARAH, I.O. Effects of aqueous suspensions of titanium dioxide nanoparticles on *Artemia salina*: assessment of nanoparticle aggregation, accumulation, and toxicity. **Environmental Monitoring and Assessment**, v. 185, p. 3339–3348, 2013. Doi: 10.1007/s10661-012-2794-7

53. HUND-RINKE, K.; SIMON, M. Ecotoxic effect of photocatalytic active nanoparticles (TiO_2) on algae and daphnids. **Environmental Science and Pollution Research**, p. 1-8, 2006. Doi: 10.1065/espr2006.06.311.

54. PETERSEN, E.; AKKANEN, J.; KUKKONEN, J. K.; WEBER JR., W. J. Biological uptake and depuration of carbon nanotubes by *Daphnia magna.* **Environmental Science & Technology**, v. 43, p. 2969–2975, 2009. Doi: 10.1021/es8029363

55. ZHAO, C-M.; WANG, W-X. Size-dependent uptake of silver nanoparticles in *Daphnia magna*. **Environmental Science and Technology**, v. 46, p. 11345−11351, 2012. Doi: 10.1021/es3014375

56. RINNA, A.; MAGDOLENOVA, Z.; HUDECOVA, A.; KRUSZEWSKI, M.; REFSNES, M.; DUSINSKA, M. Effect of silver nanoparticles on mitogen-activated protein kinases activation: role of reactive oxygen species and implication in DNA damage. **Mutagenesis**, v. 30, p. 59–66, 2015. Doi: 10.1093/mutage/geu057

57. FABREGA, J.; LUOMA, S. N.; TYLER, C. R.; GALLOWAY, T. M.; LEAD, J. R. Silver nanoparticles: Behaviour and effects in the aquatic environment. **Environment International**, v. 37, p. 517–531, 2011. Doi: 10.1016/j.envint.2010.10.012

58. BEER, C.; FOLDBJERG, R.; HAYASHI, Y.; SUTHERLAND, D. S.; AUTRUP, H. Toxicity of silver nanoparticles: Nanoparticle or silver ion? **Toxicology Letters**, v. 208, p. 286–292, 2012. Doi:10.1016/j.toxlet.2011.11.002

59. IVASK, A.; KURVET, I.; KASEMETS, K.; BLINOVA, I.; ARUOJA, V.; SUPPI, S.; VIJA, H.; KÄKINEN, A.; TITMA,T.; HEINLAAN, M.; VISNAPUU, M.; KOLLER, D.; KISAND, V.; KAHRU, A. Size-dependent toxicity of silver nanoparticles to bacteria, yeast, algae, crustaceans and mammalian cells in vitro. **Plos One**, v. 9, n. 7, p. e102108, 2014. Doi:10.1371/journal.pone.0102108

60. KUMAR, R.; MÜNSTEDT, H. Silver ion release from antimicrobial polyamide/silver composites. **Biomaterials**, v. 26, p. 2081–2088, 2005.

61. BIANCHINI, A.; WOOD, C. M. Mechanism of acute silver toxicity in *Daphnia magna.* **Environmental Toxicology and Chemistry**, v. 22, n. 6, p. 1361–1367, 2003.

62. ZHAO, C-M.; WANG, W-X. Regulation of sodium and calcium in daphnia magna exposed to silver nanoparticles. **Environmental Toxicology and Chemistry**, v. 32, n. 4, p. 913–919, 2013. Doi: 10.1002/etc.2133

63. ZHAO, C-M.; WANG, W-X. Comparison of acute and chronic toxicity of silver nanoparticles and silver nitrate to *Daphnia magna*. **Environmental Toxicology and Chemistry**, v. 30, n. 4, p. 885–892, 2011. Doi: 10.1002/etc.451

64. ZHANG, Z.; YANG, X.; SHEN, M.; YIN, Y.; LIU, J. Sunlight-driven reduction of silver ion to silver nanoparticle by organic matter mitigates the acute toxicity of silver to *Daphnia magna*. **Journal of Environmental Sciences**, v. 35, p. 62-68, 2015. Doi: 10.1016/j.jes.2015.03.007

65. CHOI, O.; CLEVENGER, T. E.; DENG, B.; SURAMPALLI, R. Y.; ROSS JR., L.; HU, Z. Role of sulfide and ligand strength in controlling nanosilver toxicity. **Water Research**, v. 43, p. 1879–1886, 2009. Doi: 10.1016/j.watres.2009.01.029

66. ERICKSON, R. J.; BROOKE, L. T.; KAHL, M. D.; VENTER, F.V.; HARTING, S. L.; MARKEE, T.P.; SPEHAR, R. L. Effects of laboratory test conditions on the toxicity of silver to aquatic organisms. **Environmental Toxicology and Chemistry**, v. 17, n. 4, p. 572–578, 1998.

67. GAO, J.; POWERS, K.; WANG, Y.; ZHOU, H.; ROBERTS, S.M.; MOUDGIL, B.M.; KOOPMAN, B.; BARBER, D.S.; Influence of Suwannee River humic acid on particle properties and toxicity of silver nanoparticles. **Chemosphere**, v. 89, p. 96–101, 2012. Doi: 10.1016/j.chemosphere.2012.04.024

68. BRANT, J.; LECOANET, H.; WIESNER, M.R. Aggregation and deposition characteristics of fullerene nanoparticles in aqueous systems. **Journal of Nanoparticle Research**, v. 7, p. 545–553, 2008. Doi: 10.1007/s11051-005-4884-8

69. WARHEIT, D. B.; WEBB, T. R.; REED, K. L.; FRERICHS, S.; SAYES, C. M. Pulmonary toxicity study in rats with three forms of ultrafine-TiO_2 particles: Differential responses related to surface properties. **Toxicology**, v. 230, p. 90–104, 2007. Doi: 10.1016/j.tox.2006.11.002

70. CAI, R.; KUBOTA, Y.; SHUIN, T.; SAKAI, H.; HASHIMOTO, K.; FUJISHIMA, A. Induction of cytotoxicity by photoexcited TiO_2 particles. **Cancer Research**, v. 52, p. 2346-2348, 1992.

71. KAKINOKI, K.; YAMANE, K.; TERAOKA, R.; OTSUKA, M.; MATSUDA, Y. Effect of relative humidity on the photocatalytic activity of titanium dioxide and photostability of famotidine. **Journal of Pharmaceutical Sciences**, v. 93, n. 3, p. 582-589, 2004.

72. SAYES, C. M.; WAHI, R.; KURIAN, P. A.; LIU, Y.; WEST, J. L.; AUSMAN, K. D.; WARHEIT, D. B.; COLVIN, V. L. Correlating nanoscale titania structure with

toxicity: a cytotoxicity and inflammatory response study with human dermal fibroblasts and human lung epithelial cells. **Toxicological Sciences**, v. 92, n. 1, p. 174–185, 2006. Doi:10.1093/toxsci/kfj197

73. TURCI, F.; PEIRA, E.; CORAZZARI, I.; FENOGLIO, I.; TROTTA, M.; FUBINI, B. Crystalline phase modulates the potency of nanometric TiO_2 to adhere to and perturb the stratum corneum of porcine skin under indoor light. **Chemical Research in Toxicology**, v. 26, p. 1579−159, 2013. Doi: 10.1021/tx400285
74. GEYS, J.; NEMMAR, A.; VERBEKEN, E.; SMOLDERS, E.; RATOI, M.; HOYLAERTS, M. F.; NEMERY, B.; HOET, PETER H.M. Acute toxicity and prothrombotic effects of quantum dots: impact of surface charge. **Environmental Health Perspectives**, v. 116, n. 12, p. 1607-1613, 2008.
75. ARNDT, A. **Carbon nanomaterials in freshwater ecosystems: an chronic, Multi-generational, and genomic assessment of toxicity to *Daphnia magna*.** 2014. 129 p. Doctor of Philosophy in Freshwater Sciences - The University of Wisconsin-Milwaukee, Milwaukee, 2014
76. SHA, B.; GAO, W.; CUI, X.; WANG, L.; XU, F. The potential health challenges of TiO2 nanomaterials. **Journal of Applied Toxicology**, v. 35, p. 1086–1101, 2015. Doi: 10.1002/jat.3193

8 IMPACT OF SILVER IONS AND SILVER NANOPARTICLES ON THE PLANT GROWTH AND SOIL MICROORGANISMS[5]

Abstract
There is a growing consumer market for products that proclaim to decrease microorganism counts to prevent infections. Most of these products are loaded with silver in its ionic or nanoparticle form. Through use or during production, these particles can find their way into the soil and cause an impact in microbial and plant communities. This study aims to evaluate the impact of silver based particles in Avena byzantina (oat), Lactuca sativa (lettuce) and Raphanus sativus (radish) development and in the soil microorganism abundance. Oat, lettuce and radish plants were cultivated in soil contaminated with particles of bentonite organomodified with silver (Ag^+_bentonite), silver phosphate glass (Ag^+_phosphate) and silver nanoparticles adsorbed on fumed silica (AgNp_silica). Plant development and microorganisms' abundance were evaluated. To some degree, Ag^+_bentonite impacted plants development and AgNp_silica causes an adverse effect on microbial abundance. The impact on plants and microorganisms was contradictory and varied according to soil and particles physicochemical characteristics.

Keywords: Microbial population; Silver ions; Silver nanoparticles; Soil health; Terrestrial ecotoxicity.

8.1 INTRODUCTION

The use of silver (Ag) in functionalized products became widespread because of its biocidal effect [1]. Silver ions released from loaded materials can end up in the environment and have a negative impact [2]. A study accomplished by Sun et al. [3] highlights that in the European Union silver nanoparticles (AgNps) released from consumer goods have as final destination landfills (79 µg kg^{-1}) and sewage treatment plants (61 µg kg^{-1}). The action of AgNps can vary depending on particle sizes, characteristics and transformation pattern in the environment. Regarding the size, the AgNp damage relies on its ability to enter cells and be oxidized, generating reactive oxygen species (ROS) [4, 5]. The chemical characteristics of particle coating will influence the agglomeration and dissolution properties [6]. Moreover, the interaction of AgNp with the soil can modify physical and chemical characteristics which will influence stability, availability and, in turn, impact the toxicity of nanoparticles [7]. For example, the conversion of silver to Ag-sulfide has greater

[5] TOMACHESKI, D.; PITTOL, M.; SIMÕES, D. N.; FERREIRA, V. F.; SANTANA, R. M. C. Impact of silver ions and silver nanoparticles on the plant growth and soil microorganisms. **Global Journal of Environmental Science and Management**, 3(4): …-… 2017 (*In press*). Doi: 10.22034/gjesm.2017.03.04.00*.

impact on its toxicity because of the lower solubility of this modified silver specie [8]. Microbial communities are responsible for the maintenance of soil health. This way, an impact on these communities will affect agricultural production safety [9]. Plant growth based bioassay has been used to verify metal particle toxicity on the terrestrial environment [10, 11]. Soil ensure the life on earth through the ecosystem services [12, 13]. In this ecosystem, the concern rests on the fact that these particles can affect the composition of microbial communities [14], plant growth [15], reproduction of earthworms [16] and furthermore, can accumulate in the food chain [17]. Concerns related to the degradation of soil ecosystem prompted the development of monitoring and remediation projects [18]. With that in mind, it is important to understand the toxic aspects related to soil communities and potential pollutants to achieve the balance between the technological development and ecosystem health. Thus, the aim of this study is to evaluate the impact of three commercial silver-based biocide additives for use in polymers, being them: silver ions (silver phosphate glass, bentonite organomodified with silver) and silver nanoparticles (silver nanoparticles adsorbed on fumed silica), in the development of three plant species (oat, radish and lettuce), as well as the effects of such materials on soil microorganism abundance. This study has been carried out in South of Brazil in 2015-16.

8.2 MATERIAL AND METHODS

For the studies soil samples were experimentally contaminated with particles of bentonite organomodified with silver (referred to here as “Ag+_bentonite”), silver phosphate glass (referred to here as “Ag^{+}_phosphate”) and silver nanoparticles adsorbed on fumed silica (referred to here as “AgNp_silica”). Particle characteristics were previously determined in Tomacheski et al. [19], Figure 8.1 shows particles morphology determined by Transmission Electron Microcopy (TEM), Table 8.1 presents the average size determined by TEM, specific surface area (SSA) and zeta potential (ZP).

Figure 8.1 Transmission electron microscopy of the additives evaluated: (a) AgNp_silica, (b) Ag^+_phosphate and (c) Ag^+_bentonite

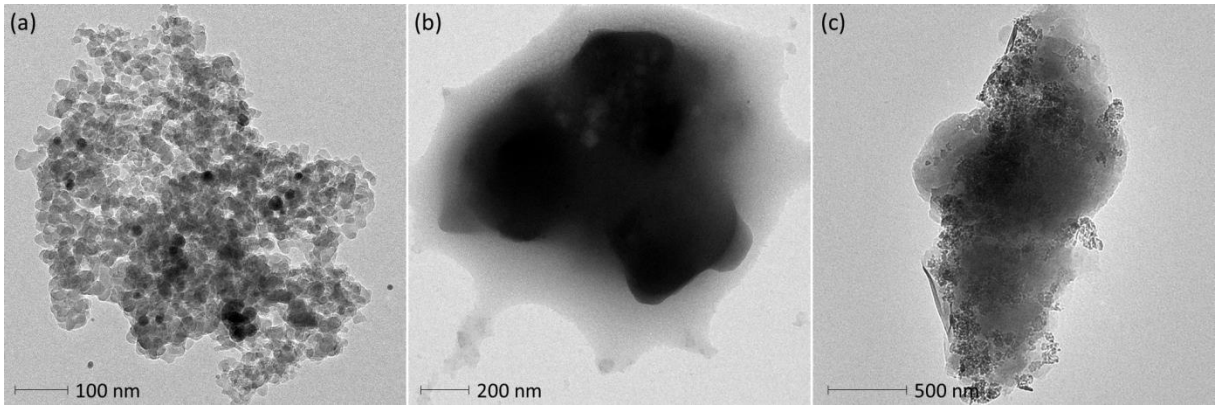

Table 8.1 Physical-chemical characteristics of the additives evaluated

Additive	Main information	Average diameter by TEM, µm	Specific Surface Area, $m^2 g^{-1}$	Zeta Potential at pH, mV	
AgNp_silica	Silver nanoparticles adsorbed on fumed silica (SiO_2)	0.02	293.90	3	0.12
				5	-6.48
				7	-27.70
				9	-27.53
				11	-35.77
Ag^+_phosphate	Silver ions supported on phosphate glass	1.0	6.16	3	15.7
				5	6.82
				7	-21.80
				9	-1.06
				11	-3.64
Ag^+_bentonite	Bentonite compounded by cristobalite and montmorillonite 22A, organomofied with silver ions.	1.5	36.73	3	-8.31
				5	-3.77
				7	-33.53
				9	-32.17
				11	-42.30

It was noted that in Ag^+_phosphate at pH 7, occurred a decrease in zeta potential and then at pH 9 it rises again. One explanation is that at pH 9 an oxidation of silver ions occurred forming silver oxide (Ag_2O). Thus, considering that the oxide surface has compatibility with the phosphate [20], the increase in ZP at pH 9 may be due to the rise in surface charge density on Ag_2O promoted by phosphate ions [21]. Anyway, particles with zeta potential below 30 mV or above -30 mV are deemed instable and with high capacity to form aggregates [22, 23] and, in this study, all three particles presented ZP between or near to 30 mV and -30 mV.

8.2.1 Germination assay

Germination assay was conducted using seeds of three plant species: *Avena byzantine* (oat), *Lactuca sativa* (lettuce) and *Raphanus sativus* (radish). The seeds were obtained commercially and sorted according to size and appearance and kept in dark, at room temperature before use. The mean germination rates of all plant seeds were greater than 90% as tested in a preliminary study (results not shown). The germination assay was performed using vessels (15 cm x 45 cm) containing 2,000 g of Organosol. It was used three vessels per additive. The particles were added in three vessels at a final concentration of 10 g kg^{-1}. Three vessels were used as control (no additive). Sowing was carried out in July 2015 (winter in the south of Brazil-29º40'54"S and 51º03'25"W). The plants were watered with 100 mL of water collected from rain every other day. A seed was considered as having germinated when shoots were evident above the soil surface. Figure 8.2 show the apparatus used for the germination assay.

Figure 8.2 Germination assay: (a) greenhouse used in the test and (b) vessels arrangement within the greenhouse.

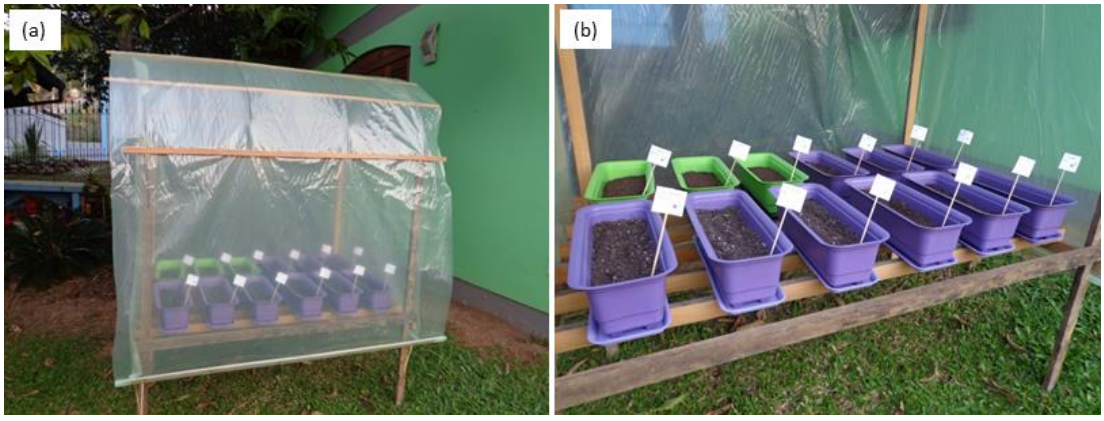

After a period of 35 days the plants were carefully removed from the soil and root length and dry weight measurements were taken after drying (48 h at 58 °C) the washed plants. The percentage of relative seed germination was calculated considering the total germination in the control sample as 100%. The lengths of the seedling roots were measured with a digital caliper rule. Each treatment was conducted with 25 seeds of lettuce, 25 seeds of radish, and 5 seeds of oat, and the results were presented as mean ± SD (standard deviation). Differences between treatments were analyzed using Analysis of Variance (ANOVA) followed by Tukey comparison tests using PAST version 3.14 software [24]. Each of the experimental

values was compared to its corresponding control. The level of significance was set at (p) less than 0.05.

8.2.2 Soil characterization

After harvesting, a composite sample of each additive type was prepared by mixing the three vessels of soil with same additive. For verify the concentration of silver a composite soil was acid digested based on the standard Environmental Protection Agency 3050B and the Inductively Coupled Plasma Optical Emission Spectrometry (ICP-OES) performed using a Thermo Scientific iCAP 6300 Model. Total nitrogen was measured by the Kjeldahl process based on British Standard 1309/7 and the International Union of Research Commission 10. Soil pH was measured using the potentiometric method with 1:10 dilution of soil, deionized water. Total phosphorus was measured by colorimetric assay, based on 4500 system from Standard Methods for the Examination of Water and Wastewater [25].

8.2.3 Isolation of soil microorganisms

Four composite soil samples were used for microbial isolation (three contaminated samples and one control sample). For the enumeration of microorganisms, 25 g of each composite soil sample was suspended in 225 mL peptone salt solution (0.1 %) and homogenized in Stomacher for 60 s (10^{-1} dilution). For the enumeration of mesophilic aerobe microorganisms 1 mL (10^{-4}) of soil suspension was placed in sterile Petri dishes and molten Plate Count Agar (Oxoid) was added to these plates and incubated for 48 h at 36 ± 1 °C. For yeast and fungi isolation the dilution (10^{-4}) was placed in Potato Dextrose Agar (MERCK) for 7 days at 25 ± 1 °C. *Pseudomonas aeruginosa* (*P. aeruginosa*) counts were performed according to the Most Probable Number test. Soil suspension (10^{-1}) was inoculated in *Pseudomonas* Asparagine Broth (BIOLOG) and incubated for 24-48 h at 35-37 ± 1°C. The positive test was confirmed with Acetamide Broth after the incubation for 24-36 h at 35-37 ± 1°C.

For the enumeration of *Bacillus* sp. 10 g of each composite soil sample was suspended in 90 mL of dilution water and homogenized in Stomacher for 60s. Then, 10 mL of diluted samples (10^{-4}) were heat-shocked at 80°C for 12 min and cooled at

4°C for 5 min. After this process, the suspension was placed in Nutrient Agar (Oxoid) and incubated for 24 h at 30°C.

8.3 RESULTS AND DISCUSSION

It is known that the soil physicochemical characteristics have an influence on the availability and consequently the toxicity of pollutants [26]. Table 8.2 shows the chemical characteristics of the soil contaminated and not contaminated used in this study. The addition of Ag^+_phosphate reduced the soil pH, while Ag^+_bentonite made it more alkaline and AgNp_silica had no effect compared to the control. The percentage of nitrogen (N) was greater than the control in all soil samples, mainly in AgNp_silica. The phosphorus (P) content was detected in high amounts in all soil samples. However, the concentration of P in Ag^+_bentonite soil was fairly high, showing a concentration ten-fold higher than the control. The high amount of P in soil with Ag^+_bentonite can be related to capability of clays to retain P in soil [27]. According to ICP-OES results, high amounts of silver were found in the sample loaded with Ag^+_phosphate followed by Ag^+_bentonite and AgNp_silica.

Table 8.2 Physicochemical characteristics of metal loaded soil

	Control	**Ag^+_phosphate**	**Ag^+_bentonite**	**AgNp_silica**
pH	7.9	7.4	8.4	8.0
Nitrogen (%)	0.33	0.37	0.38	0.77
Phosphorus (mg kg^{-1})	109	141	1082	175
Silver (mg kg^{-1})	0	176.0	65.1	49.9

It has been reported that the reaction of plants to metal present in soil can vary depending on plant species and characteristics of the particle tested [11]. In this study the toxicity of each additive was manifested in distinct ways. Table 8.3 shows germination; relative germination; root growth and dry mass values of plants cultivated in the control soil (without additive) and in the metal contaminated soil. Pictures of oat, lettuce and radish after harvest are shown in Figure 8.3, Figure 8.4 and Figure 8.5 respectively.

Table 8.3 Oat, lettuce and radish germination (%), relative germination (%, comparing loaded soil with the control), root growth (mm) and dry mass (g)

	Control	Ag^+_phosphate	Ag^+_bentonite	AgNp_silica
Oat				
Germination (%)	80	120	40	120
Relative germination (%)	-	150	50	150
Root growth (mm)	133 ± 25^a	233 ± 68^a	362 ± 47^a	103 ± 56^b
Dry mass (g)	0.026 ± 0.003^a	0.046 ± 0.015^a	0.042 ± 0.013^a	0.034 ± 0.006^a
Lettuce				
Germination (%)	80	64	36	40
Relative germination (%)	-	80	45	50
Root growth (mm)	23 ± 0.00^a	31 ± 7^a	24 ± 9^a	28 ± 7.85^a
Dry mass (g)	0.07 ± 0.00^a	0.06 ± 0.00^a	0.06 ± 0.00^a	0.04 ± 0.00^a
Radish				
Germination (%)	88	84	88	92
Relative germination (%)	-	95%	100%	105%
Root growth (mm)	92 ± 39^a	81 ± 23^a	52 ± 14^b	79 ± 27^a
Dry mass (g)	0.025 ± 0.01^a	0.035 ± 0.01^b	0.016 ± 0.01^c	0.031 ± 0.0^a

Values are given as mean ± SD. Averages that sharing the same superscript letter (a, b or c) are not significantly different from each other (p>0.05, Tukey's test).

Figure 8.3 Oat cultivated in soils containing (a) Control, (b) Ag^+_bentonite, (c) Ag^+_phosphate and (d) AgNp_silica

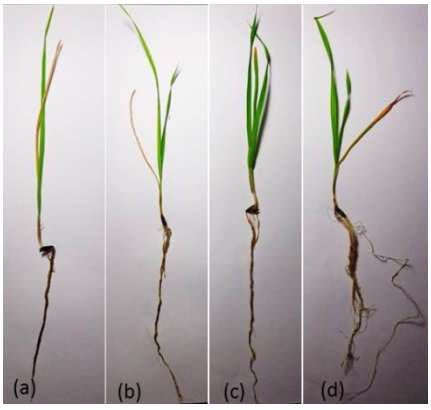

Figure 8.4 Lettuce cultivated in soils containing (a) Control, (b) Ag^+_bentonite, (c) Ag^+_phosphate and (d) AgNp_silica

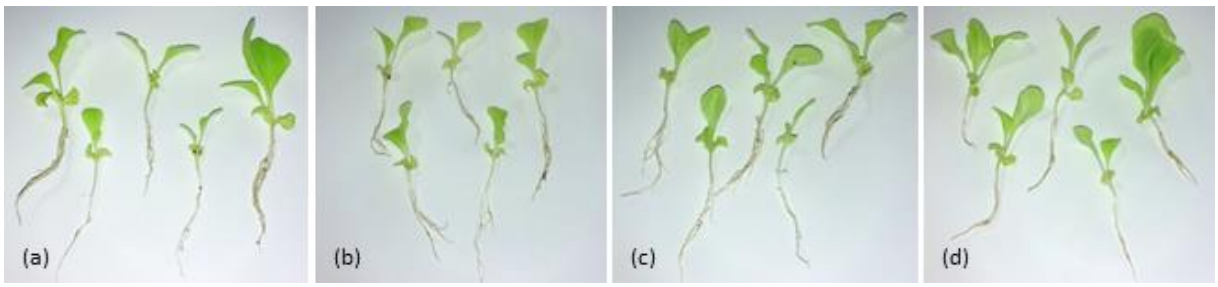

Figure 8.5 Radish cultivated in soils containing (a) Control, (b) Ag^+_bentonite, (c) Ag^+_phosphate and (d) AgNp_silica

Oat plants had lower germination rate in the soil with Ag^+_bentonite, however low root growth was observed in the soil loaded with AgNp_silica ($p<0.05$) (Table 8.3 and Figure 8.3). Root growth and dry mass values of lettuce presented no difference among the additives tested; however the germination was lower in the soil with Ag^+_bentonite (Table 8.3 and Figure 8.4). Root growth and dry mass of radish varied between the additives ($p<0.05$), with lower values found in the soil loaded with Ag^+_bentonite (Table 8.3 and Figure 8.5). Moreover, in Ag^+_phosphate and AgNp_silica soils it was verified enhance of dry mass values of radish plants compared to the control. Plant development was significantly lower in the soil loaded with Ag^+_bentonite, which presented high P levels. Phosphorus uptake is regulated according to plant growth rate and thus its concentration will vary in different plant species [28]. Nevertheless, the imbalance of phosphorus concentration causes the depletion of organic matter and nutrients and may have reflected in plant growth in Ag^+_bentonite loaded soils.

The main theory to explain silver toxicity is that silver ions generate reactive oxygen species (ROS, such as oxygen superoxide and hydrogen peroxide) which injures cell membrane and impacts DNA [29]. In the case of nanoparticles (AgNps), silver can be oxidized as shown in equation (1), resulting in the liberation of silver ions as shown in equation (2) [30, 31].

$$4Ag_{(0)} + O_2 \rightarrow 2Ag_2O \quad (1)$$

$$2Ag_2O + 4H^+ \rightarrow 4Ag^+ + 2H_2O \quad (2)$$

Soil pH influences the oxidation of Ag nanoparticles and the release of ions [26]. The modification of pH can change the potential zeta of particle (as seen in

Table 8.1) modifying particle agglomeration [32], hence the pH of the medium and the nanosilver coating influences its toxicity by making them unstable [15, 33].

Soil pH suitable for oat and lettuce growth is near 5.5-6.5. So, neutral to alkaline pH observed in the soil with Ag^+_bentonite (pH 8.4) and AgNp_silica (pH 8.01) may have contributed to the low relative germination rates in oat (50% - Ag^+_bentonite), lettuce plants (45% - Ag^+_bentonite and 50% - AgNp_silica) and the root growth of radish (52 mm-Ag^+_bentonite).

In oat plants, low root growth was observed in the soil loaded with AgNp_silica ($p<0.05$). Joshi et al. [34] suggest that silver nanoparticles are toxic due to their ability to translocate to the shoots, entering the cell membrane and being oxidized within the cell. After exposure to AgNp, plant roots showed a differential expression of proteins related to plant defense system against oxidative stress [35]. Coutris et al. [36] has shown that some forms of AgNp can be more dangerous, since in this format Ag is more promptly available than Ag ions.

In contrast, previous studies have shown that silver nanoparticles presented lower toxicity to plants than Ag^+ [5]. Besides that, studies revealed growth promotion in different species of plants [37, 38]. Particularly in the case of AgNps, Mustafa et al. [38] depict these nanoparticles as beneficial to the growth of soybean exposed to flooding. During the experiments carried out by these authors, the weight of the plant increased when cultivated with particles of 15 nm at a concentration of 2 ppm. Proteomic analysis suggested that the soybeans would suffer less with the absence of oxygen when treated with AgNps. Thus, plants growing in flooding conditions could have their development favored by the ROS generated from silver. Pokhrel and Dubey [4] studies revealed that the development and root growth of maize and cabbage was less affected by metal nanoparticles than the ionic form. Kaveh et al. [31] evaluated the action of AgNps and ionic silver on *Arabidopsis thaliana*. The exposure to 1.0 and 2.5 mg L^{-1} AgNps (20 nm) allowed for biomass gain; the same concentration of Ag^+ did not affect growth. However, by increasing the concentration to 5.0 and 20 mg L^{-1} of both AgNp and Ag^+ the weight of the plants presented lower values compared to the control. These divergent effects in plants exposed to nanoparticles or ionic silver can be explained by the hormesis mechanism. This process is characterized by enhanced growth at low concentrations of a toxic substance and an inhibition in higher doses [39]. In addition, the binding of sulfur and silver (Ag_2S - Ag sulfidation) or other sulfur-bound forms may be related to the low

toxicity of AgNp to plant development [8, 40]. The sulfidation of AgNp renders these particles less bioavailable due to the insolubility property of sulfidized nanoparticles [41, 42]. Once that the susceptibility of plants to toxic metals can vary not merely between plant species, but either between cultivars, it becomes difficult to make a connection among the presence of silver in soil and its toxic effects in plants. Priac et al. [43] observed different ecotoxicological responses from lettuce cultivars after be irrigated with the same metal-loaded wastewater.

Microorganisms perform key role in soil biological processes [37]. Due to silver's well-documented toxicity for microbes [44, 45], negative effect to both bacteria and fungi was expected upon Ag-exposure. Interestingly, despite the varying levels of negative effects of metal based additives on plant development, Ag^+_phosphate and Ag^+_bentonite improved the proliferation of Bacillus, mesophilic bacteria and fungi population. Table 8.4 shows the abundances of microorganisms in different metal loaded soil.

Table 8.4 Soil microbiota after harvest

	Control	Ag^+_phosphate	Ag^+_bentonite	AgNp_silica
***Bacillus* sp. (CFU g^{-1})**	2.47×10^5	2.82×10^5	4.18×10^5	7.76×10^4
Mesophilic bactéria (CFU g^{-1})	2.47×10^6	4.47×10^6	3.12×10^6	3.14×10^5
Fungi and yeasts (CFU g^{-1})	1.39×10^4	1.68×10^3	3.74×10^4	2.08×10^3
***P. aeruginosa* (MPN g^{-1})**	<0.2	<0.2	<0.2	<0.2

Note: CFU g^{-1}: Colony Forming Units per gram; MPN g^{-1}: Most Probable Number per gram

According to Schlich and Hund-Rinke [26] soil pH between 5.5 and 7.5 was found to have weak microbial toxicity. In the present study, the lowest bacterial toxicity was associated with acid (Ag^+_phosphate, pH 7.4) and alkaline (Ag^+_bentonite, pH 8.4) soils. The growth of bacteria and fungi populations in Ag^+_bentonite soil may be related to the ability of bentonite (clay) to absorb silver ions [44, 46]. Given that ionic silver have an inclination to interact with inorganic ligands and organic matter [47], the high concentration of phosphorus in Ag^+_bentonite soil (Table 8.2) may have provided a decrease in Ag toxicity for microorganisms. Moreover, extracellular polymeric substances produced by bacteria provide protection for the cells [34]. Judy et al. [37] reported that Ag_2S forms, which are produced in soil and wastewater environments, are less toxic to Gram-negative, Gram-positive bacteria and fungi populations than ionic Ag and polyvinylpyrrolidone

coated Ag nanomaterials. Reinsch et al. [41] observed that sulfidation decreases the toxic potential of AgNps against the *Escherichia coli* bacteria.

In contrast, in AgNp_silica loaded soils negative effect was noted on microbial development, oat and radish growth. This toxicity may be related to Ag connection with thiol groups found in enzymes and proteins of bacteria [48]. Furthermore, the AgNp_silica additive analyzed in this study has a specific surface area which provides high contact with microorganism cells in soil; besides of the described action in inhibit the plant growth by dropping chlorophyll content [49].

There was no detection of *P. aeruginosa* in the standard neither in metal loaded soil, which was expected once that this bacterium occurs in aquatic environment [50], being also reported in soil contaminated with untreated waste or subjected to hydrocarbon [51].

At the same time that plants and soil microorganisms are sensible to the presence of metals, some groups of inedible plants and microbes can be used for soil remediation. Researchers have reported the capability of Rhodes grass (*Chloris gayana*) to uptake antimony, arsenic, cadmium, lead, silver and zinc [52], and also *Jatropha curcas* and *Puccinellia frigida* to remove mercury [53] and boron [54] from soil, respectively. Alaribe and Agamuthu [55] mentioned the use of *Lantana camara* for phytoremediation of soil contaminated with lead. Moreover, some bacteria can be used to mitigate harmful effects of metals in soil, such as *Pseudomonas tolaasii*, *Pseudomonas fluorescens*, *Alcaligenes* sp. and *Mycobacterium* sp. [56].

Despite the natural filtration process that occurs when the effluent permeates the soil layers, attention must be taken in the metal-contaminated wastewater discard, once these xenobiotics substances can still reach groundwater [57].

8.4 CONCLUSIONS

It can be conclude that the responses of plants and microorganisms to the Ag present in soil vary according to size and chemical characteristics of the particle as well as to soil characteristics and the sensitivity of the plant. Silver nanoparticles and silver ions can be used as antimicrobial additives to avoid microbial proliferation in everyday use products, but attention must be taken on disposal of these materials in the environment.

8.5 REFERENCES

1. WAKSHLAK, R. B-K.; PEDAHZUR, R.; AVNIR, D. Antibacterial activity of silver-killed bacteria: the "zombies" effect. **Scientific Reports**, 5, p. 9555(1-5), 2005. Doi: 10.1038/srep09555
2. NOWACK, B.; KRUG, H. F.; HEIGHT, M. 120 years of nanosilver history: implications for policy makers. **Environmental Science and Technology**, v. 45, p. 1177-1183, 2011. Doi: 10.1021/es103316q
3. SUN, T. Y.; BORNHÖFT, N. A.; HUNGERBÜHLER, K.; NOWACK, B. Dynamic probabilistic modeling of environmental emissions of engineered nanomaterials. **Environmental Science and Technology**, v. 50, p. 4701-4711, 2016. Doi: 10.1021/acs.est.5b05828
4. POKHREL, L. R.; DUBEY, B. Evaluation of developmental responses of two crop plants exposed to silver and zinc oxide nanoparticles. **Environmental Science and Technology**, v. 452-453, p. 321–332, 2013. Doi: 10.1016/j.scitotenv.2013.02.059
5. SINGH, D.; KUMAR, A. Effects of nano silver oxide and silver ions on growth of vigna radiate. **Bulletin of Environmental Contamination and Toxicology**, 95, p. 379-384, 2015. Doi: 10.1007/s00128-015-1595-4
6. FURTADO, L. M.; BUNDSCHUH, M.; METCALFE, C. D. Monitoring the fate and transformation of silver nanoparticles in natural waters. **Bulletin of Environmental Contamination and Toxicology**, 97, p. 449-455, 2016. Doi: 10.1007/s00128-016-1888-2
7. ANJUM, N.A.; GILL, S. S.; DUARTE, A. C.; PEREIRA, E.; AHMAD, I. Silver nanoparticles in soil–plant systems. **Journal of Nanoparticle Research**, v. 15, p. 1896, 2013. Doi: 10.1007/s11051-013-1896-7
8. DOOLETTE, C. L.; MCLAUGHLINA, M. J.; KIRBY, J. K.; NAVARRO, D. A. Bioavailability of silver and silver sulfide nanoparticles to lettuce (*Lactuca sativa*): Effect of agricultural amendments on plant uptake. **Journal of Hazardous Materials**, v. 300, p. 788-795, 2015. Doi: 10.1016/j.jhazmat.2015.08.012
9. MCGEE, C. F.; STOREY, S.; CLIPSON, N.; DOYLE, E. Soil microbial community responses to contamination with silver, aluminium oxide and silicon dioxide nanoparticles. **Ecotoxicology**, 2017. Doi: 10.1007/s10646-017-1776-5
10. DIMKPA, C. O.; MERTEN, D.; SVATOS, A.; BÜCHEL, G.; KOTHE, E. Metal-induced oxidative stress impacting plant growth in contaminated soil is alleviated by microbial siderophores. **Soil Biology and Biochemistry**, v. 41, 154-162, 2009. Doi: 10.1016/j.soilbio.2008.10.010
11. DE OLIVEIRA, V. H.; MELO, L. C. A.; ABREU, C. A.; COSCIONE, A. R. Influences of soil pH on cadmium toxicity to eight plant species. **Ecotoxicology and Environmental Contamination**, v. 11, n. 1, p. 45-52, 2016. Doi: 10.5132/eec.2016.01.07
12. MOL, G.; KEESSTRA, S. Soil science in a changing world. **Current Opinion in Environmental Sustainability**, v. 4, p. 473–477, 2012. Doi: 10.1016/j.cosust.2012.10.013

13. BREVIK, E. C.; CERDÀ, A.; MATAIX-SOLERA, J.; PEREG, L.; QUINTON, J. N.; SIX, J.; OOST, K. V. The interdisciplinary nature of SOIL. **Soil**. v. 1, p. 117–129, 2015. Doi: 10.5194/soil-1-117-2015

14. ZHAI, Y.; HUNTING, E. R.; WOUTERS, M.; PEIJNENBURG, W. J. G. M.; VIJVER, M. G. Silver nanoparticles, ions, and shape governing soil microbial functional diversity: nano shapes micro. **Frontiers in Microbiology**, v. 7, p. 1123, 2016. Doi: 10.3389/fmicb.2016.01123

15. DIMKPA, C. O.; MCLEAN, J. E.; MARTINEAU, N.; BRITT, D. W.; HAVERKAMP, R.; ANDERSON, A. J. Silver nanoparticles disrupt wheat (*Triticum aestivum l.*) growth in a sand matrix. **Environmental Science and Technology**, v. 47, p. 1082-1090, 2013. Doi: 10.1021/es302973y

16. TSYUSKO, O. V.; HARDAS, S. S.; SHOULTS-WILSON, W. A.; STARNES, C. P.; JOICE, G.; BUTTERFIELD, D. A.; UNRINE, J. M. Short-term molecular-level effects of silver nanoparticle exposure on the earthworm, *Eisenia fetida*. **Environmental Pollution**, v. 171, p. 249-255, 2012. Doi: 10.1016/j.envpol.2012.08.003

17. SERVIN, A. D.; MORALES, M. I.; CASTILLO-MICHEL, H.; HERNANDEZ-VIEZCAS, J. A.; MUNOZ, B.; ZHAO, L.; NUNEZ, J. E.; PERALTA-VIDEA, J. R.; GARDEA-TORRESDEY, J. L. Synchrotron Verification of TiO2 accumulation in cucumber fruit: a possible pathway of TiO_2 nanoparticle transfer from soil into the food chain. **Environmental Science and Technology**, v. 47, p. 11592-11598, 2013. Doi: 10.1021/es403368j

18. KEESSTRA, S. D.; BOUMA, J.; WALLINGA, J.; TITTONELL, P.; SMITH, P.; CERDÀ, A.; MONTANARELLA, L.; QUINTON, J. N.; PACHEPSKY, Y.; VAN DER PUTTEN, W. H.; BARDGETT, R. D.; MOOLENAAR, S.; MOL, G.; JANSEN, B.; FRESCO, L. O. The significance of soils and soil science towards realization of the United Nations Sustainable Development Goals. **Soil**, v. 2, p. 111–128, 2016. Doi: 10.5194/soil-2-111-2016

19. TOMACHESKI, D.; PITTOL, M.; SIMÕES, D. N.; RIBEIRO, V. F.; SANTANA, R. M. C. Effects of silver adsorbed on fumed silica, silver phosphate glass, bentonite organomodified with silver and titanium dioxide in aquatic indicator organisms**. Journal of Environmental Sciences**, 2016. Doi: 10.1016/j.jes.2016.07.018

20. WU, W.; HE, Q.; JIANG, C. Magnetic Iron Oxide Nanoparticles: Synthesis and Surface Functionalization Strategies. **Nanoscale Research Letters**, 3: 397–415, 2008. Doi: 10.1007/s11671-008-9174-9

21. BROOKHAVEN INSTRUMENTS CORPORATION. **Colloidal Stability in Aqueous Suspensions**. Technical Information. Avaiable on: http://www.brookhaveninstruments.com/literature/pdf/ZetaPlus/ColloidalStabilityOctober.pdf, accessed on May 10, 2017.

22. SHIEH, Y-T.; CHEN, J. Y.; TWUC, Y. K.; CHENA, W-J. The effect of pH and ionic strength on the dispersion of carbon nanotubes in poly(acrylic acid) solutions. **Polymer International**, v. 61, p. 554–559, 2011. Doi: 10.1002/pi.3203

23. TAVARES, K. P.; CALOTO-OLIVEIRA, Á.; VICENTINI, D. S.; MELEGARI, S. P.; MATIAS, W. G.; BARBOSA, S.; KUMMROW, F. Acute toxicity of copper

and chromium oxide nanoparticles to *Daphnia similis*. **Ecotoxicology and Environmental Contamination**, v. 9, n. 1, p. 43-50, 2014. Doi: 10.5132/eec.2014.01.006

24. HAMMER, Ø.; HARPER, D. A. T.; RYAN, P. D. PAST: Paleontological statistics software package for education and data analysis. **Palaeontologia Electronica**, v. 4, n. 1, 9 pp. 2001.

25. RICE, E. W.; BAIRD, R. B.; EATON, A. D.; CLESCERI, L. S. **Standard methods for the examination of water and wastewater**, 22nd. Ed. APHA, AWWA, WEF, 2012.

26. SCHLICH, K.; HUND-RINKE, K. Influence of soil properties on the effect of silver nanomaterials on microbial activity in five soils. **Environmental Pollution**, v. 196, p. 321-330, 2015. Doi: 10.1016/j.envpol.2014.10.021

27. ULÉN, B.; ETANA, A. Phosphorus leaching from clay soils can be counteracted by structure liming. **Acta Agriculturae Scandinavica, Section B — Soil & Plant Science**, v. 64, n. 5, p. 425–433, 2014. Doi: 10.1080/09064710.2014.920043

28. NARANG, R. A.; BRUENE, A.; ALTMANN, T. Analysis of phosphate acquisition efficiency in different arabidopsis accessions. **Plant Physiology**, v. 124, p.1786–1799, 2000. Doi: 10.1104/pp.124.4.1786

29. KUMARI, M.; MUKHERJEE, A.; CHANDRASEKARAN, N. Genotoxicity of silver nanoparticles in *Allium cepa*. **Science of the Total Environment**, v. 407, p. 5243-5246, 2009. Doi: 10.1016/j.scitotenv.2009.06.024

30. XIU, Z-M.; ZHANG, Q-B.; PUPPALA, H. L.; COLVIN, V. L.; ALVAREZ, P. J. J. Negligible particle-specific antibacterial activity of silver nanoparticles. **Nano Letters**, v. 12, p. 4271-4275, 2012. Doi: 10.1021/nl301934w

31. KAVEH, R.; LI, Y-S.; RANJBAR, S.; TEHRANI, R.; BRUECK, C. L.; AKEN, B. A. Changes in arabidopsis thaliana gene expression in response to silver nanoparticles and silver ions. **Environmental Science and Technology**, v. 47, p. 10637-10644, 2013. Doi: 10.1021/es402209w

32. PRATHNA, T. C.; CHANDRASEKARAN, N.; MUKHERJEE, A. Studies on aggregation behaviour of silver nanoparticles in aqueous matrices: Effect of surface functionalization and matrix composition. **Colloids and Surfaces A: Physicochemical and Engineering Aspects**, v. 390, p. 216- 224, 2011. Doi: 10.1016/j.colsurfa.2011.09.047

33. EL BADAWY, A.; LUXTON, T. P.; SILVA, R.; SCHECKEL, K. G.; SUIDAN, M. T.; TOLAYMAT, T. Impact of environmental conditions (pH, ionic strength, and electrolyte type) on the surface charge and aggregation of silver nanoparticles suspensions. **Environmental Science and Technology**, v. 44, p. 1260-1266, 2010. Doi: 10.1021/es902240k

34. JOSHI, N.; NGWENYA, B. T.; FRENCH, C. E. Enhanced resistance to nanoparticle toxicity is conferred by overproduction of extracellular polymeric substances. **Journal of Hazardous Materials**, v. 241-242, p. 363-370, 2012. Doi: 10.1016/j.jhazmat.2012.09.057

35. VANNINI, C.; DOMINGO, G.; ONELLI, E.; PRINSI, B.; MARSONI, M.; ESPEN, L.; BRACALE, M. Morphological and proteomic responses of *Eruca sativa*

exposed to silver nanoparticles or silver nitrate. **Plos One**, v. 8, n. 7, p. e68752, 2013. Doi: 10.1371/journal.pone.0068752

36. COUTRIS, C.; JONER, E. J.; OUGHTON, D. H. Aging and soil organic matter content affect the fate of silver nanoparticles in soil. **Science of the Total Environment**, v. 420, p. 327-333, 2012. Doi: 10.1016/j.scitotenv.2012.01.027
37. JUDY, J. D.; KIRBY, K. K.; CREAMER, C.; MCLAUGHLIN, M. J.; FIEBIGER, C.; WRIGHT, C.; CAVAGNARO, T. R.; BERTSCH, P. M. Effects of silver sulfide nanomaterials on mycorrhizal colonization of tomato plants and soil microbial communities in biosolid-amended soil. **Environmental Pollution**, v. 206, p. 256-263, 2015. Doi: 10.1016/j.envpol.2015.07.002
38. MUSTAFA, G., SAKATA, K., HOSSAIN, Z, KOMATSU, S. 2015. Proteomic study on the effects of silver nanoparticles on soybean under flooding stress. **Journal of Proteomics**, v. 122, p. 100-118. Doi: 10.1016/j.jprot.2015.03.030
39. POSCHENRIEDER, C.; CABOT, C.; MARTOS, S.; GALLEGO, B.; BARCELÓ, J. Do toxic ions induce hormesis in plants? **Plant Science**, v. 212, p. 15-25, 2013. Doi: 10.1016/j.plantsci.2013.07.012
40. LEVARD, C.; HOTZE, E. M.; LOWRY, G. V.; BROWN JR, G. E. Environmental transformations of silver nanoparticles: impact on stability and toxicity. **Environmental Science and Technology**, v. 46, p. 6900-6914, 2012. Doi: 10.1021/es2037405
41. REINSCH, B. C.; LEVARD, C.; LI, Z.; MA, R.; WISE, A.; GREGORY, K. B.; BROWN, JR. G. E.; LOWRY, G. V. Sulfidation of silver nanoparticles decreases *Escherichia coli* growth inhibition. **Environmental Science and Technology**, v. 46, p. 6992-7000, 2012. Doi: 10.1021/es203732x.
42. LEVARD, C.; HOTZE, E. M.; COLMAN, B. P.; DALE, A. L.; TRUONG, L.; YANG, X. Y.; BONE, A. J.; BROWN JR. G.E.; TANGUAY, R. L.; DI GIULIO, R. T.; BERNHARDT, E. S.; MEYER, J. N.; WIESNER, M. R.; LOWRY, G. V. Sulfidation of silver nanoparticles: natural antidote to their toxicity. **Environmental Science and Technology**, v. 47, p. 13440−13448, 2013. Doi: 10.1021/es403527n
43. PRIAC, A.; BADOT, P. M.; CRINI, G. Treated wastewater phytotoxicity assessment using *Lactuca sativa*: Focus on germination and root elongation test parameters. **Comptes Rendus Biologies**, v. 340, p. 188–194, 2017. Doi: 10.1016/j.crvi.2017.01.002
44. CALDER, A. J.; DIMKPA, C. O.; MCLEAN, J. E.; BRITT, D. W.; JOHNSON, W.; ANDERSON, A. J. Soil components mitigate the antimicrobial effects of silver nanoparticles towards a beneficial soil bacterium, *Pseudomonas chlororaphis O6*. **Science of the Total Environment**, v. 429, p. 215-222, 2012. doi: 10.1016/j.scitotenv.2012.04.049
45. HE, S.; FENG, Y.; NI, J.; SUN, Y.; XUE, L.; FENG, Y.; YU, Y.; LIN, X.; YANG, L. Different responses of soil microbial metabolic activity to silver and iron oxide nanoparticles. **Chemosphere**, v. 147, p. 195-202, 2015. Doi: 10.1016/j.chemosphere.2015.12.055
46. MAGAÑA, S. M.; QUINTANA, P.; AGUILAR, D. H.; TOLEDO, J. A.; ANGELES-CHÁVEZ, C.; CORTES, M. A.; LEON, L.; FREILE-PELEGRIN, Y.; LOPEZ, T.;

SANCHEZ, R. M. T. Antibacterial activity of montmorillonites modified with silver. **Journal of Molecular Catalysis A: Chemical**, v. 281, p. 192-199, 2008. Doi: 10.1016/j.molcata.2007.10.024

47. YANG, Y.; WANG, J.; XIU, Z.; ALVAREZ, P. J. J. Impacts of silver nanoparticles on cellular and transcriptional activity of nitrogen-cycling bacteria. **Environmental Toxicology and Chemistry**, v. 32, n. 7, p. 1488-1494, 2013. Doi: 10.1002/etc.2230

48. LEMIRE, J. A.; HARRISON, J. J.; TURNER, R. J. Antimicrobial activity of metals: mechanisms, molecular targets and applications. **Nature Reviews**, v. 11, p. 371-384, 2013. Doi: 10.1038/nrmicro3028

49. QIAN, H.; PENG, X.; HAN, X.; REN, J.; SUN, L.; FU, Z. Comparison of the toxicity of silver nanoparticles and silver ions on the growth of terrestrial plant model Arabidopsis thaliana. **Journal of Environmental Sciences**, v. 25, n. 9, p. 1947-1955, 2013. Doi: 10.1016/S1001-0742(12)60301-5

50. SELEZSKA, K.; KAZMIERCZAK, M.; MÜSKEN, M.; GARBE, J.; SCHOBERT, M.; HÄUSSLER, S.; WIEHLMANN, L.; ROHDE, C.; SIKORSKI, J., Pseudomonas aeruginosa population structure revisited under environmental focus: impact of water quality and phage pressure. **Applied and Environmental Microbiology**, v. 14, n. 8, p. 1952–1967, 2012. Doi: 10.1111/j.1462-2920.2012.02719.x

51. DEREDJIAN, A.; COLINON, C.; HIEN, E.; BROTHIER, E.; YOUENOU, B.; COURNOYER, B.; DEQUIEDT, S.; HARTMANN, A.; JOLIVET,C.; HOUOT, S.; RANJARD, L.; SABY, N. P. A.; NAZARET, S. Low occurrence of Pseudomonas aeruginosa in agricultural soils with and without organic amendment. **Frontiers in Cellular and Infection Microbiology**, v. 4, p. 1-12, 2014. Doi: 10.3389/fcimb.2014.00053

52. KEELING, S. M.; WERREN, G. Phytoremediation: The uptake of metals and metalloids by rhodes grass grown on metal-contaminated soil. **Remediation Journal**, v. 15, n. 2, p. 53-61, 2005. Doi: 10.1002/rem.20042

53. MARRUGO-NEGRETE, J.; DURANGO-HERNÁNDEZ, J.; PINEDO-HERNÁNDEZ, J.; OLIVERO-VERBEL, J.; DÍEZ, S. Phytoremediation of mercury-contaminated soils by *Jatropha curcas*. **Chemosphere**, v. 127, p. 58–63, 2015. Doi: 10.1016/j.chemosphere.2014.12.073

54. RÁMILA, C. D. P.; LEIVA, E. D.; BONILLA, C. A.; PASTÉN, P. A.; PIZARRO, G. E. Boron accumulation in *Puccinellia frigida*, an extremely tolerant and promising species for boron phytoremediation. **Journal of Geochemical Exploration**, v. 150, p. 25–34, 2015. Doi: 10.1016/j.gexplo.2014.12.020

55. ALARIBE, F. O.; AGAMUTHU, P. Assessment of phytoremediation potentials of Lantana camara in Pb impacted soil with organic waste additives. **Ecological Engineering**, v. 83, p. 513–520, 2015. Doi: 10.1016/j.ecoleng.2015.07.001

56. DELL'AMICO, E.; CAVALCA, L.; ANDREONI, V. Improvement of *Brassica napus* growth under cadmium stress by cadmium-resistant rhizobacteria. **Soil Biology and Biochemistry**, v. 40, p. 74–84, 2008. Doi: 10.1016/j.soilbio.2007.06.024

57. KEESSTRA, S. D.; GEISSEN, V.; MOSSE, K.; PIIRANEN, S.; SCUDIERO, E.; LEISTRA, M.; VAN SCHAIK, L. Soil as a filter for groundwater quality. **Current Opinion in Environmental Sustainability**, v. 4, p. 507–516, 2012. Doi: 10.1016/j.cosust.2012.10.007

9 CONCLUSÃO GERAL

Os resultados obtidos nesta pesquisa levaram as seguintes conclusões:

As variações nas propriedades físicas e mecânicas dos compostos, após a incorporação dos aditivos (avaliadas no Capítulo 4), estão dentro do desvio padrão de fabricação do produto e não afetam a aplicação comercial do mesmo. O aditivo AgNp_sílica teve o melhor desempenho antibacteriano, mesmo na concentração de 0,025%, eliminando 96% da população de *E. coli* e 81% da população de *S. aureus*. O aditivo Ag^+_bentonita atingiu a ação antibacteriana próxima de AgNp_sílica somente com a adição de 2,0% no composto.

O envelhecimento natural, avaliado no Capítulo 5, mostrou ser um fator importante na redução do desempenho mecânico assim como na atividade antibacteriana contra *E. coli* para todos os compostos independentemente da presença dos aditivos antimicrobianos. A ação contra *S. aureus* teve redução de eficiência com os aditivos AgNp_sílica e Ag^+_bentonita. Ao contrário do esperado, a amostra aditivada com 0,3% de Ag^+_fosfato teve maior eficiência contra *S. aureus* após 6 meses de exposição.

A análise de superfície dos corpos de prova expostos ao intemperismo, realizada no Capítulo 6, mostrou que alterações como aumento da energia superficial específica e redução da hidrofobicidade tornam o composto mais propício ao desenvolvimento das bactérias e fungos, mesmo sem perda de aditivo.

No ensaio de respirometria, também realizado no Capítulo 5, a amostra aditivada com AgNp_sílica teve uma menor produção de gás carbônico (CO_2), provavelmente, decorrente da liberação de nanopartículas de prata, as quais podem ter afetado o mecanismo de biodegradação dos micro-organismos presentes no solo.

No Capítulo 7, todos os aditivos se demonstraram letais aos microcrustáceos aquáticos (*D. magna*), não sendo possível estabelecer uma relação entre as características dos aditivos (composição, tamanho, forma, potencial zeta ou área de superfície) e a toxicidade.

No ensaio de germinação realizado no Capítulo 8, os resultados foram diversos e inconclusivos; em comparação com o solo controle, a alface (*Lactuca sativa*) apresentou menor índice relativo de germinação, mas sem variação nos índices de massa seca e crescimento de raiz. A aveia (*Avena sativa*) teve maior

massa quando em solo aditivado e o crescimento de raiz foi menor somente no solo com AgNp_sílica, a germinação foi menor no solo com Ag^+_bentonita. Para o rabanete (*Raphanus sativus*), o índice de germinação foi semelhante para todas as amostras, com maior massa seca para as amostras em solo com Ag^+_fosfato e Ag^+_bentonita e menor para AgNp_silica. O crescimento de raiz foi menor no solo com Ag^+_bentonita.

A avaliação dos efeitos ecotoxicológicos dos aditivos realizados nos capítulos 7 e 8 se mostrou complexa devido à enorme quantidade de variáveis existentes na avaliação da toxicidade nos ecossistemas, como tipo de micro-organismos e plantas presentes, características do solo como pH e níveis de nutrientes, os quais podem contribuir para mitigar ou reforçar os efeitos tóxicos dos aditivos. A revisão da literatura mostra que os resultados dos testes ecotoxicológicos são contraditórios e que mais estudos são necessários para atestar ou não a segurança do uso dos aditivos antimicrobianos.

Como são materiais 100% recicláveis e a taxa de migração da prata é baixa, o maior risco para o meio ambiente ocorre caso os compostos sejam descartados diretamente no solo, reforçando a importância da correta gestão dos resíduos sólidos.

Nesse contexto, observando-se a destinação correta dos resíduos, como a reciclagem ou disposição final em aterros sanitários normatizados e fiscalizados, os compostos termoplásticos com propriedades antimicrobianas são seguros para o meio ambiente e podem auxiliar no controle da disseminação de doenças.